O-GLYCOSYLATION AND THE NOTCH SIGNALING PATHWAY

by

RACHEL K. LOPILATO

(Under the Direction of Robert S. Haltiwanger)

ABSTRACT

The Notch signaling pathway is an evolutionarily conserved mechanism for cell-to-cell communication in metazoan development. Significant pathway regulation occurs through glycosylation of the Notch receptor extracellular domain by the Fringe family of glycosyltransferases at numerous *O*-fucosylated Epidermal Growth Factor-like (EGF) Repeats. In this study we investigated the *in vivo* contributions of two Fringe-modified *O*-fucose sites in NOTCH1 by using CRISPR/Cas9 knock-in technology to generate two lines of C57BL/6J mice carrying point mutations at *O*-fucose sites in NOTCH1 previously shown to alter signaling *in vitro*. Because T/V point mutation of EGF8 *O*-fucose results in reduced Notch receptor activation when stimulated by both Delta-like and Jagged ligands in cellular assays, we predicted that mice carrying two mutated gene copies would have *Notch1*-null phenotypes and embryonic lethality. Another Fringe-elongated *O*-fucose site in EGF6 was of great interest for its ability to inhibit Notch activation by Jagged ligand, despite its location outside the NOTCH1 ligand-binding region, without enhancing activation by Delta-like ligand. Moreover, T/V mutation of EGF6 *O*-fucose *in vitro* causes no change to Notch activation when unmodified, suggesting that its role is solely regulatory. We chose to monitor changes in the well-documented developmental process of retinal angiogenesis due to its dependence on the coordinated expression of *Notch1*,

Jag1, *Dll4*, and the three mammalian Fringe genes *Lfng*, *Mfng*, and *Rfng*. Unexpectedly, the EGF8 mice were viable and fertile, indicating that the point mutation did not sufficiently lower pathway activation to cause embryonic lethality, although the *O*-fucose residue directly participates in ligand-binding events. However, vessels in the EGF8 retinas were densely clustered, consistent with the predicted *Notch1* loss-of-function phenotype. Retinas from the EGF6 mice presented with the opposite phenotype, a decrease in vessel density associated with our predicted *Notch1* gain-of-function outcome. Overall, these *in vivo* results recapitulate the *in vitro* data and confirm the significance of individual NOTCH1 *O*-glycans in pathway function during mammalian development.

INDEX WORDS: Glycobiology, Notch Signaling Pathway, Development, Angiogenesis

O-GLYCOSYLATION AND THE NOTCH SIGNALING PATHWAY

by

RACHEL LOPILATO

BS, University of Georgia, 2015

A Dissertation Submitted to the Graduate Faculty of The University of Georgia in Partial Fulfillment of the Requirements for the Degree

DOCTOR OF PHILOSOPHY

ATHENS, GEORGIA

2023

O-GLYCOSYLATION AND THE NOTCH SIGNALING PATHWAY

by

RACHEL LOPILATO

Major Professor:	Robert S. Haltiwanger
Committee:	Michael Tiemeyer
	Neil Grimsey
	James D. Lauderdale

Electronic Version Approved:

Ron Walcott

Vice Provost for Graduate Education and Dean of the Graduate School

The University of Georgia

May 2023

DEDICATION

I would like to dedicate this dissertation to my mother Carole and grandmother Katy, aunts Eva, Celeste, Linda, Joanne, Karen, Jan, uncle David, cousins Michelle, Alicia, Erin, Jonathan, Melissa, Jay, Matt, Andrew, Laura, nephews Jack and Avery, sisters-in-law Allison and Laura, and my brothers Alex and Daniel.

ACKNOWLEDGEMENTS

I would like to acknowledge several of the many people who contributed to my scientific development and have gone above and beyond to support me over the years. These people are Shinako Kakuda, Heike Kroeger, Neil Grimsey, Steven Berardinelli, Nick Kegley, Kelvin Luther, Youxi Yuan, Nancy Manley, Jenna Wingfield, Alexis Gibson, Hannah Fullenweider, Carly Duffy, and Bob and Kim Haltiwanger

TABLE OF CONTENTS

Page

LIST OF TABLES

LIST OF FIGURES

CHAPTER 1

LITERATURE REVIEW AND SPECIFIC AIMS

Historical and Biological Overview of the Notch Signaling Pathway

Discovery of the Notch gene is credited to both John S. Dexter and Thomas Hunt Morgan during the model organism boom in the early 1900s. Significant recent advancements had primed their discovery of Notch – *Drosophila* researchers developed the use of balancer chromosomes for maintaining strains carrying alleles of interest, genetic screens were accelerated by the introduction of radiation mutagenesis, and Morgan had demonstrated X-linked inheritance of *Drosophila* eye color [1]. First documented by Morgan in a radiation mutagenesis study, a cluster of *Drosophila* phenotypes ranging from ripples along wing edges to severe absence of wing tissue was categorized as the 'Beaded' strain of mutants. Crosses sometimes resulted in lethality or reversion to wildtype, complicating the study of its inheritance. When John S. Dexter took up study of the Beaded strain and awarded the title 'Perfectly Notched' to a female isolate **(Figure 1.1, right panel)**, he noted that Perfectly Notched only presented in females and caused lethality in males. He concluded that the causative allele was X-linked dominant. Shortly after publication, however, John S. Dexter lost the Perfectly Notched stock while away on travel [2].

Thomas Hunt Morgan integrated Dexter's findings into a commentary on Darwin's theory of evolution by natural selection, laying the foundation for modern synthesis of evolutionary biology. Morgan also provided the first illustration of a *notch+/-* female **(Figure 1.1, left panel)** and described the inheritance of *notch* as X-linked dominant with respect to its

wing phenotype and X-linked recessive with respect to its lethality. Morgan reported that *notch*+/- females could revert to wildtype through numerous backcrosses selecting for wildtype traits. One outcross could recover the *notch*+/- phenotype, however, thus refuting Darwin's idea that unique traits are erased when crossed into background and at the same time supporting the Darwinian theory of natural selection based on chance variation. More importantly, Morgan inferred the presence of a modifying gene elsewhere in the *Drosophila* genome which was selected for during backcross while the *notch* mutant allele itself remained intact [3].

Further study of the *notch*-null *Drosophila* embryo defined the lethal phenotype in greater detail, earning the name 'neurogenic' due to its overabundance of neuroblasts at the expense of epithelial progenitors originating from the ectoderm. Defining this phenotype helped classify future genes in relation to *notch*, such as *delta* and *mastermind* [1]. In 1985 the *notch* locus was cloned for the first time and analyzed for its protein structure. In addition to discerning an intracellular domain with probable DNA-binding capacity, researchers identified regions of protein homologous to human proteins containing Epidermal Growth Factor (EGF) repeats, cysteine-rich regions usually found in protein extracellular regions. Human proteins known to contain EGF-like repeats include the LDL receptor and blood coagulators Human Factors IX and X. Unlike these proteins, Notch appeared to have 36 tandem EGF-like repeats, compared to the one or several repeats found in the extracellular domains of the LDL receptor and Human Factor IX [4]. Although not exact, the homology pointed to a degree of conservation between Notch in *Drosophila* and vertebrates. The homology also hinted to the function of Notch protein in a cellular context for the first time. Because EGF-like repeats are located in extracellular regions known for protein-protein interactions, the high density of EGF-like repeats suggested the

presence of a large extracellular domain, likely for engaging in cell-to-cell communication during binary cell fate decisions exemplified by the neurogenic phenotype [4].

In 1991, the human *NOTCH1* gene was cloned by happenstance when researchers were studying a chromosomal translocation event associated with T-Cell Acute Lymphoblastic Leukemia (T-ALL) at the gene region encoding for a β T-cell receptor. Not only did cloning *NOTCH1* confirm a high degree of conservation between *Drosophila* Notch and mammalian Notch, but it also related the Notch family to human disease for the first time. Additionally, researchers identified lymphoid tissue from both human and mouse samples as particularly rich in *NOTCH1*/*Notch1* transcript [5].

The broad involvement of Notch in mammalian embryonic development and organogenesis was demonstrated for the first time in a mouse carrying two copies of a *Notch1*-null allele. The null embryos were shown to arrest by embryonic day 10.5 with heart and neural defects, as well as a strikingly small body size **(Figure 1.2, left panel)** [6]. A later study linked *Notch1* to somitogenesis and showed that somite formation in *Notch1 -/-* embryos was delayed and asymmetric during skeletal development **(Figure 1.2, right panel)** [7]. These studies established major *Notch1* phenotypes in the murine model that would facilitate future research into *NOTCH1* gene function in humans.

At the time of these first mouse studies, *Drosophila* researchers uncovered a *notch* modifier named *fringe*. Its discovery grew from the concurrent study of homeobox genes regulating anatomical positioning during embryogenesis. A mutagenesis screen by transposable P-element insertion with a β-galactosidase reporter under the hox transcription factor *apterous* known to specify dorsal wing fate, generated several mutants displaying wing margin defects at the apparent dorsal-ventral boundary **(Figure 1.3, left panel)** [8].

Other modifiers of *notch* were found to include the *serrate* and *delta* ligand genes. Both ligand proteins were found to contain EGF-like repeats, suggesting that they were also involved in direct cell-to-cell communication [9]. A positive feedback loop in the expression of *notch* and both ligands was identified at the dorsal-ventral boundary in the wing where activation of *notch* appeared to be elevated. The spatial component to this feedback loop was indicative of cell-to-cell interactions [10]. Both *fringe* and *serrate* expression are restricted to the dorsal compartment, while *delta* expresses broadly throughout the wing disc **(Figure 1.3, middle and right panels)** [11].

The mechanism underpinning elevated expression of *notch* in a strip at the dorsal-ventral boundary was shown to involve ligand-specific responses influenced by *fringe*. In the presence of *fringe*, signaling by *serrate* is reduced while signaling by *delta* is enhanced **(Figure 1.3, middle panel)** [11]. Biochemical characterization of this phenomenon reported that the *fringe* gene encodes a Golgi glycosyltransferase which transfers N-acetylglucosamine to *O*-fucosylated EGF-like repeats on Notch protein to increase its binding affinity for Delta at the expense of Serrate [12, 13] **(Figure 1.4)**.

Structure-function studies were performed to identify specific regions of the Notch receptor protein important for signaling. Truncation of the entire extracellular domain and transmembrane region caused the remaining intracellular region to translocate to the nucleus and resulted in gain-of-function phenotypes [14]. It was also revealed that EGFs 11-12 were necessary for receptor association with ligand in an aggregation assay with *Drosophila* S2 cells [15]. Considering the high conservation of this region across vertebrates, it was hypothesized to function as the ligand-binding domain [14].

When comparing the putative structures of *Drosophila* Notch to its human orthologs NOTCH1, 2, 3, and 4, conservation of the extracellular domain is evident. *Drosophila* Notch and human NOTCH1 and NOTCH2 contain 36 EGF-like repeats **(Figure 1.5)**. Directly C-terminal of the EGF-like repeats is the mechanosensitive Lin-repeat region necessary for receptor regulation. One definite difference between *Drosophila* Notch and members of the human Notch family is the absence of a furin cleavage site, meaning that mature *Drosophila* Notch is expressed as a monomer while mammalian Notch is expressed as a heterodimer stabilized by disulfide bonds and interactions with Ca^{2+}. However, Notch from either group needs Ca^{2+} interactions for stabilizing EGF-like repeats and maintaining the negative regulatory state of the Lin-repeat regions [16-18].

The level of conservation extends to the Notch ligands as well **(Figure 1.6)**. Both *Drosophila* Serrate and Delta ligands are comprised of extensive extracellular regions that are packed with cysteine-rich EGF-like repeats. Serrate has a longer extracellular domain and a greater number of EGF-like repeats than Delta. These characteristics are also observed in the several mammalian/human Delta-like Ligands (DLL1, DLL3, and DLL4) and Jagged ligands (Jagged1 and Jagged2) [19-21].

While studies into receptor/ligand structure, function, and signaling dynamics were underway, other researchers worked to define the transcriptional machinery, target genes, and necessary proteolytic events in the context of a cell-to-cell membrane environment that induces mechanical force. **Figure 1.7** summarizes these findings beginning with mammalian receptor translation and *O*-fucosylation in the ER, Fringe modification and Furin cleavage in the Golgi compartment, and expression of the mature heterodimer at the cell surface. Following ligand binding and the mechanical force of endocytosis, the Notch extracellular domain is shed by

ADAM proteolytic cleavage. The intracellular domain is released by intramembrane secretases and translocates directly to the nucleus for co-activation of target genes [22, 23].

Biochemical characterization of EGF-like repeats identified *O*-fucosylation and Fringe elongation on both *Drosophila* Notch and Mouse Notch1 at EGF12, where the sugars were predicted to interact with ligand due to their location in the ligand-binding domain. A putative consensus sequence for EGF-like repeat *O*-fucosylation was collated to $C^2XXXX\underline{S/T}C^3$ at otherwise heterologous EGF-like repeats **(Figure 1.8)** [15, 24]. A short fragment of NOTCH1 carrying a GlcNAc-Fuc disaccharide at EGF12 was shown to substantially increase binding affinity with ligands JAG1 and DLL1 compared to fragment carrying monosaccharide only [25], further highlighting the importance of this region.

The advent of more powerful mass spectrometry enabled detection of post-translational modifications and site-mapping EGF-like repeats to confirm the presence of *O*-glycans [26]. Of the 36 EGF-like repeats found in *Drosophila* Notch, 22 contain a putative consensus sequence for *O*-fucosylation, and mapping by mass spectrometry confirmed that all 22 sites were *O*-fucosylated **(Figure 1.9)**. Among these sites, 17 were found to carry some degree of Fringe modification, notably EGFs 8 and 12 in the ligand binding domain and several within the abruptex region [27-29].

Elongation of *O*-fucose by Fringe in mammals is more diverse, given that there are three mammalian Fringes named Lunatic, Manic, and Radical. To initially establish their functionality, the mouse genes *Lfng*, *Mfng*, or *Rfng* were cloned and ectopically misexpressed along the Anterior-Posterior boundary in the *Drosophila* wing disc, which was predicted to disrupt the Dorsal-Ventral boundary by perpendicular intersection with cells expressing high levels of receptor and ligands [30]. Only *Mfng* and *Rfng* caused loss of distal wing tissue consistent with

disruption at the Dorsal-Ventral boundary and confirming their interaction with *notch*. Although *Lfng* had no effect on wing tissue, this was likely because *Drosophila* lacks a Furin enzyme capable of cleaving the pro-protein site, which is not found in either Manic or Radical Fringe. Despite the presence of a cleavage site in both Lunatic Fringe and D-Fringe, their cleavage sites differ slightly in sequence and thus likely in enzyme sensitivity, likely causing ectopically misexpressed *Lfng* to have no impact on wing boundary formation [30].

Later discoveries would show that the Fringe enzymes differ in kinetics [13, 31], specificity [15, 32, 33], expression [30, 34], and levels of Notch activation [32, 33, 35]. For a pathway which is already heavily influenced by expression combinations of the three receptors and five ligands, distinct activities of the individual Fringe enzymes further increase variation of mammalian pathway outcomes. To follow in the remaining sections is greater discussion into the biological roles of Notch *O*-glycans, molecular mechanisms behind the unique influence of each Fringe, and background into the Notch-driven developmental process of angiogenesis that is specifically assessed in the research study explored in this dissertation.

Figure 1.1 The ‘notch’ wing phenotype in *Drosophila*

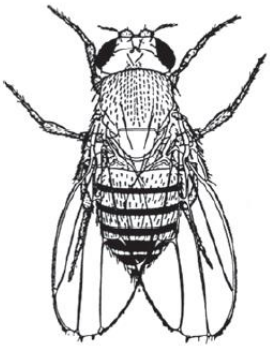

FIG. 44.
Notch-wing, a dominant sex-linked, recessive lethal of Drosophila melanogaster.

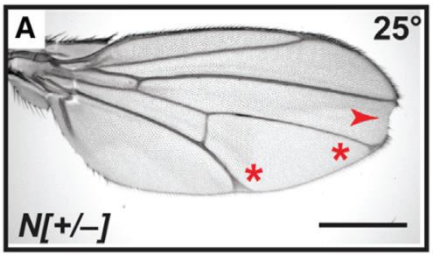

(Left) T.H. Morgan’s first illustration of the notch phenotype observed in *notch*+/- female *Drosophila* published by Yale University’s *The Theory of the Gene* in 1926 [36]. **(Right)** Arrow indicates loss of distal wing tissue in *notch*+/- female, and asterisks emphasize the wing vein thickening phenotype [27].

Figure 1.2 *Notch1*-/- mice display severe defects in pericardial and somite development resulting in lethality by E10.5

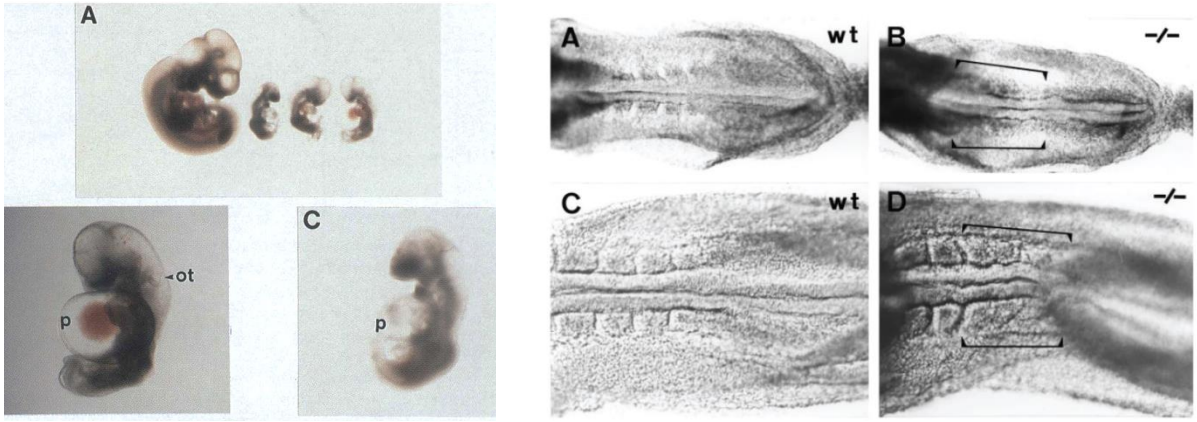

(Left) Top panel compares the size of the Wildtype littermate control embryo to three *Notch1*-/- embryos at E10.5. Bottom panels show magnified images of two *Notch1*-/- embryos at E10.5. Attention is drawn to the Otic Vesicle (ot) in the hindbrain where there is tissue necrosis and to the pericardium (p) which swells outward in the *Notch1*-/- embryos [6]. **(Right)** Comparing wildtype littermate controls to *Notch1*-/- embryos during early somitogenesis E8.5 – 9.5. In Panel A, the wildtype embryo has developed four pairs of somites, while in Panel B, the mutant has developed none. In Panel C, the wildtype littermate has developed 5 pairs of evenly segmented somites, while in Panel D, the mutant has only developed 2 pairs of segmented somites and 3 asymmetrical, condensed somites [7].

Figure 1.3 *Drosophila* Fringe gene expression in the developing wing disc sharply raises Notch activation at the dorsal-ventral boundary in coordination with expression of ligands Delta and Serrate to define the wing margin

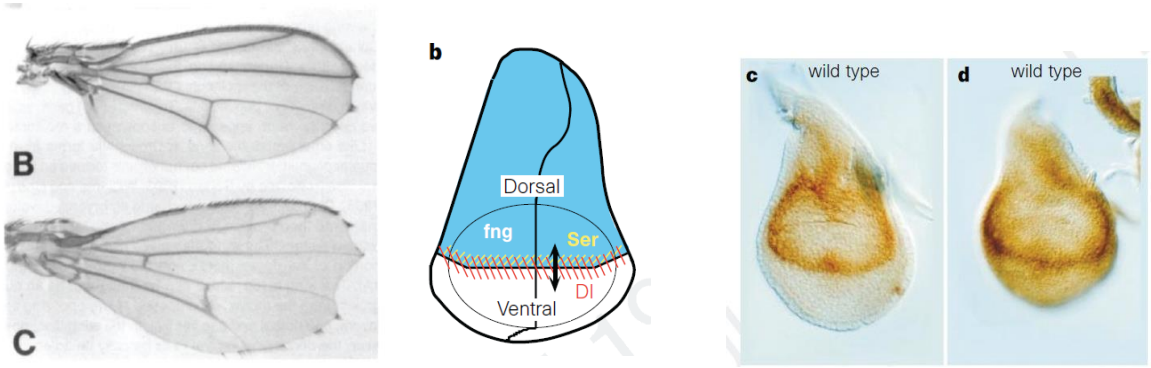

(Left Panel) Two *fringe* hypomorphs identified from a mutagenesis screen targeted to the gene region regulated by the hox transcription factor *ap*. Similar to the Notch phenotype, there is loss of tissue at the distal tip and some wing vein thickening [8]. **(Middle Panel)** Expression of *fringe* (in blue) is restricted to the dorsal compartment of the wing disc and ends abruptly at the dorsal-ventral boundary. Expression of *fringe* enhances *notch* activation by *delta* on the dorsal side of the boundary (yellow hatching) while restricting *notch* activation by *serrate* to the ventral side (red hatching) and inhibiting activation by *serrate* throughout the dorsal compartment [11]. **(Right Panel)** Expression of *serrate* is restricted to the dorsal compartment of the developing wing disc, and *delta* is expressed broadly throughout [11].

Figure 1.4 Fringe is a GlcNAc-transferase that modifies fucose *O*-linked to EGF-like repeats in the extracellular domain of the Notch receptor to enhance activation by Delta and inhibit activation by Serrate

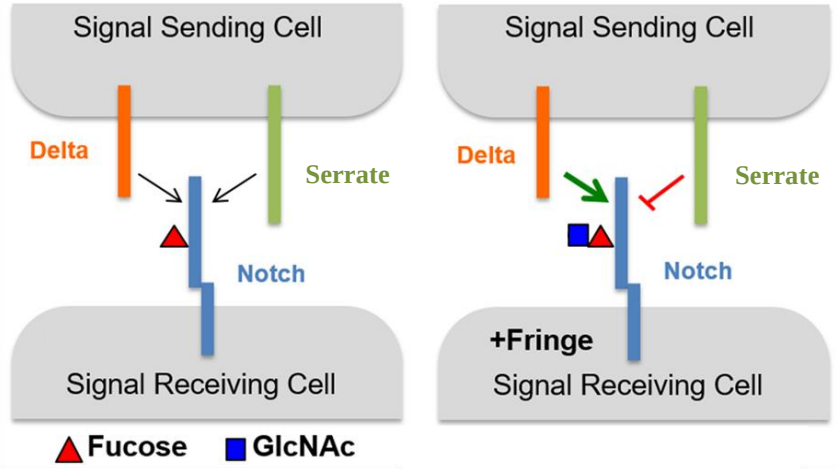

(Left panel) In the absence of Fringe, both ligands Serrate and Delta have equal capacity to activate Notch. **(Right panel)** Fringe adds N-acetylglucosamine (blue square) to *O*-fucose (red triangle) on Notch EGF-like repeats to enhance activation by Delta and inhibit activation by Serrate [13].

Figure 1.5 *Drosophila* Notch is structurally similar to its mammalian orthologs with some exceptions

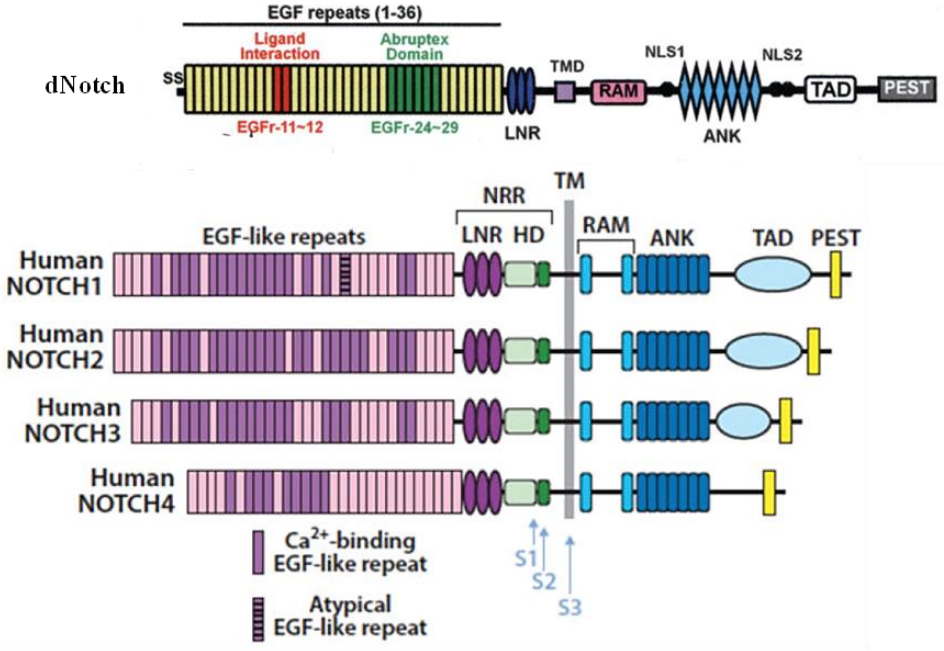

(Top Panel) *Drosophila* Notch is a monomeric, single-pass transmembrane receptor [17]. At the N-terminus, there are 36 tandem EGF-like repeats which bind Ca^{2+} and associate with ligand at EGFs 8-12 [17]. Directly C-terminal to the EGF-like repeats is the Lin-repeat region, a highly folded, mechanosensitive region sensitive to cleavage by ADAM metalloproteases. Cleavage by γ-secretase occurs within the membrane, and the intracellular tail contains the RAM (RBPJ-associated molecule) domain and DNA-binding ankyrin repeat region, stabilized by a Transactivation Domain (TAD) [37]. The PEST domain, a Pro, Glu, Ser, Thr rich region, is necessary for NICD turnover via phosphorylation and ubiquitination [23]. **(Bottom Panel)** The four mammalian Notch receptors differ in the number of EGF-like repeats in their extracellular domain, but otherwise they are structurally similar. Unlike *Drosophila* Notch, mammalian Notch receptors have a Furin cleavage site N-terminal of the transmembrane region, which results in a heterodimeric, mature receptor expressed at the cell surface [16].

Figure 1.6 Notch ligands are structurally conserved

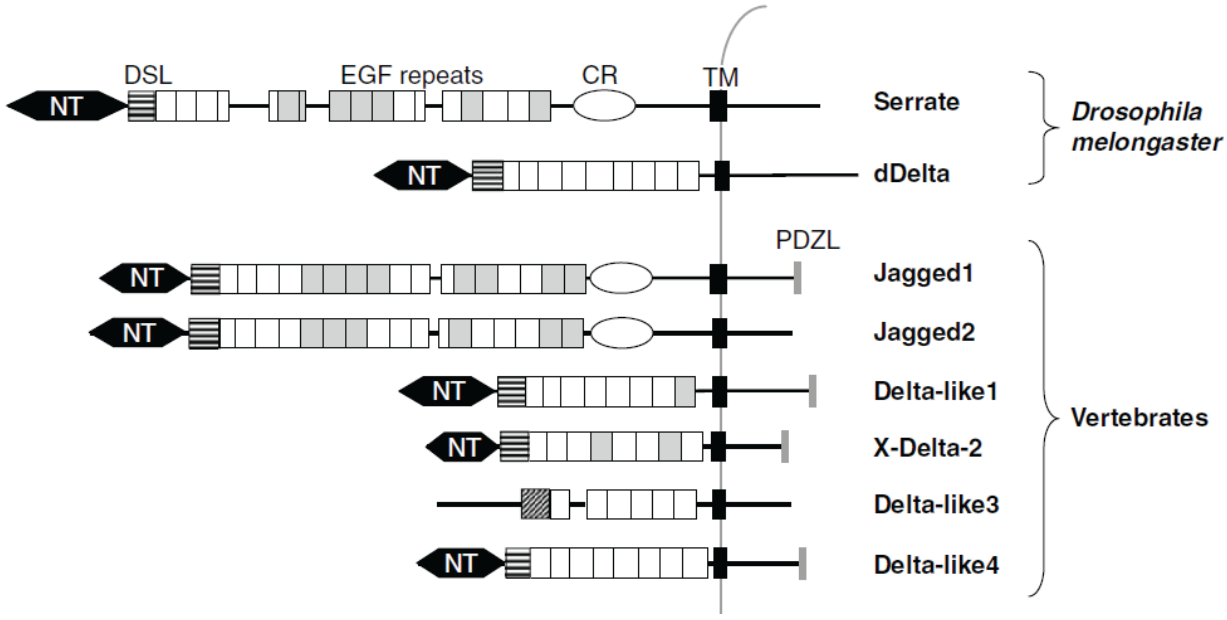

The structures of *Drosophila* ligands Delta and Serrate and mammalian ligands Jagged1, Jagged2, Delta-like Ligand 1, Delta-like Ligand 3, and Delta-like Ligand 4. The DSL (Delta-Serrate-Ligand) domain at the N-terminus of the ligands is the region which makes physical contact with receptor. The remainder of the ligand extracellular domains are made of EGF-like repeats [20].

Figure 1.7 The canonical Notch signaling pathway in mammals

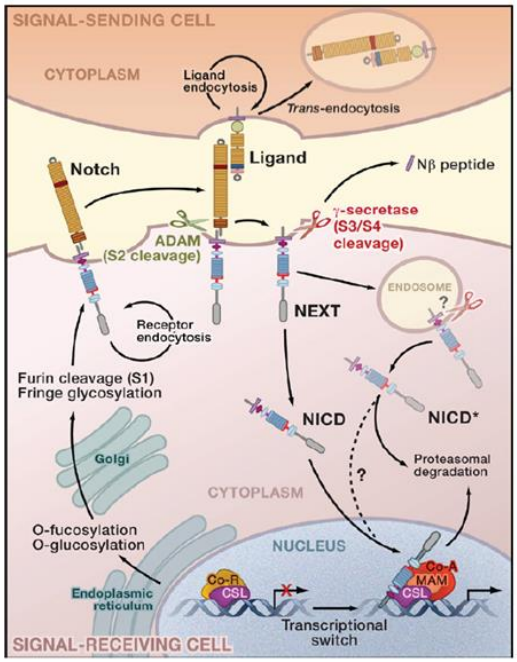

The Notch receptor is translated in the ER where resident *O*-glycosyltranferases modify a Ser/Thr in EGF-like repeats of the extracellular domain. In the Golgi, *O*-glycans are extended by the Fringe family of glycosyltransferases, and receptor is cleaved by Furin to generate a mature, heterodimer that is expressed at the cell membrane where the Notch ligand binding domain at EGFs 8-12 can bind to the DSL/EGF region in ligand extracellular domain. Endocytosis of the ligand-receptor complex generates a pulling force on the Negative-Regulatory Region (NRR) of the receptor, which undergoes a conformational change to expose a proteolytic site for cleavage by the ADAM 10/17 family of metalloproteases. Intramembrane γ-secretases cleave at the transmembrane domain to release the Notch intracellular domain for direct translocation to the nucleus where it can complex with CSL and Mastermind to co-activate downstream target genes. Finally, phosphorylation and ubiquitination of the PEST domain targets Notch for endosomal degradation and turnover [23].

Figure 1.8 Representative cartoon of a single EGF-like repeat that is *O*-fucosylated by POFUT1, elongated to GlcNAc-Fuc disaccharide by Fringe, and galactosylated by β4-Galactosyltransferase 1

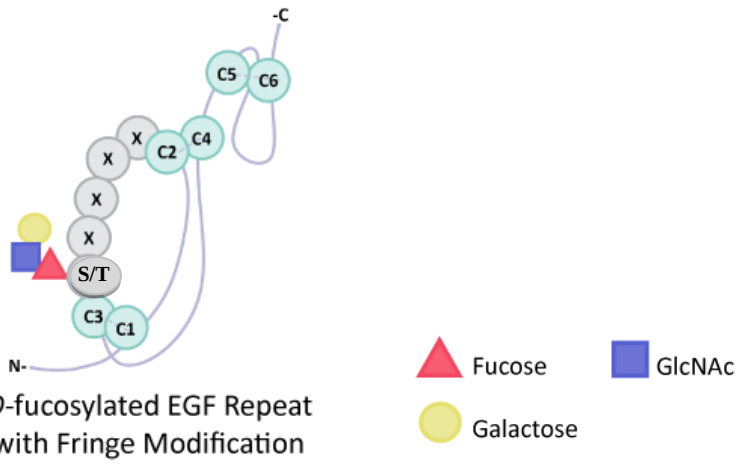

Cartoon representation of a single EGF-like repeat with significant amino acids represented by circles. Cysteines 1 and 6 bookend a single EGF-like repeat at the N-terminus and C-terminus. The disulfide bonding pattern is specific to an EGF-like repeat: $C^1 – C^3$, $C^2 – C^4$, and $C^5 – C^6$. The resulting structure is a highly folded cluster of loops containing approximately 40 amino acids. *O*-Fucosylation, represented by the red triangle, occurs at S/T adjacent to C^3 and preceded by four amino acids of any composition (represented by X) adjacent to C^2. Fringe elongates *O*-fucose with GlcNAc (blue square), which can be galactosylated in mammals. Not depicted here is the possible addition of a terminal Sialic acid [38, 39].

Figure 1.9 Cartoon representation of the extracellular domain from *Drosophila* Notch depicting *O*-fucosylation and Fringe elongation of its EGF-like repeats

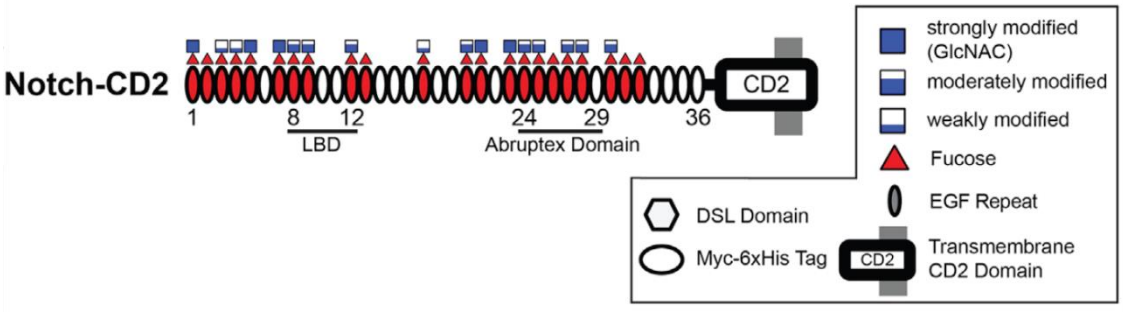

Ovals represent EGF-like repeats, and red ovals signify an EGF-like repeat containing a putative consensus sequence for *O*-fucosylation (22 EGF-like repeats of 36 total). The presence of a red triangle (representing fucose) confirms the presence of *O*-fucosylation (all 22 EGF-like repeats with consensus sequences). The squares represent the presence of Fringe modification consistent with the addition of GlcNAc to fucose with the relative stoichiometry of GlcNAc extension indicated by blue coloring, where fully blue squares represent very high relative abundance of GlcNAc-Fuc disaccharide in that EGF-like repeat (17 of 22 fucose residues carry some degree of modification by GlcNAc) [27].

O-glycans and Receptor Trafficking, Stability, and Binding

Notch receptors and ligands belong to a family of proteins that are *O*-glycosylated at repeating cysteine-rich regions found in EGF-like repeats and Thrombospondin Type Repeats [40]. EGF-like repeat regions were named for their homology to EGF, a secreted peptide first identified in human urine. EGF is 53 amino acids in length when cleaved from its 1200 amino acid, membrane-spanning precursor [41] and activates cell proliferation through the RAS/RAF/MAPK and PI3K-Akt pathways after binding its cognate ligand EGFR, a member of the erbB family of receptor tyrosine kinases [42]. Secreted EGF contains three disulfide bonds between Cys^1 – Cys^3, Cys^2 – Cys^4, and Cys^5 – Cys^6 **(Figure 1.10)**. Homology to EGF was first identified in the extracellular matrix proteins laminin and thrombospondin which appeared to have roughly 10 repeats in their extracellular domains [41]. Because of the many EGF-like repeats in Notch and the EGF homology found in known extracellular matrix proteins, researchers hypothesized that the extracellular domain of Notch was significant in length and influenced cell signaling transduction in some capacity [4].

In 1987 the biotechnology company Genentech gained FDA approval for Activase, a recombinant tissue plasminogen activator (tPA) capable of dissolving blood clots, for the treatment of myocardial infarctions and ischemic stroke [43]. Research into tPA continued at academic institutions and Genentech for optimizing its production, stability, and application. One academic group isolated tPA glycoforms by reduction, alkylation, protease digestion, and sequencer degradation coupled with reverse phase liquid chromatography. They identified three N-glycan sites and another site suspected to carry an unusual *O*-glycan modification due to the detection of a hexosamine byproduct [44].

A Genentech group pursued analysis of the suspicious peptide region by mass spectrometry. They observed a mass reflecting a single fucose linked to the same peptide, either at Thr or a closely situated Ser, and in high abundance relative to the non-glycosylated form. An additional protease digestion shedding Thr and preserving Ser corresponded to an unmodified peptide, suggesting that fucose modified Thr only or it modified any hydroxy-amino acid at that specific position. The Thr-containing peptide was also sensitive to α-fucosidase, which released the mass of one fucose [45].

Additional scrutiny of the *O*-fucose modification within the context of the tPA peptide sequence and other sequence homologies drew attention to the position of the modified Thr within a single EGF-like repeat. Until this time, *O*-linked fucose modifications had not yet been observed in the literature, likely owing to the acid-labile nature of *O*-linked glycans [45], with exception of one other group that had very recently published a report on a new post-translational modification identified in the EGF domain of the urinary plasminogen pro-urokinase. Other than designating the modification as a covalently attached fucose within the EGF domain, the study did not comment on the nature of the linkage or to which amino acid it was linked [46].

The group at Genentech surmised that the location of the modification site within a single EGF domain was likely significant because closer sequence analysis uncovered strong homology between the region of the fucose modification in tPA and the putative modification site in pro-urokinase, both carrying Thr directly adjacent to Cys^3 in their EGF domains **(Figure 1.10)**. The researchers predicted the same *O*-fucose attachment to Thr in this position within the EGF region of other coagulation and matrix proteins such as Human Factor XII, Transforming Growth Factor α, and Protein C. Proteins with a Ser in this position such as Human Factor VII and IX were also

predicted to carry the modification, while Factor X and the LDL receptor lacking a Ser or Thr in this position were not candidates [45]. In the same year, a study on the biological function of pro-urokinase showed that TFA could remove *O*-linked fucose without altering the protein structure. The non-fucosylated form could bind cell surface receptor with similar affinity as its fucosylated form; however, the non-fucosylated pro-urokinase could not activate cell proliferation, opening the possibility that a single *O*-fucose could participate in recruitment of accessory proteins or directly alter the structure-function of its receptor to activate cellular events [47].

The same group at Genentech published a follow-up study two years later, this time investigating a Ser residue within Human Factor IX they had previously predicted to carry the *O*-fucose modification. Instead of finding *O*-fucose, however, the mass spectral data repeatedly revealed a mass corresponding to their peptide carrying a tetrasaccharide composed of NeuAc, Hex, HexNAc, and Fuc. An NMR study definitively confirmed the sugar identities and their linkages as NeuAc α2, 6 – Gal β1, 4 – GlcNAc β1, 3 – Fuc α1 – Ser **(Figure 1.10)**. Digestion with α-fucosidase was performed on the Ser glycopeptide from Human Factor IX and the Thr glycopeptide from tPA followed by mass spectrometry. As expected, the tPa glycopeptide carrying *O*-fucose monosaccharide was sensitive to α-fucosidase, which cleaves terminal fucose only, while the tetrasaccharide-carrying glycopeptide from Human Factor IX was not. Finally, the authors concluded that *O*-fucosylation was restricted to the sequence Cys^2 – X – X – Gly – Gly – <u>Ser/Thr</u> – Cys^3 where X is any amino acid **(Figure 1.10)** [48]. It is not clear from this study if the authors considered the differing origins of their protein samples, tPA from a cancer cell line and Factor IX from human plasma, or if there was a structural determinant for tetrasaccharide vs. monosaccharide. Connection between the novel EGF, *O*-linked

tetrasaccharide, and mammalian Fringe would not develop until further genetic and structural studies in *Drosophila* and mammalian Notch converged roughly five years later.

In a report published the same year (1993), an academic group used radiolabeled GDP-fucose to detect *O*-fucosylated glycoproteins in a CHO cell line lacking GlcNAc Transferase I (named Lec1 cells), the enzyme which commits N-glycans to the core-fucosylated, complex type. The significant radiolabeling detected in proteins from a cell lysate lacking core-fucosylated N-glycans suggested that many *O*-fucosylated glycoproteins were yet to be identified [49].

Research into glycosylation of Human Factor IX was ongoing prior to the tPA finding in 1989. As part of the growing body of research into the blood coagulation pathway, researchers were investigating the location of serine protease sites within the pro-forms of human clotting factors when their GC-MS peptide screen was unable to detect a region of Factor IX between Cys^1 and Cys^2 of its EGF domain. The MS spectra instead reproduced the mass of a peptide carrying glucose and xylose moieties. More specifically, they calculated the ratio of abundance as two molecules of xylose per one molecule of glucose covalently linked to a Ser residue [50].

In a comprehensive follow-up report on Human Factor IX, Factor VII, and Protein Z, the authors opted to manually release the suspicious Xyl-Xyl-Glc modifications by acid hydrolysis paired with GC-MS. Glycan release from a highly conserved peptide sequence between Cys 1 and 2 of the EGF domain from all proteins generated the reducing-end derivative form of glucose each time, without exception, thus verifying glucose as the initiating *O*-linked glycan at the Ser residue between Cys^1 and Cys^2 of EGFs **(Figure 1.10)** [51]. The trisaccharide and disaccharide forms were far more abundant than monosaccharide with some protein-specific heterogeneity. Highly conserved sequence homology generated a stringent consensus sequence

for *O*-glucosylation of Ser at $C^1X\underline{S}XPC^2$ within EGF domains **(Figure 1.10)**. Finally, the authors noted that the consensus sequence for *O*-glucosylation was frequent in *Drosophila* Notch EGF-like repeats [51]. However, the biological function of Notch EGF *O*-glucosylation would remain unknown until later genetic studies into the Notch-related *O*-glucosyltransferase named Rumi [52].

The enzyme responsible for EGF *O*-fucosylation was identified in 1996 in a study which first attempted to use short, synthesized peptide sequences previously reported as *O*-fucosylated in native protein. The peptides were used as substrates in an assay detecting transfer of radiolabeled GDP-fucose when mixed with CHO cell extract presumably containing active *O*-fucosyltransferase. However, none of the peptide samples tested positive for transfer of radiolabeled fucose. The researchers hypothesized that linear polypeptide alone was not sufficient for acceptor-donor transfer and turned to recombinant expression of the full EGF domain from human Factor VII purified out of an *E. coli* expression system. Their suspicions were confirmed when the recombinantly expressed EGF yielded high levels of fucose transfer in their radioactivity assay [53].

To enrich for *O*-fucosyltransferase, the CHO cell extract was separated by anion-exchange, and fractions testing positive for fucose transfer activity were pooled, buffer exchanged, and stored. After successful transfer of heavy fucose to recombinant EGF, the modified EGF was digested with proteases to regenerate the linear polypeptide carrying the putative consensus sequence for *O*-fucosylation. Mass spectral analysis validated a mass corresponding to fucose attached to the target peptide. In addition, raising the electrospray voltage showed loss of fucose from the peptide, as glycosidic linkages are very labile and frequently dissociate during ionization [53]. This was the first publication to suggest that *O*-

fucosylation of EGF-like repeats was permitted exclusively when in their native structure, theorizing that distinctive folds generated by the conserved disulfide bonding patterns **(Figure 1.10)** enable enzyme recognition of EGF [53].

In a follow-up report by the same group, donor-substrate transfer was further studied with pure enzyme. They observed that full-length, recombinantly expressed EGF repeats could not be *O*-fucosylated after reduction/alkylation locked them into a linear form. Another experiment identified several peaks from reverse-phase chromatography of native, recombinant EGF after incubation with pure *O*-fucosyltransferase. There were small but significant differences in retention times, suggesting that the individual peaks reflected EGF variants rather than aggregates. All peaks were confirmed by mass spectrometry to have the same mass, but only one peak showed a mass increase equal to the addition of fucose. The researchers proposed that the other peaks contained separate species of EGF which were improperly folded due to disulfide bonding patterns differing from $C^1 – C^3$, $C^2 – C^4$, and $C^5 – C^6$ [54]. These findings proposed that a requirement for *O*-fucosylation went beyond native EGFs with any secondary structure. They concluded that *O*-fucosylation of Ser/Thr between Cys^2 and Cys^3 **(Figure 1.10)** was exclusive to properly folded EGFs [54].

Continuing their interest in the *O*-fucosyltransferase, active enzyme pooled from CHO cells was subjected to peptide sequence analysis, and gene homology searches were performed with the putative cDNA. Homologous genes were identified in *Drosophila*, humans, mice, and others. The genes were named human *POFUT1*, mouse *Pofut1* (Protein *O*-fucosyltransferase 1), and *Drosophila Ofut1* **(Figure 1.10)**. Enzyme localization was predicted to be the ER or Golgi, and it harbored a conserved DXD motif commonly found in the catalytic region of

glycosyltransferases. Otherwise, the genetic analysis showed little homology with known glycosyltransferases [55].

Cloning of the *POFUT1* gene overlapped with studies into *O*-fucosylation of Notch. Building off an earlier study using a line of CHO cells lacking complex N-glycans (Lec1 cells), and thus lacking core-fucosylation of N-glycans, researchers used tritium-labeled L-fucose to trace proteins carrying fucose modifications exclusively *O*-linked to Ser or Thr residues. After confirming endogenous expression of mammalian Notch1 in Lec1 cells by antibody recognition of the intracellular/transmembrane region, Notch1 was immunoprecipitated out of a Lec1 lysate metabolically labeled with tritiated L-fucose. The precipitated protein was separated by SDS-PAGE, and radiolabeled fucose was visualized by fluorography. A single, bright band appeared at 200kDa, a molecular weight corresponding to the predicted mass of the extracellular domain fragment. Although the antibody used for immunoprecipitation bound the intracellular region of Notch, it was able to capture extracellular domain heterodimerized to the intracellular/transmembrane fragment. Reducing conditions in during gel electrophoresis then broke the 300kDa full fragment into 100kDa and 200kDa fragments. Significantly, the 100kDa intracellular/transmembrane fragment was not visualized on the radiographed gel because it did not contain EGF-like repeats for tritiated fucose to modify [56]. This confirmed the Notch1 extracellular domain, which contains 36 tandem EGF-like repeats, to be heavily *O*-fucosylated **(Figure 1.13)**.

To take the analysis a step further, β-elimination was performed to release *O*-glycans from Notch. In this reaction, the sugar at the reducing end would be converted to a sugar alcohol, freeing glycans *O*-linked to Ser/Thr. The released products were separated by size exclusion chromatography paired with scintillation counting. Two tritium-containing peaks appeared, a

larger peak sharing retention times with the monosaccharide standard, and a smaller peak eluting at an earlier time than the dextran pentasaccharide standard, likely due to an oligosaccharide composition other than standard glucose/dextran. Because the peak corresponding to tritiated monosaccharide was much larger than the tritiated oligosaccharide fraction, *O*-fucose monosaccharide was likely the predominant *O*-fucose glycoform on Notch [56].

Fractions collected from the tritium-labeled monosaccharide peak co-eluted with the fucitol standard when separated by anion exchange, validating the initiating sugar *O*-linked to Ser/Thr as fucose. The size exclusion fractions containing oligosaccharide were subjected to acid hydrolysis to indiscriminately break glycosidic linkages between individual glycans. When analyzed by anion exchange, the fraction containing tritiated monosaccharide also co-eluted with the fucitol standard, confirming that the oligosaccharide was also initiated by *O*-fucosylation of Ser/Thr [56].

To verify the composition of the oligosaccharide predicted to be the tetrasaccharide NeuAc α2, 6 – Gal β1, 4 – GlcNAc β1, 3 – Fuc α1 – Ser first identified in Human Factor IX [48], the fractions containing oligosaccharide released by β-elimination were digested by a series of glycosidases and separated by size exclusion. Consecutive shifts in the tritium-containing peak were observed after sequential digestion with Sialidase, Galactosidase, and Hexosaminidase. The hexosamine was confirmed to be GlcNAc by incubating disaccharide with a galactosyltransferase specific for addition to GlcNAc, as opposed to another hexosamine such as GalNAc [56]. This was definitive evidence that *O*-fucose tetrasaccharide modifies the extracellular domain of Notch and that its composition was NeuAc -α2,3 Gal -β1,4 GlcNAc -β1,3 -Fuc **(Figure 1.10)**. The authors hypothesized that sugar hydroxyl groups might engage ligand through hydrogen-bonding to influence the biological activity of Notch, similar to *O*-

fucosylation of urokinase operating as a molecular switch when activating its receptor [47]. This prediction would later gain confirmation in biophysical studies [57, 58].

After confirmation that Notch was modified with *O*-fucose, it appeared even more likely that its extracellular domain would also carry *O*-glucose modifications characterized earlier in Human Factor IX, Factor VII, and Protein Z EGFs between Cys^1 and Cys^2 at the conserved sequence $C^1X\underline{S}XPC^2$ **(Figure 1.10)** [51]. To demonstrate this would be more challenging, however, because radiolabeled glucose could participate in multiple biosynthetic events that might label any number of glucose-derived species modifying proteins. Because the biosynthetic endpoint of UDP-galactose is either direct N-glycan incorporation or epimerization to UDP-glucose, tracing tritiated galactose epimerized to glucose was the clever solution. Lec8 cells defective in transport of UDP-Galactose (causing an 80 – 90% loss of galactosylation overall) were metabolically labeled with tritiated galactose. This increased the likelihood that the radiolabel was transported into the ER from the cytosol as UDP-glucose only [56].

Immunoprecipitation of Notch resulted in the same 200kDa band when imaged by fluorography, confirming that only the extracellular domain was radiolabeled with tritiated glucose. Glycans were released by β-elimination and separated by size exclusion. Two peaks eluted, the larger peak having a similar retention time to the dextran standard containing three glycans, while the retention time for the smaller peak overlapped with the monosaccharide standard, indicating that trisaccharide was the more abundant *O*-glucose glycoform. Analysis of the monosaccharide by anion exchange chromatography confirmed the presence of glucitol, verifying glucose as the initiating sugar *O*-linked to Ser. The trisaccharide form was acid hydrolyzed and anion exchange to again confirm presence of glucitol and that trisaccharide is an *O*-glucose glycoform. However, the authors could not define the composition of trisaccharide at

the time of publication, although previous publications suggested that it might be Xyl – Xyl – Glc **(Figure 1.10)** [56].

The experimental workflow developed by these authors would prove useful in demonstrating the biochemical activities of Fringe, which shared homology with some bacterial glycosyltransferases, particularly the catalytic DXD motif unique to glycosyltransferase activity [12]. They were motivated to pursue biochemical studies because *fringe* was recently shown to modulate *notch/delta/serrate* feedback loops during *Drosophila* development [11], and there were compelling lines of evidence hinting to its biochemical activity. A few years prior, the EGF *O*-fucosyltransferase POFUT1 had been purified from CHO cells, characterized, and used to modify Human Factor VII [53, 54]. This implied that the *O*-fucose monosaccharide on Notch was likely added by POFUT1 and opened the possibility that Fringe elongated *O*-fucose. Similarly, Fringe might have transferred *O*-glucose, as that enzyme was yet unknown, or it could have elongated *O*-glucose. This was less likely because RNA analysis of the CHO cell line used to characterize Notch *O*-glycans showed low expression of the mammalian Fringes [13]. The *O*-glucose trisaccharide was relatively abundant, whereas the *O*-fucose monosaccharide was more abundant than its corresponding tetrasaccharide. Therefore, Fringe likely modified *O*-fucose [56].

Because the mammalian Fringes named Lunatic Fringe, Manic Fringe, and Radical Fringe had recently been cloned and ectopically expressed in *Drosophila* [30], the authors were able to use the expression construct for Manic Fringe developed by this group to transfect a CHO cell line incubated with radiolabeled sugar, immunoprecipitate Notch, and analyze the released glycans by size exclusion chromatography. When *Mfng* was transfected into the Lec8 cells metabolically labeled with tritiated galactose, the authors observed no change in the *O*-glucose

modifications on Notch. When they transfected *Mfng* into the Lec1 cells metabolically labeled with tritiated fucose, they observed an increase in the proportion of tritiated sugar elongated beyond monosaccharide, including tetrasaccharide, trisaccharide, and disaccharide. Because all species disaccharide and beyond appeared to increase in abundance, the authors theorized that Fringe was elongating *O*-fucose to generate the disaccharide glycoform. When examining the β-eliminated disaccharide by anion exchange column, the disaccharide eluted at the same retention time as a synthetic GlcNAc β1,3 – Fucitol, confirming that Fringe was transferring GlcNAc to *O*-fucose **(Figure 1.10)** [13].

Significant transfer activity was measured when Fringe (D-FNG, LFNG, and MFNG were all tested) was affinity purified and incubated with tritiated UDP-GlcNAc in the presence of the EGF Human Factor VII carrying *O*-fucose monosaccharide [59]. Radioactive transfer was not observed when other tritium labeled UDP donors (UDP-Gal, GalNAc, and Glc) were incubated with Fringe and EGF. Thus, the authors were able to show that Fringe was a GlcNAc-transferase specific for *O*-fucose **(Figure 1.10)** [13].

Once the landscape of Notch *O*-glycans was somewhat mapped out, the next line of inquiry was their functional significance. In a *Drosophila Ofut1* (*Pofut1/POFUT1*) knockdown study, significant wing notching was observed [60], such as that seen in the first *notch*-null and *fringe* mutants in *Drosophila* [3, 8, 61]. Knockout of *Pofut1* in a mouse caused embryonic lethality at a similar developmental timepoint as the *Notch1* knockout, between E9.5 – E10.5 with significant defects. The study documented low vascularization of the yolk sac and brain, a 'kinked' neural tube, asymmetrical somite formation, pericardial swelling, and significant body size reduction [62]. These phenotypes heavily overlapped with those published on *notch1*-null mice **(Figure 1.2)** [6, 7].

In 2005, another *Drosophila Ofut1* knockdown study was published. This time, the authors stained for Notch protein in the wing imaginal disc, showing localization at the cell membrane in the control and accumulation inside the cell after *Ofut1* knockdown. When co-stained with ER and Golgi markers, Notch staining overlapped with ER markers only. Notch protein that was not *O*-fucosylated appeared to become trapped in the ER [63].

The experiment was repeated in *Drosophila* S2 cells which lack functional *notch* but express *Ofut1*. Cells transfected with *notch* showed cell surface expression of Notch protein and substantial accumulation in the ER consistent with general protein overexpression. When *Ofut1* was knocked down, staining of Notch could not be detected at the cell surface, and only ER staining remained, supporting the idea that *O*-fucosylated Notch reaches the cell surface while Notch lacking *O*-fucosylation is retained in the ER [63].

A cellular fractionation study had already shown that full-length, mammalian NOTCH1 is the ER-retained form that has not yet been processed in the Golgi [64]. When staining endogenous NOTCH1 in a mammalian cell lysate using antibody raised to the intracellular domain, two fragments appeared. An abundant fragment migrated at 112kDa, corresponding to the intracellular/transmembrane portion. Extracellular domain could not be detected due to lack of antibody recognition site, however, a fragment at 300kDa was observed in low abundance. This fragment corresponded to full-length protein which had not been cleaved into its mature heterodimer, as the disulfide bonds holding the heterodimer intact would have been broken by the reducing conditions of gel electrophoresis, and the antibody could only detect intracellular domain (~100kDa). After treatment with Befeldin A which blocks traffic across the Golgi network, only this full-length, immature fragment could be detected in the lysate. Passage over a

sucrose gradient showed full-length NOTCH1 in the nuclear pellet only, suggesting that immature, mammalian NOTCH1 is found in the ER before Furin cleavage in the Golgi [64].

After knockdown of *Ofut1* in S2 cells, only the full-length fragment of *Drosophila* Notch protein was detected in the lysate [63]. Because *Drosophila* Notch is a monomer that does not undergo Furin cleavage in the Golgi, this result suggested that Notch retained its full-length form because it was not reaching the cell surface for cleavage by ADAM or γ-secretase. The cleaved fragment reappeared after co-transfection with mouse *Pofut1*. Because staining of Notch shifted from the ER to the cell-surface before/after introducing exogenous *Pofut1*, these experiments showed that Notch requires expression of *Ofut1* to leave the ER. This was a surprising finding, however, because transport of GDP-fucose had only been observed in the Golgi (remains true to this day). Staining for OFUT1 also showed co-localization with the ER marker and not with the Golgi marker, which meant that OFUT1, lacking a transmembrane region, is a soluble resident of the ER that is retained by its KDEL sequence, despite the lack of apparent GDP-fucose transporter in the ER [63].

Because no GDP-fucose transporter had been identified in the ER, the authors hypothesized that OFUT1 had chaperone activity independent of its catalytic activity. They generated an *Ofut1* construct with a point mutation in its catalytic domain and showed that the enzyme was catalytically inactive. Then they ectopically expressed the catalytically inactive *Ofut1* in the imaginal disc into cells they engineered to endogenously express only the null allele for *Ofut1*. Ectopic expression of the inactive focosyltransferase restored some Notch localization to the cell membrane. They again repeated the experiment in S2 cells after knockdown of endogenous *Ofut1*. The 100 kDa fragment corresponding to activated intracellular/transmembrane fragment was partially rescued by transfection with the inactive

fucosyltransferase, suggesting that OFUT1 has chaperone activity independent of *O*-fucosylation. One mechanism for this could be that OFUT1 binds to EGF repeats that are correctly folded as a form of quality control prior to fucosylation [63]. Later studies would show that POFUT1 chaperone activity was not observed in mouse or human tissues [65].

During a chemical mutagenesis screen in 2007, the gene responsible for *O*-glucosylation of Notch in flies was isolated and named *rumi* [52]. The mutant flies showed a loss of bristle development, a Notch-dependent process resulting from a defect in prosensory neuron specification. The phenotype was temperature-sensitive and could only be observed when raised at 25°C or higher, suggesting that the mutation caused instability of the gene product. When raised at 18°C, bristle appearance was indistinguishable from wildtype. When raised at 28°C, a neurogenic phenotype arose, and embryonic development was not completed. In mutants raised at 25°C, bristle loss could be rescued by adding one copy of Notch, and in mutants raised at 18°C bristle loss could be induced by removing one copy of Notch. These genetic experiments signaled that, before identifying *rumi* as an *O*-glucosyltransferase, the mutant gene interacted with Notch in some way [52].

Wing disc extracts were prepared, and lysates were analyzed for full-length and active, cleaved fragment detected by antibody raised to the intracellular domain (*Drosophila* Notch is not processed by Furin and remains monomeric until cleavage by ADAM/γ-secretase. Thus, the full-length fragment runs at a single band on a reducing gel.). Cleaved, activated Notch was detected in the lysate from *rumi* mutants raised at 18°C but not in *rumi* mutants shifted to 28°C at the start of wing disc development; the *rumi* mutation was certainly impacting activation of Notch by an unknown mechanism. To exclude defects in γ-secretase cleavage, an active, membrane bound form of Notch, identical to Notch cleaved by ADAM metalloproteases, was

overexpressed in *rumi* mutants at 28°C. Because transcription of Notch target genes was restored, the defect was likely occurring prior to cleavage by γ-secretase. A cell-based ligand binding assay performed in S2 cells overexpressing Notch during RNA-mediated knockdown of *rumi* showed no changes in binding to soluble Delta at room temperature or at 28°C, excluding ligand binding as the primary effect. Cellular staining checking for defects in trafficking showed accumulation of Notch inside the cell but also at the cell surface, ruling out trafficking defects as the cause for Notch accumulation as well [52].

The mutant was genetically mapped to a family of CAP10-containing glycosyltransferases in bacteria and contained an ER-retention signal. Because the enzyme for *O*-glucosylation of Notch was unknown at this time, the authors tested glucosylation of Notch by purifying a fragment of extracellular domain from S2 cells under *rumi* knockdown conditions and analyzed glycopeptides by mass spectral analysis. The mass spectral data showed intact *O*-fucosylation and a significantly greater relative abundance of peptides lacking *O*-glucosylation compared to control conditions. Thus, the authors showed that the *rumi* gene product encodes the enzyme for *O*-glucosylation of Notch EGF repeats **(Figure 1.10)** [52].

Finally, the authors identified a point mutation in their most severe *rumi* mutant fly that likely rendered the enzyme catalytically inactive due to its location in the DXD motif. When this *rumi* mutant gene was overexpressed in S2 cells, the Rumi protein expressed well and localized to the ER. When the Rumi protein was purified, it could not modify EGF from Human Factor VII, confirming it inactive. Because this catalytically inactive *rumi* mutant gene causes the neurogenic phenotype in the *Drosophila* system, their experiment suggested that, unlike OFUT1, Rumi does not have independent chaperone activity which could rescue Notch function under catalytically inactive conditions. The authors hypothesized that, while Notch lacking *O*-glucose

was able to localize to the cell membrane, it was possibly forming aggregates or associations with other molecules which blocked interaction with ligand under endogenous conditions [52]. A later study would echo this theory, suggesting that *O*-glucose modifications may shield hydrophobic residues from unintended interactions [65].

A comprehensive study demonstrated that *O*-fucosylation and *O*-glucosylation of Notch facilitates efficient cell-surface expression in an additive manner [65]. The authors generated three HEK293 cell lines, including CRISPR/Cas9 knockouts of *POFUT1*, *POGLUT1*, and both *POFUT1/POGLUT1*. Cell surface staining and FACS analysis showed that both single knockouts caused a 50% reduction in the cell surface expression of endogenous NOTCH1. The *POFUT1/POGLUT1* double knockout cells caused a ~90% reduction in cell surface staining, meaning that *O*-fucosylation and *O*-glucosylation serve non-redundant functions that individually contribute to secretion of NOTCH1 out of the ER [65].

Structural study of a single EGF repeat from Human Factor IX containing the consensus sequences for both *O*-fucosylation and *O*-glucosylation was expressed in *E. coli* and modified by pure POFUT1 or POGLUT1 (Rumi in flies) *in vitro*. The resulting EGFs were subjected to reduction by DTT and GnHCl followed by TFA acid-trapping to quench at varying timepoints. Analysis by reverse-phase HPLC could separate species of EGF in different states of denaturation, the more hydrophobic, unfolded EGFs eluting later than the folded EGFs. Consequently, longer exposure to reducing conditions would cause EGFs to elute later [65].

A time series experiment was performed on *O*-fucosylated or *O*-glucosylated EGF repeats. Addition of one fucose or one glucose extended the time needed to unfold 50% of total EGF by roughly 3-4x each, demonstrating that each *O*-glycan imparted significant stability alone. When both *O*-fucosylation and *O*-glucosylation of EGF were performed *in vitro*, EGFs

needed 5-10x more time in reducing conditions to produce the unfolded species, greater than either *O*-fucose or *O*-glucose alone and reflective of a non-redundant, additive influence. The authors also noted that buffer lacking Ca^{2+} reduced the effect by half, confirming that interactions with Ca^{2+} are necessary for individual EGF stability as well [65].

Interestingly, the Xyl-Glc disaccharide destabilized the EGF repeat compared to *O*-glucose monosaccharide, and addition of a second Xyl rescued the stability while imparting further stability beyond *O*-glucose monosaccharide alone [65]. The identified *Drosophila* gene *shams* (*GXYLT1/2* in humans) **(Figure 1.10)** responsible for addition of Xyl to *O*-Glc also has a negative effect on cell-surface expression of Notch under normal conditions in S2 cells, which might be explained by the instability it causes in EGFs [66]. While the loss of Xyloside Xylosyltransferase I **(Figure 1.10)** responsible for adding the second Xyl residue in the Xyl-Xyl-Glc trisaccharide does not cause a *Drosophila* phenotype on its own, the human gene XXYLT1 is frequently overexpressed in cancers [67].

The *O*-GlcNAc which modifies EGFs at Cys^5-X-X-Gly-X-Ser/Thr-Gly-X-X-Cys^6 is added by an ER-localized *O*-GlcNAc transferase specific to EGFs called EOGT **(Figure 1.10)** [68]. *O*-GlcNAc can be elongated by Galactose transferases and capped with a terminal Sialic Acid. Knockout of *Eogt* in flies causes embryonic lethality without the typical Notch phenotypes, likely due to the many *O*-GlcNAc sites within the highly modified protein named Dumpy that may dominate the phenotype in the fly wing. In the mammalian cell system, loss of *EOGT* causes reduced DLL4-NOTCH1 binding but no change to JAG1-NOTCH1 binding. *Eogt* knockout in mice results in viable animals and a minor phenotype observed in retinal angiogenesis due to loss of DLL4-NOTCH1 signaling. In humans, defects in *EOGT* cause the congenital disorder Adams-Oliver Syndrome [68].

The final *O*-glycan to be discovered on Notch is an unusual *O*-Glucose identified at EGF11 in the mammalian NOTCH1-DLL4 co-crystal structure published in 2015 and again in the NOTCH1-JAG1 co-crystal structure published in 2017 [57, 58]. Its origin was traced to two enzymes homologous to POGLUT1 called POGLUT2/POGLUT3 which modify at the consensus sequence Cys^{3}-X-Asn-Thr-X-Gly-Ser-Phe-X-Cys^{4} **(Figure 1.10)**. Loss of the *O*-glucose site at EGF11 exacerbates defects in binding, activation, and cell-surface expression caused by loss of *O*-fucose at EGF8 but does not cause significant changes in these events alone [69]. Further inquiry into these enzymes revealed that they heavily modify the Fibrillin proteins at high stoichiometry, so their role is more important in the context of extracellular matrix biology rather than Notch [70]. Preliminary data from the lab agrees with this hypothesis, as mice that are null for either *Poglut2* or *Poglut3* have fibrillin-related phenotypes, and mice that are null for both *Poglut2* and *Poglut3* show perinatal lethality with deficits in body size and bone development consistent with loss of effective fibrillin function (unpublished).

This novel *O*-glucose wasn't the only finding from the NOTCH1/DLL4 or NOTCH1/JAG1 co-crystal structures [57, 58]. Both structures depicted NOTCH1 EGF12 *O*-fucose (T466) directly engaging ligand through hydrogen bonding with amino acid sidechains from either Tyr^{65} in the MNNL domain of DLL4 or Tyr^{82} in the C2 region of JAG1 [57, 58]. The direct involvement of the EGF8 *O*-fucose (T311) was confirmed in the NOTCH1/JAG1 co-crystal showing hydrogen bonding with the sidechain of Asn^{298} as well [58].

Not only did these studies confirm the importance of Notch *O*-fucose in binding ligand, but they also revealed some unique features. When the EGF12 GlcNAc-Fuc disaccharide was modeled into the NOTCH1/DLL4 co-crystal, new H-bonds and Van der Waals interactions were facilitated, supporting the experimentally confirmed idea that Fringe raises affinity of Notch for

Delta-like ligands [57]. Additionally, the NOTCH1/JAG1 co-crystal revealed a significant degree of pivoting in the N-terminal region of JAG1 from the unbound state to the bound state. It is unclear if the 'flexing' of JAG1 occurs by the force of unbound endocytic recycling or if JAG1 pivots during the process of binding receptor. However, significant hinge activity is found under the circumstances of a 'catch bond', a protein-protein interaction phenomenon where bond lifetime increases as greater pulling force is applied [58]. The catch bond was first characterized in P-selectin bound to ligand during leukocyte rolling, possibly explaining the observation that platelets have no problem adhering to clotting factors expressed on highly stressed arterial walls [71]. Analysis of the bond lifetime under increasing force showed that both JAG1 and DLL4 form catch bonds with NOTCH1 [58].

This finding adds to the understanding of Notch activation in the context of a cellular membrane environment. It was experimentally demonstrated that unfolding the Negative-Regulatory Region of Notch requires 6pN of force before the region can be cleaved by ADAM metalloproteases [72]. Although tested on short fragments of Notch and ligand, the results from force-clamp assays for Notch bound to either JAG1 or DLL4 are similar in their maximum bond lifetime observed at 10pN of force [58]. The biological implications of this might be to ensure enough force is passed from the N-terminal ligand binding domain of receptor into its more C-terminal NRR, while at the same time ensuring that the bond endures as long as possible for increasing the chances of encountering ADAM metalloproteases [58].

In this section we have discussed the sequence of events leading to the discovery of unique *O*-glycans that modify EGF-like repeats in the Notch receptor extracellular domain. These glycans and their glycosyltransferases are depicted in a fictional cartoon representation of an EGF-like repeat carrying consensus sites for every mammalian Notch *O*-glycan **(Figure 1.10)**

as well as a map of the mouse NOTCH1 extracellular domain identifying EGF-like repeats containing consensus sequences for *O*-glycosylation **(Figure 1.13)** [68]. The biological significance of *O*-glycans can be categorized by their effects on the stability of individual EGF-like repeats, ER quality control and secretion, and involvement in binding ligand. In the next section, the Fringe family of glycosyltransferases will be discussed in greater detail.

Figure 1.10 Cartoon representation of a fictional EGF repeat modified by all known Notch *O*-glycans

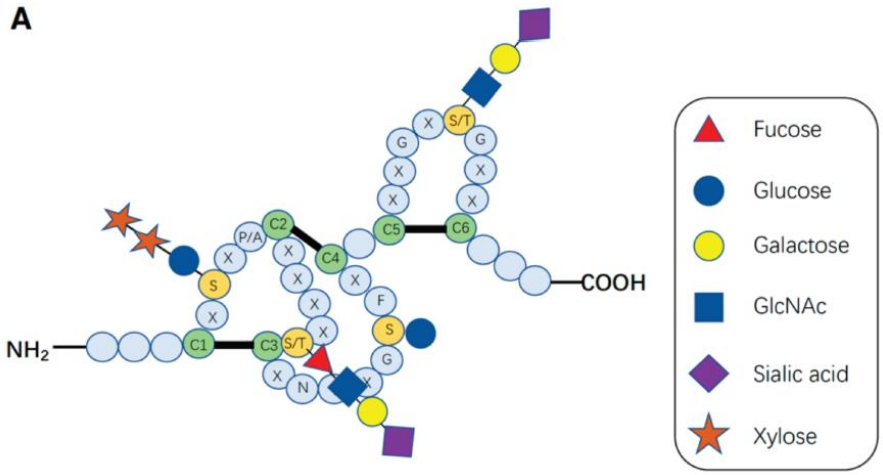

O-Glucosylation by Rumi/POGLUT1 at Cys[1]-Pro/Ala-X-Ser-X-Cys[2] followed by addition of xylose catalyzed by Shams/GXYLT1/2 and capped with a terminal xylose by XXYLT1. *O*-Fucosylation by OFUT1/POFUT1 at Cys[2]-X-X-X-X-Ser/Thr-Cys[3] which can be elongated with GlcNAc by D-FNG/LFNG/MFNG/RFNG, galactosylated by β4-GALT1, and capped with Sialic Acid by Sialyltransferases. *O*-Glucosylation by POGLUT2/3 at Cys[3]-X-Asn-Thr-X-Gly-Ser-Phe-X-Cys[4]. *O*-GlcNAcylation by Eogt/EOGT at Cys[5]-X-X-Gly-X-Ser/Thr-Gly-X-X-Cys[6], galactosylated by β4-GALT1, and capped with Sialic Acid by Sialyltransferases [73].

Figure 1.11 The Notch1-DLL4 co-crystal structure

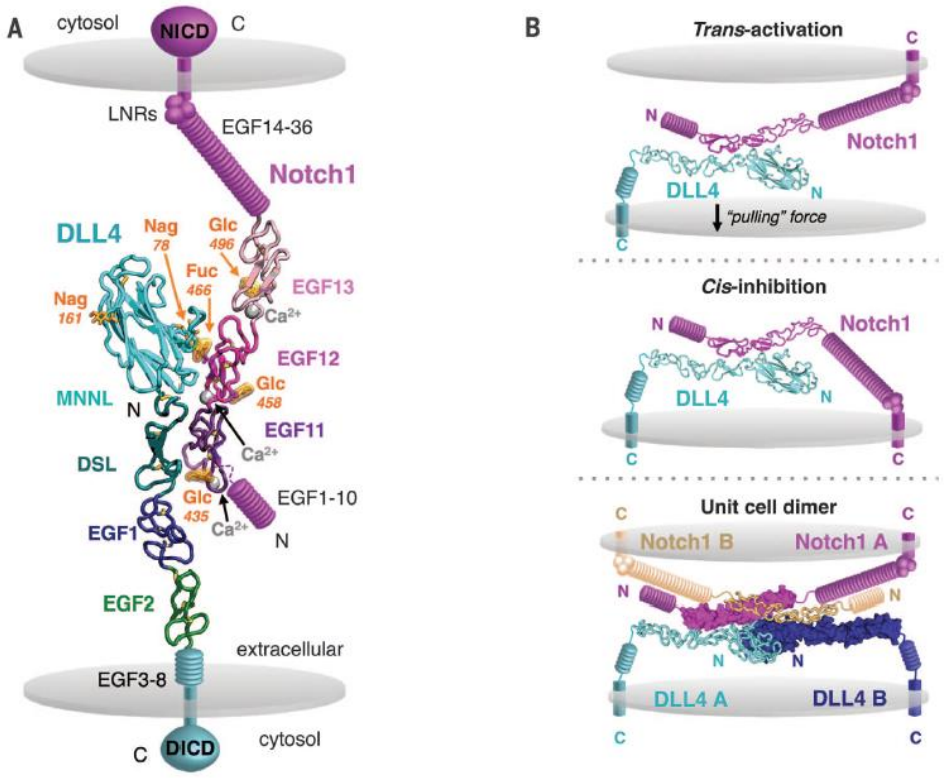

(Panel A) Co-crystal structure of Notch1-DLL4 showing H-bonding between EGF12 *O*-fucose at Thr^{466} and the sidechain of Tyr^{65} from the MNNL domain of DLL4 [57] **(Panel B)** and proposed models for *trans* and *cis*-activation with representation consistent with the anti-parallel interaction. Bottom cartoon depicts the 2:2 dimer observed in the crystals, although the soluble complex occurred in 1:1 [57].

Figure 1.12 The Notch1-JAG1 co-crystal structure

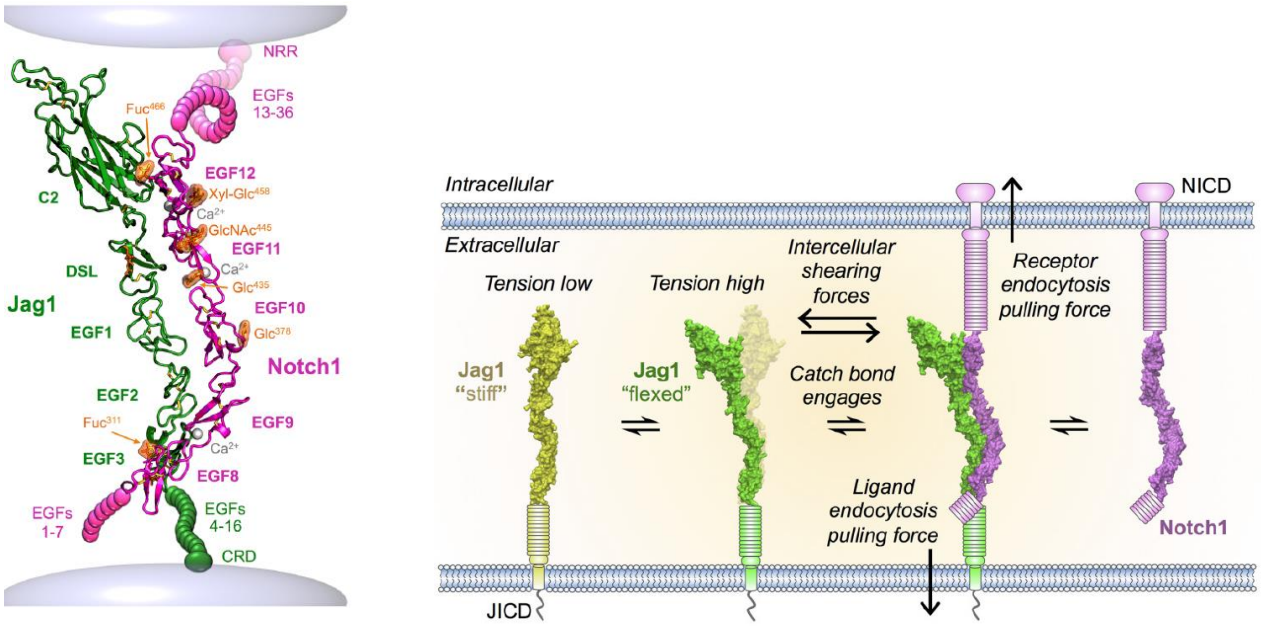

(Left Panel) Notch1 and Jagged1 proteins form an anti-parallel interaction which interfaces at EGF8 and EGF12 of Notch1 and the DSL/EGF regions of Jagged1. *O*-Fucose residues at EGF8 Thr^{311} and EGF12 Thr^{466} are depicted in H-bonds with sidechains from Asn^{298} and Tyr^{82} of Jagged1. The sugars engage in additional Van der Waals interactions as well [58]. **(Right Panel)** Cartoon representation of Jagged1in a flexed conformation in complex with Notch1 which forms a resilient 'Catch Bond' under the force of endocytosis [58].

Figure 1.13 A map of the mouse NOTCH1 extracellular domain identifying EGF-like repeats carrying consensus sites for specific *O*-glycans

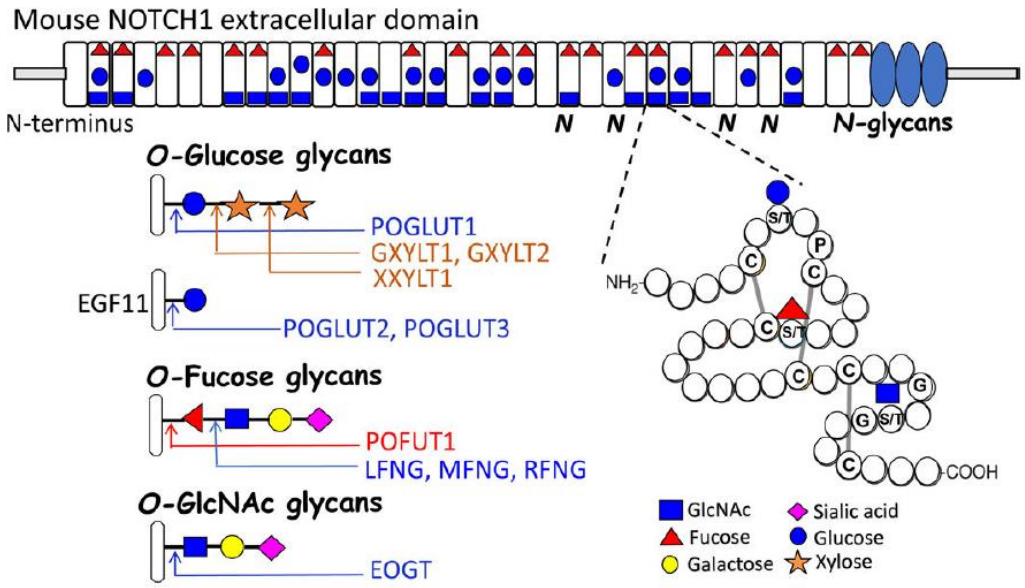

This map shows where specific consensus sites for *O*-glycosylation are located within the extracellular domain of mouse NOTCH1 but does not represent the actual glycosylation status detected [68]. For example, the map is labeled with fucose at EGFs 23 and 24, but those sites are unmodified when analyzed by mass spectrometry [32].

The Mammalian Fringes and Retinal Angiogenesis

The mammalian Fringe enzymes Lunatic, Manic, and Radical were cloned in 1997 [30]. The gene homology for Lunatic Fringe most closely resembles *Drosophila* Fringe – both appearing to have pro-forms which are proteolytically cleaved in the Golgi. RNA *in situ* hybridization experiments in mouse embryos showed that all three Fringe genes are expressed to varying degrees at somite boundaries, the hindbrain, and along the neural tube [74]. Knockout of *Lfng* in a mouse causes substantial malformation of the ribs and vertebral column in neonates, often leading to death by respiratory impairment. These mice also have a shortened trunk size and irregularly sized somites frequently fusing at their boundaries [75].

Cell signaling assays for probing activation of Notch have proven especially useful in differentiating the biological footprint of each Fringe. In a co-culture assay of cells overexpressing *Notch1* incubated with cells stably expressing *Delta-like ligand 1*, co-expression of *Lfng* enhanced activation of Notch1. By comparison, co-expression of either *Mfng* or *Lfng* caused inhibition of *Notch1* activation when co-cultured with cells stably expressing Jagged1, indicating ligand-specific effects with some functional overlap [74]. When *Rfng* was studied in co-culture with Jagged1 cells, it showed an interesting enhancement of *Notch1* activation, unlike the inhibition caused by *Lfng* and *Mfng* [35]. Therefore, it appears that Lunatic and Manic Fringes are more similar in their effects while Radical Fringe is more of an outlier.

Localization of the Fringe proteins may play a role in their functioning. Cleavage of Lunatic Fringe at its pro-protein site by Furin in the Golgi causes secretion of LFNG out of the cell, and its short half-life inside the cell may contribute to the cyclic nature of the vertebral segmentation clock. Radical Fringe appears to be a Golgi resident, and a chimeric Lunatic Fringe

protein carrying the RFNG N-terminal sequence which replaces the LFNG cleavage site increased the half-life of LFNG in the golgi from 90 minutes to 130 minutes [35]. LFNG also possesses more efficient transfer of UDP-GlcNAc to substrate than either MFNG or *Drosophila* D-FNG [13], which may facilitate its activity within a short timeline inside the cell.

In one intriguing study, researchers repeated the swapping experiment where the N-terminus of LFNG containing its Golgi cleavage site was swapped with the N-terminus of RFNG, except that this chimeric protein (RLFNG) was engineered into a mouse [76]. Given that the RLFNG mutant protein showed an increase in its Golgi half-life while retaining enzymatic activity *in vitro*, the authors predicted that this phenotype would likely cause gain-of-function with respect to *Lfng* and lead to dysregulation of the vertebral segmentation clock. Although the outward appearance of these mutants was similar to the *Lfng-/-* mice, differences were identified when comparing skeletal stain preparations. There were noted differences in the *RLfng+/+* ribs especially, exhibiting more severe fusion and clustering than *Lfng-/-*. Their vertebral columns also displayed bony outgrowths and greater disorganization of the individual vertebrae [76].

Numerous attempts to untangle the roles of the three mammalian Fringes during development have been made. When mice carrying null alleles for *Rfng* and *Mfng* were generated, the homozygotes for either Fringe gene did not show any outward defects or change to viability, unlike the *Lfng-/-* mice [75, 77, 78]. Double homozygotes of either *Rfng*-null or *Mfng*-null in combination with *Lfng*-null alleles were also generated. Mice carrying two null alleles of both *Rfng* and *Lfng* were examined for any exacerbation of *Lfng* skeletal defects. The authors did not observe any significant changes in the double homozygote compared to the *Lfng*-null mouse alone, nor any significant reduction in viability [78]. This experiment was repeated with a *Mfng*-null mouse, and the authors also reported no changes to skeletal defects or viability

in the double homozygote compared to *Lfng*-null alone. The authors then generated a triple knockout mouse null for all three Fringes. The increased inbreeding decreased viability across all genotypes, but one generation of outcrossing helped maintain viability of the triple-null mouse. To the authors' surprise, the triple mutant showed no significant increase in skeletal defects either [77].

On the hunt for a phenotype in their Fringe triple homozygote, the authors performed whole-mount immunohistochemistry to stain neurofilaments in the E10.5 hindbrain, a region where they had detected RNA expression of all three fringes previously. They examined the embryos for changes in cranial nerve organization but found no significant phenotypes in any of the homozygotes, including the triple homozygote [77]. The conclusion from this study was that no synergism was at play in skeletal development, nor was there redundancy because single homozygotes could not reproduce the skeletal phenotype observed in the *Lfng*-null mice [78]. This was also surprising because RNA expression for all three Fringe genes had been detected at somite boundaries [30].

The conservation of three Fringe homologs across organisms (Xenopus, Zebrafish) suggests a level of redundancy for maintaining important developmental functions. However, the authors also considered that redundant genes are not necessarily conserved more frequently than non-redundant genes. There existed the possibility of other tissue phenotypes that could differentiate the *in vivo* function of the Fringe genes, and thymic T-cell development became the next promising target [77].

The involvement of Notch in immune development was discovered early on when analyzing causative mutations for T-cell Acute Lymphoblastic Leukemia (T-ALL). Gene expression analysis also showed a high level of *NOTCH1* activity in lymphoid tissue [5], and

another study demonstrated that conditional inactivation of *Notch1* in mouse bone marrow caused loss of T-cell development [79].

After it was established that mouse NOTCH1 is Fringe elongated at EGFs in the Ligand-Binding Domain [15], that the function of the Ligand Binding Domain in EGFs 8 – 12 is necessary for embryonic development in mice [80], point mutation at Fringe-modified *Drosophila* Notch EGF12 causes a loss-of-function phenotype [81], and finally, that *Lfng* expression enhances DLL4 binding to influence β-selection in Double Negative T cells [82], the function of Fringe in immune development became a significant area of study. Researchers generated at mouse carrying a T/A mutation at the EGF12, Fringe elongated *O*-fucose site located in the NOTCH1 ligand binding domain and measured a decrease in thymus size, thymocyte number, a greater proportion of Single Positive T cells compared to Double Positive T cells, and an arrest at the T cell Double Negative - Double Positive transition, consistent with hypomorphic Notch signaling [83].

Next, the Fringe-null mice were examined for changes in immune development [84]. *Lfng*-null mice showed reduced body size, thymus size, and spleen size, as well as fewer thymocytes and splenocytes. However, all *Rfng*-null and *Mfng*-null mice yielded the same ratio of thymus/spleen size and numbers of thymocytes/splenocytes in relation to their body sizes. This was consistent with the observation that the proportions of T cell and B cell subsets were unaffected in the thymus of *Lfng*-null mice, therefore implying that an immune phenotype in the *Lfng*-null mouse was not functionally observed [84].

The authors moved on to analyzing the Triple Knockout mice, which had smaller thymi than single knockout mutants. Again, the size of their thymi reduced proportionately with their body size, similar to observations in the double knockout mice and functionally insignificant.

When analyzing the frequencies of T cell subpopulations from thymus, however, the triple knockout mice showed an increased frequency of Single Positive CD4+ and CD8+ T cells as well as a reduced frequency in the DN1 and DN2 subpopulations. In the spleen, there were lower percentages of CD4+ and CD8+ T cells, as well as Marginal Zone B cells [84].

Next, T cell frequencies in mice homozygous for one functional allele of Fringe were compared to the T cell frequencies observed in the Triple Knockouts. Homozygosity for any functional Fringe gene could rescue the relative loss of Double Positive T cells from the thymus of Triple Knockout mice. This was a surprising observation, especially for Radical Fringe, which seems to influence Notch activation uniquely in comparison to Lunatic and Manic Fringes [35, 74]. In the spleen, mice homozygous for functional *Rfng* or *Lfng* could restore the percent reduction of CD4+ and CD8+ Single Positive T cells observed in the Triple Knockouts, while *Mfng* contributed partial rescue. Finally, *Lfng* was the only Fringe gene which restored the Marginal Zone B cell population in the spleen. The authors suggested that there may be functional consequences in immune response to pathogen or uniquely derived leukemias influenced by inappropriate Fringe activity as a consequence of these differences [84].

One main idea from these exhaustive studies into the *in vivo* functions attributed to each mammalian Fringe gene is that there is overlap in some tissues and contexts but not others. Skeletal development, for examples, is likely coordinated by the efficient catalytic activity and rapid secretion of Lunatic Fringe alone [35], whereas Radical Fringe and Manic Fringe play a greater role in development of sensory organs in the inner ear [85]. Still of interest, however, were their mechanistic effects most clearly observed in cell-based assays under the same expression conditions.

In a comprehensive study on NOTCH1 activation in the presence or absence of Lunatic, Manic, and Radical Fringes, numerous cell co-culture assays detected the relative differences in their abilities to enhance or inhibit mouse NOTCH1 activation when incubated with cells stably overexpressing Delta-like Ligand 1 or Jagged1 [32]. Experiments were performed in human NIH3T3 cells specifically for their low expression levels of endogenous Fringes, and cells were co-transfected with mouse constructs for NOTCH1, Fringe, a β-galactosidase control plasmid, and a luciferase reporter which expresses after complexing with the Notch DNA-binding complex upon receptor activation. After 24hrs, cells were coated with a layer of L cells stably overexpressing either mouse DLL1 or JAG1 ligands at their cell surfaces [32].

Notch1 co-expressed with *Lfng* and stimulated by co-culture with DLL1-presenting cells showed the greatest enhancement of NOTCH1 activation, approximately 3.5x the level of activation compared to without co-expression of any Fringes. Under the same conditions, co-expression of *Mfng* induced a NOTCH1 response approximately 2.5x greater than *Notch1* expression alone. *Rfng* exerted the least influence on NOTCH1 activation by increasing its luciferase reporter response 1.5x above signal in the absence of Fringe co-expression **(Figure 1.14)** [32].

This data is in congruence with abundant mass spectral data from mouse NOTCH1 purified in the presence or absence of Lunatic, Manic, or Radical Fringe. Detected by glycopeptide analysis of the entire extracellular domain from mouse NOTCH1, LFNG was shown to modify the greatest number of *O*-fucosylated EGF-like repeats, particularly EGF12 in the ligand binding domain. This is the only *O*-fucose site which MFNG did not share with LFNG, and because MFNG did not elongate any *O*-fucose residues outside those modified by

LFNG, the EGF12 *O*-fucose site is likely responsible for the maximum level of NOTCH1 activation observed in the presence of LFNG **(Figure 1.15)** [32].

The intermediate level of signal generated by co-expression of *Mfng* can also be explained in relation to site-specific modifications detected in NOTCH1 purified in the presence of RFNG [32]. In comparison to MFNG, *O*-fucosylated EGFs 6, 9, 26, 30, 35, and 36 were not modified by RFNG. However, RFNG did modify EGF12, unlike MFNG, and this likely accounts for the 1.5x enhancement of Notch1 activation by DLL1 **(Figure 1.15)**. In summary, Fringe modification of NOTCH1 EGF12 *O*-fucose is likely the element responsible for elevating activation by DLL1, and other sites modified by MFNG likely compensate for its lack of EGF12 elongation **(Figure 1.16)** [32].

The hierarchical levels of DLL1-Notch1 signal paralleled by a hierarchy of site modifications by Lunatic, Manic, and Radical Fringes is a significant finding. Taken together with the developmental roles and biological characteristics discussed above, it is an intuitive explanation for how *Lfng* expression might dictate phenotype in the expression context of all three Fringe genes, such as somite boundary formation [30] and immune development [84]. This, however, does not address the outcomes of Fringe-modified NOTCH1 activation by JAG1.

To define NOTCH1 responses to co-culture with JAG1-expressing cells when NOTCH1 is modified by Lunatic, Manic, and Radical Fringes, the co-culture assays were repeated with L cells stably overexpressing *Jag1*. When *Notch1* was co-expressed with either *Lfng* or *Mfng* and stimulated by JAG1, NOTCH1 activation, as measured by luciferase response, was suppressed in comparison to the absence of either Fringe. By contrast, co-expression of *Rfng* and *Notch1* followed by JAG1 stimulus resulted in a 1.5x increase in activation, approximately equal to

levels observed when *Rfng* was co-expressed with *Notch1* and co-cultured with cells presenting DLL1 at their cell surfaces **(Figure 1.14)** [32].

Upon re-examination of the mass spectral data, there are several Fringe-elongated *O*-fucose sites which only Lunatic Fringe and Manic Fringe share exclusively that might mediate their inhibitory effects when stimulated by JAG1. These sites include EGFs 6, 9, 27, 30, 35, and 36 **(Figure 1.15)**. Because there are quite a few sites on that list, the signaling assays were repeated with constructs carrying conservative T/V point mutations at the specific *O*-fucosylated Ser or Thr. Notably, mutation at EGF6 or EGF36 rescued signal when the co-culture was repeated with *Lfng* or *Mfng* expression and stimulation with JAG1. When performed with expression of *Rfng*, the level of NOTCH1 activation by JAG1 was unaffected while the *Notch1* expression construct encoded for either EGF6 T/V or EGF36 T/V in the NOTCH1 protein. Repeating with a double mutant carrying T/V point mutations at EGF6 and EGF36 rescued NOTCH1 activation to the level of unmodified, WT NOTCH1. Again, the double mutation in the context of *Rfng* expression did not change the elevated level of activation **(Figure 1.16)** [32].

Mutation of the other EGF *O*-fucose sites identified in the mass spectral screen failed to rescue signal and also impacted activation of unmodified NOTCH1. What is interesting about EGFs 6 and 36 is not only did mutation rescue signal inhibited by LFNG or MFNG with no effect on signal elevated by RFNG, mutation at either site also had no effect on unmodified NOTCH1 stimulated by JAG1. This suggests that the function of these sites is primarily regulatory. Moreover, these mutations also had no effect on NOTCH1 activation by DLL1 in the presence or absence of any Fringe expression, meaning that the mutations are specific to NOTCH1 inhibition by JAG1 through *Lfng* or *Mfng* co-expression only **(Figure 1.16).** Mutations at EGFs 8 and 12 reduce signal activation by both JAG1 and DLL1 in the absence of Fringes,

consistent with their positioning within the ligand-binding domain and co-crystal structures showing direct involvement of those *O*-fucose residues in binding ligand **(Figures 1.11, 1.12, and 1.16)** [57, 58].

Beyond the function of *O*-fucose in ligand-binding at EGFs 8 and 12 and their sensitivity to mutation when unmodified NOTCH1 is stimulated by either JAG1 or DLL1, with mutation at both sites suppressing most all activation, a deeper analysis of Fringe-specific effects on DLL1 can pinpoint a site that favors enhancing activation of NOTCH1 by DLL1. As previously discussed when addressing shared sites, LFNG modifies both EGFs 8 and 12, while MFNG only modifies EGF8, and RFNG only modifies EGF12 **(Figure 1.15)**. The complicating factor is that mutation at either site reduces activation of unmodified NOTCH1, but normalizing NOTCH1 signal in the presence of any of the three Fringes to the signal of unmodified NOTCH1 (in the context of any mutation) and comparing to the normalized signal from co-culture of WT NOTCH1 can elucidate a specific Fringe effect that is lost when a relevant site is mutated [32].

When EGF8 is mutated, activation of NOTCH1 stimulated by DLL1 in the presence of *Mfng* equalizes to the level of activation in the absence of any Fringes, whereas a 2.5-fold increase could be observed with WT NOTCH1 in the presence of *Mfng* shown previously. Further, the fold-change in activation observed in the presence of *Lfng* is reduced from 3.5x to 3x, and activation in the presence of *Rfng* is still about 1.5-fold increased **(Figure 1.16)** [32]. When EGF12 is mutated, the fold change in activation in the presence of *Rfng* is narrowed to about 1.2-fold. The fold-change activation in the presence of *Mfng* is about 2x, and in the presence of *Lfng*, NOTCH1 activation is reduced to approximately 2.3-fold **(Figure 1.16)**. Although the margin of error is larger in these calculations, the broad interpretation is that Fringes which modify the residue that is specifically mutated demonstrate a more significant

reduction in fold-change activation with respect to WT NOTCH1 in identical co-culture conditions otherwise. Therefore, Fringe modifications at EGF8 and EGF12 both significantly contribute to enhancing NOTCH1 activation by DLL1 **(Figure 1.17)** [32].

The final element for confirming the mechanism for inhibition of NOTCH1 activation by JAG1 and enhancement of NOTCH1 activation by DLL1 is to demonstrate that the mechanism applies *in vivo*. To achieve this, retinal angiogenesis will be observed when either EGF6 or EGF8 *O*-fucose is mutated in a mouse. We will be looking for the EGF6 to cause a Gain-of-Function phenotype with respect to NOTCH1 and EGF8 to cause a Loss-of-Function phenotype with respect to NOTCH1. The topic of the negative feedback loop that maintains angiogenic growth will be discussed in relation to the effects of Fringe in the system. These mutations will also be assessed for changes to T-cell development, but given the difficulty other researchers experienced when identifying immune phenotypes, it is a good thing that the process of angiogenesis is quite sensitive in comparison.

Figure 1.14 Co-expression of *Notch1* with *Lfng*, *Mfng*, or *Rfng* causes significant changes in activation of NOTCH1 when stimulated by cell-surface ligands DLL1 and JAG1

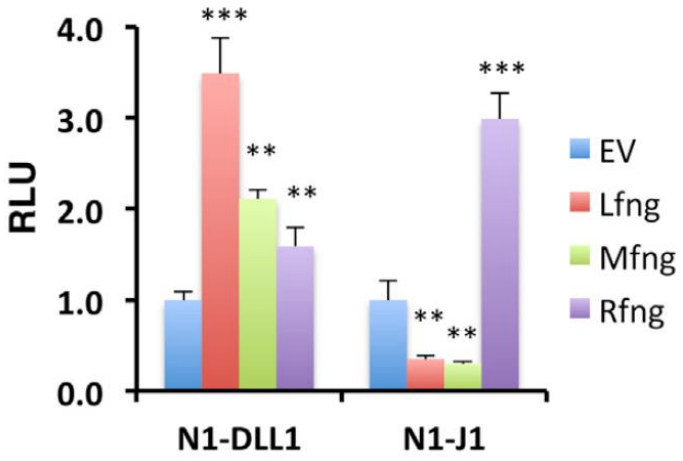

Cellular assays were performed in human 3T3 cells, in which endogenous expression of Fringes is low, co-cultured with human L cells that stably overexpress DLL1 or JAG1 ligands. First, 3T3 cells were transfected with *Notch1*, *Lfng*, *Mfng*, *Rfng*, or Empty Vector along with β-galactosidase and TP-1 luciferase reporter plasmids. Co-culture with DLL1 or JAG1-expressing L cells occurred for 24hrs., and cells were measured for luciferase activity normalized to the levels of β-galactosidase activity to control for overall transfection efficiency. The results show that *Lfng*, *Mfng*, and *Rfng* enhance NOTCH1 activation by DLL1 in descending order. When stimulated by JAG1, NOTCH1 activation is inhibited in the presence of either *Lfng* or *Mfng* but enhanced in the presence of *Rfng* [32].

Figure 1.15 Mass spectral mapping of Fringe modifications at every O-fucose site found in mouse NOTCH1 to identify differences and similarities in Fringe elongation between the three mammalian Fringes

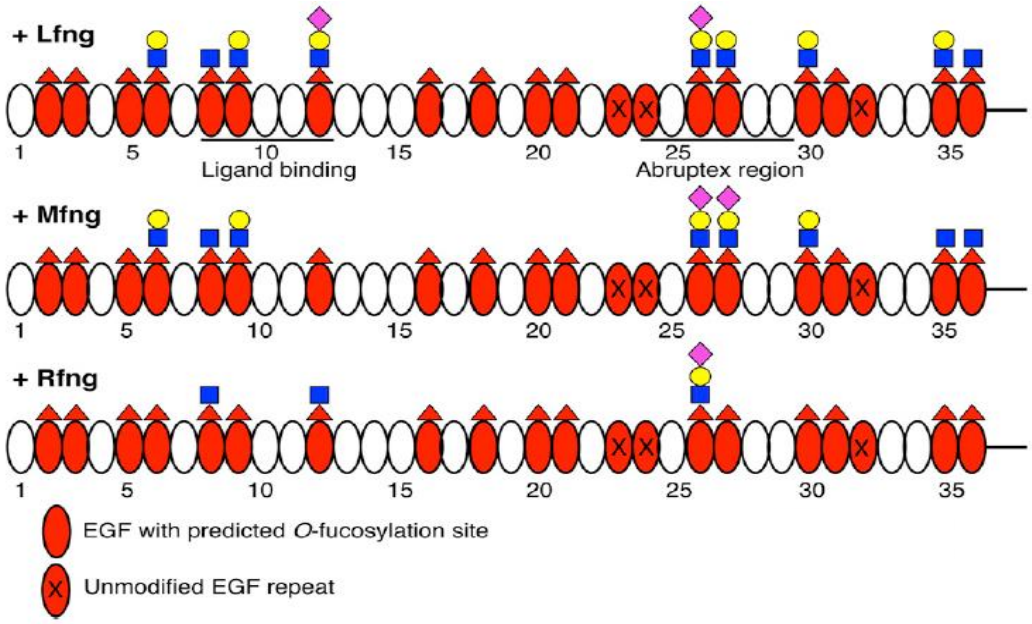

Notch1 was co-expressed with *Lfng*, *Mfng*, or *Rfng* and immunopurified for mass spectral analysis of NOTCH1 *O*-fucose sites to identify EGF-like repeats carrying GlcNAc transferred by Fringe. LFNG modified the greatest number of sites, and RFNG the fewest. The only Fringe modification site not shared by LFNG and MFNG is EGF12. RFNG modifies a subset of sites modified by LFNG, showing elongation with GlcNAc at three sites, including EGF8 which is not modified by MFNG [32].

Figure 1.16 Mutagenesis screen of EGF *O*-fucose sites modified by mammalian Fringes and assessed for changes to NOTCH1 activation by stimulation with JAG1 or DLL1

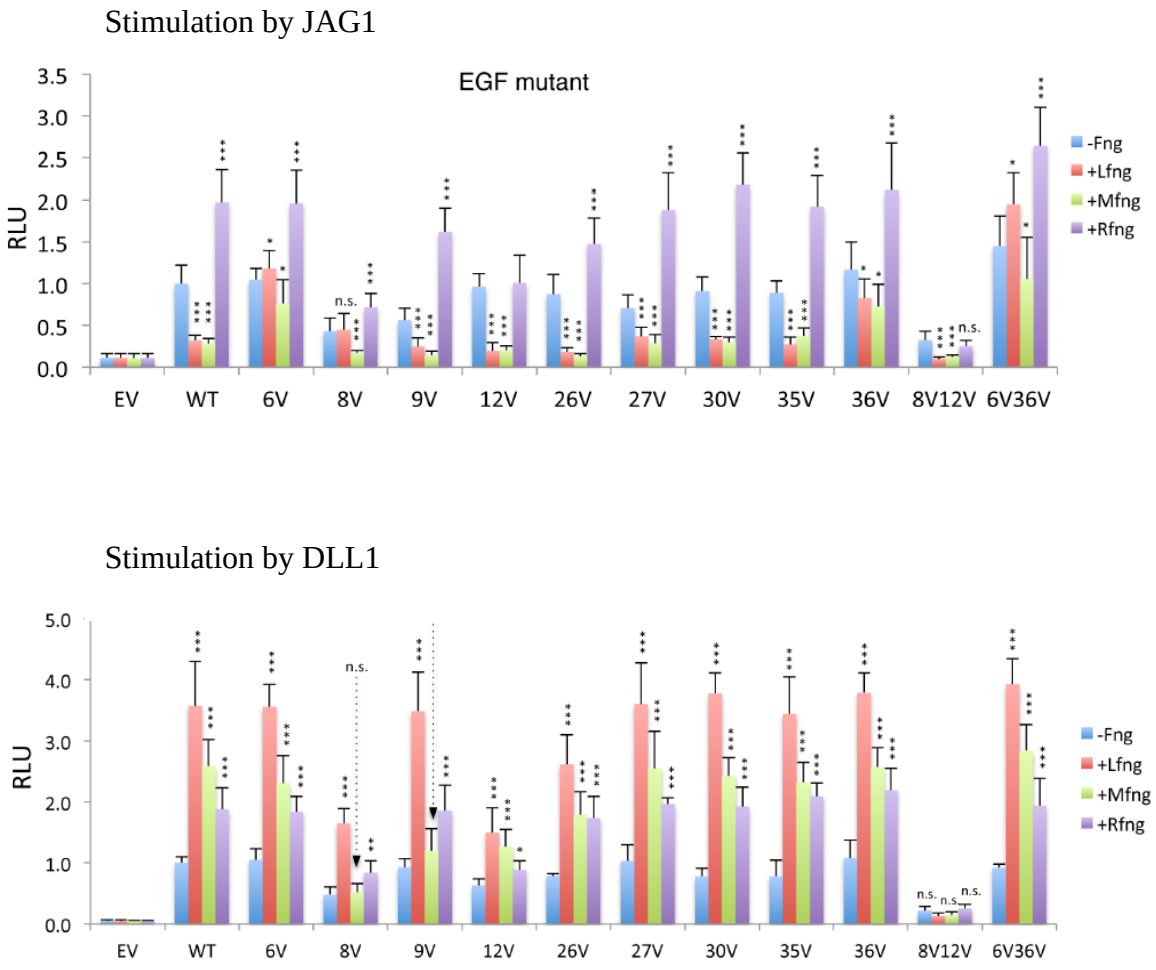

Cellular expression of *Notch1* carrying a point mutation encoding a T/V mutation at EGF-like Repeats identified in the mass spectral screen as potentially significant Fringe sites, along with expression of *Lfng*, *Mfng*, *Rfng*, or Empty Vector and control plasmids β-galactosidase and TP-1 luciferase reporter. After transfection of 3T3 cells, L cells stably expressing JAG1 **(Upper Panel)** or DLL1 **(Lower Panel)** were co-cultured for 24hrs. and measured for luciferase activity normalized to β-galactosidase activity indicating total transfection efficiency [32].

Figure 1.17 Illustrated model depicting significant Fringe-modified *O*-fucose sites on EGF-like repeats located in the extracellular domain of mouse NOTCH1 and their contributions to levels of receptor activation by either Jagged or Delta family ligands

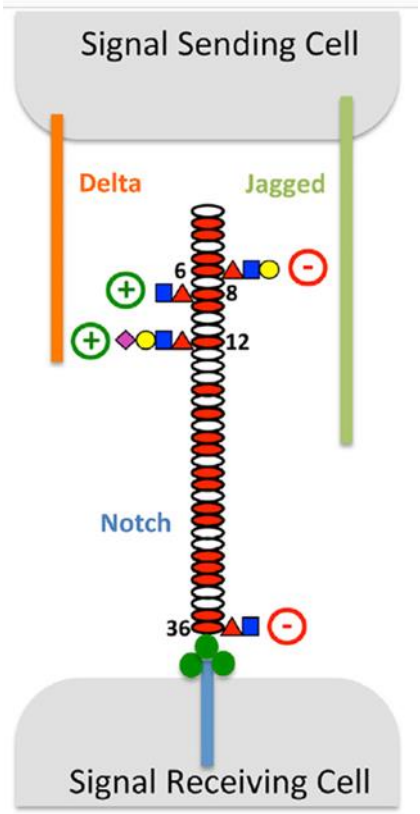

With respect to stimulation by DLL1, the Fringe-modified NOTCH1 *O*-fucose sites in EGFs 8 and 12 most significantly enhance receptor activation. With respect to stimulation by JAG1, the Fringe-modified NOTCH1 *O*-fucose sites in EGFs 6 and 36 most significantly inhibit receptor activation [32].

While early studies on *Notch1-/-* mice reported the absence of vascular defects before lethality ~E10.5 [6, 7], it was the Notch pathway disorder in humans named Alagille Syndrome which led to the connection between Notch and vessel development. Alagille Syndrome is caused by inactivating mutations in one copy of *JAG1* resulting in a spectrum of symptoms. The most devastating symptom of the disorder is lack of intrahepatic duct development which can necessitate a liver transplant in children younger than 10 years old. Other symptoms include chronic kidney disease caused by loss of properly developed nephrons, cardiac abnormalities including hypertension and narrowing of the renal artery and aorta [86], as well as ophthalmological defects, especially in the anterior chamber of the eye such as iris atrophy and displacement of the Schwalbe's line anteriorly. Eye defects affect up to 80% of Alagille patients so are often used diagnostically but does not usually cause significant loss in vision [87, 88].

To model Alagille syndrome, a group of researchers generated mice carrying one gene copy of *Jag1* lacking the most C-terminal portion of the DSL domain required for receptor interaction [89]. While the heterozygotes were normal and viable, intercross to homozygosity revealed embryonic lethality around E10.5 when blood loss from the yolk sacs was observed as well as lack of large blood vessels. Histology confirmed decrease in vascular networking in the hindbrain of the mutants **(Figure 1.18)**. When further investigated, researchers observed that a network of primitive vessels was formed prior to E10.5, and that the likely cause for lethality was not initial vascularization but the following angiogenic development [89].

To further assess the similarities of these mice to the Alagille patient population, the researchers assessed adult $Jag1_{dsl}$ heterozygotes for abnormalities, better recapitulating the *JAG1*

haploinsufficiency in the human disease. While defects in the liver, kidney, or heart were not observed, eye abnormalities were readily identifiable in ~80% of mice on a mixed background, similar to the frequency of eye abnormalities observed in Alagille patients, and nearly 100% when backcrossed into a C57BL/6J background. Iris defects and corneal clouding are both phenotypes which have been observed in Alagille patients and also observed in these mice **(Figure 1.19)** [89].

From this point onward, it was well known that Notch was involved in angiogenesis due to the requirement of Jagged1 in the process. Phenotypes in the retina, a readily accessible, 2-D tissue that is easy to image, and which undergoes the major vascular processes such as initial vascularization from P0-P3, radial expansion of the immature vascular plexus via angiogenesis between P4 – P7, vascular remodeling between P5 – P10, and vascular maturation between P8 – P15 [90]. While developing eyes in the embryo are supplied with Oxygen-rich blood via the hyaloid vasculature extending through the optic nerve head into the vitreus and the front of the eye where it exits through a facial vein. The hyaloid vasculature regresses as the primitive vessel layer grows across the neuronal network of the retina, primarily comprised of astrocytes which are derived from retinal precursors found in the optic nerve [91].

During the initial stages of astrocyte invasion into the retina, maturing astrocytes originating from the optic nerve begin to express Platelet-Derived Growth Factor Receptor-α which triggers cell division upon encountering Platelet-Derived Growth Factor A (PDGFA) secreted by retinal ganglion cells in the Nerve Fiber Layer [91]. The ultimate population size of retinal astrocytes depends on the overall level of secreted PDGFA, which correlates to the population size of ganglion cells established prior to birth [91, 92]. When the migrating and proliferating astrocyte population reaches the retinal periphery around P6, there are more

astrocytes than ganglion cells. After a period of phagocytic astrocyte culling and maturation of the astrocyte extracellular matrix environment, the final size of the astrocyte population matches the population size of the ganglion cells by P15 [93].

The migration and proliferation of astrocytes spurs angiogenesis through astrocyte secretion of hypoxia-induced Vascular Endothelial Growth Factor (VEGF) which activates angiogenic development in roughly a three-day delay, meaning that immature astrocytes begin invading the retina at E18 and trigger angiogenesis at P0, luring an observable radius of immature vessels by P3. When the astrocyte population peaks as the migrating cells reach the periphery by P6, the developing vessel networks are nearly approaching the periphery and supplying Oxygen across the retina, so astrocytes are no longer experiencing hypoxic conditions triggering VEGF secretion. Thus, the phase of angiogenic sprouting transitions into phases of network remodeling and maturation [90].

The basic steps and feedback mechanisms relating the roles of NOTCH1, DLL4, JAG1 and the mammalian Fringes LFNG, MFNG, and RFNG in mammalian angiogenesis have been broadly defined over the last 15 years. In the context of retinal angiogenic development already addressed, angiogenesis is stimulated by migrating astrocyte secretion of free VEGF and binding VEGF receptors expressed on vascular endothelial cells that have potential for angiogenic sprouting. After VEGF binding, the cell upregulates expression of *Dll4*, which is the dominant stimulant for activating NOTCH1 expressed on the endothelial cells directly adjacent. Because these endothelial cells express all Fringe genes, the highest level of expression being *Rfng*, followed by *Mfng*, and finally *Lfng*, feedback regulation can be considered under Fringe-modified conditions across all cells **(Figure 1.20)** [34].

The cell with freshly upregulated expression of *Dll4* stimulates activation of Fringe-modified NOTCH1 on the cell surfaces of its neighbors. Because NOTCH1 activation regulates expression of *Dll4*, this cell loses some cell-surface DLL4 and becomes JAG1-dominant. Finally, it inhibits activation of NOTCH1 on surrounding cells, a Notch patterning mechanism referred to as lateral inhibition because it restricts the elevated levels of NOTCH1 activation to the JAG1-dominant cells and lowers levels of NOTCH1 activation in its direct neighbors. The JAG1-cell also stimulates its original neighbor, which is already DLL4-dominant, therefore solidifying its DLL4-dominant status through inhibition of NOTCH1 activation (and because NOTCH1 activation regulates expression of *Dll4*, the expression of *Dll4* is now unregulated). The DLL4-dominant cells at the angiogenic front in contact with VEGF develop into tip cells, characterized by the growth of filopodia which determine the direction of vessel growth. The JAG1-dominant cell, on the other hand, propagates lateral inhibition downward and bi-laterally unless a cell contacts free VEGF and disrupts the cycle with induced expression of *Dll4*. Otherwise, the JAG1-dominant cells develop into stalk cells, so-called for their rectangular shape and contribution to the overall length of the developing vessel **(Figure 1.20)**. The stalk cells are where NOTCH1 co-activates downstream target genes involved in cell growth and division, so they are also named for vessel growth originating from the stalk, like a plant. Cell cycle arrest is primarily observed in tip cells, so although they give the appearance of sprouting, the actual growth takes place at the vessel stalks [34].

Confirmed phenotypes in retinal angiogenesis includes gain of vessel density and branching due to *Dll4*-heterozygosity [94], loss of vessel density in the *Jag1*-null embryo [89], and gain of vessel density in the *Lfng*-null retina [34]. An interesting experiment would be to re-introduce single Fringe genes into the Fringe triple knockout mouse and look for any changes. In

the absence of any Fringe, a realistic prediction would be disorganization of vessel networks, considering the themes discussed in this section. The Specific Aims which follow this section will focus on phenotypes related to angiogenesis, and the original research accompanying this introduction will add to the existing body of literature of Notch, Ligands, and Fringes in the context of angiogenic development and site-specific effects of individual EGF-like repeats in NOTCH1.

Figure 1.18 There is loss of embryonic vascular development in the $Jag1_{dsl}$ homozygotes and *Pofut1-/-* mice

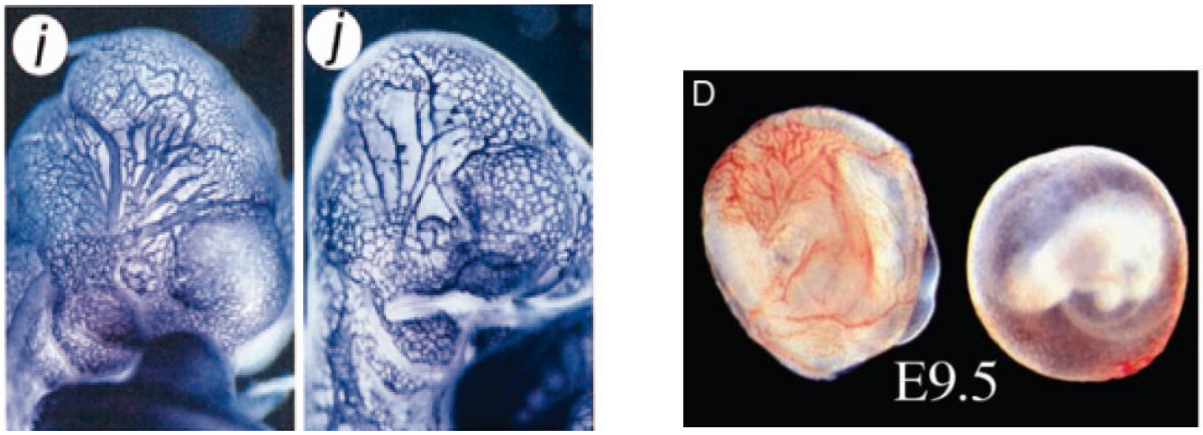

(Left Panel) Whole mounts at E10.5 showing the vasculature in the hindbrain immunostained with PECAM1. The image on the left and labeled (i) is from a WT embryo, and on the right labeled (i), is from a *$Jag1_{dsl}$* homozygous embryo showing decreased vascular density and branching as well as loss of the large vessels [89]. **(Right Panel)** Images of whole mounted embryos at E9.5 with yolk sacs intact. The WT embryo is on the left, showing a large complex of vessels, and a Pofut1-/- embryo is on the right, showing lack of functional vessel development around the time lethality is observed [62].

Figure 1.19 Eye abnormalities were observed in the *Jag1$_{dsl}$* +/- adults at similar frequency as Alagille patients

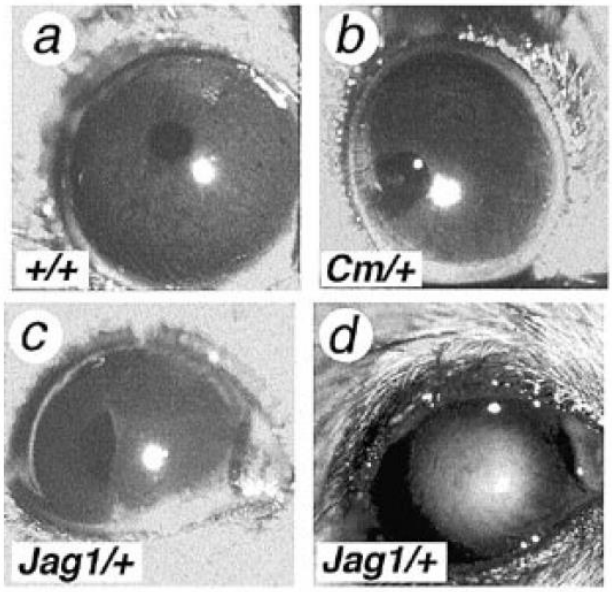

(Upper Left) Normal eye from adult WT, labeled (a) **(Upper Right)** The adult eye from a strain of mice that develop coloboma, a defect in the iris that causes the pupil to appear misshapen, labeled (b) **(Lower Left)** The adult eye from a *Jag1$_{dsl}$* heterozygote showing another coloboma making the pupil appear elliptical in shape, labeled (c) and **(Lower Right)** The adult eye from a *Jag1$_{dsl}$* heterozygote with corneal clouding, labeled (d) [89].

Figure 1.20 The negative feedback loop observed in sprouting angiogenesis

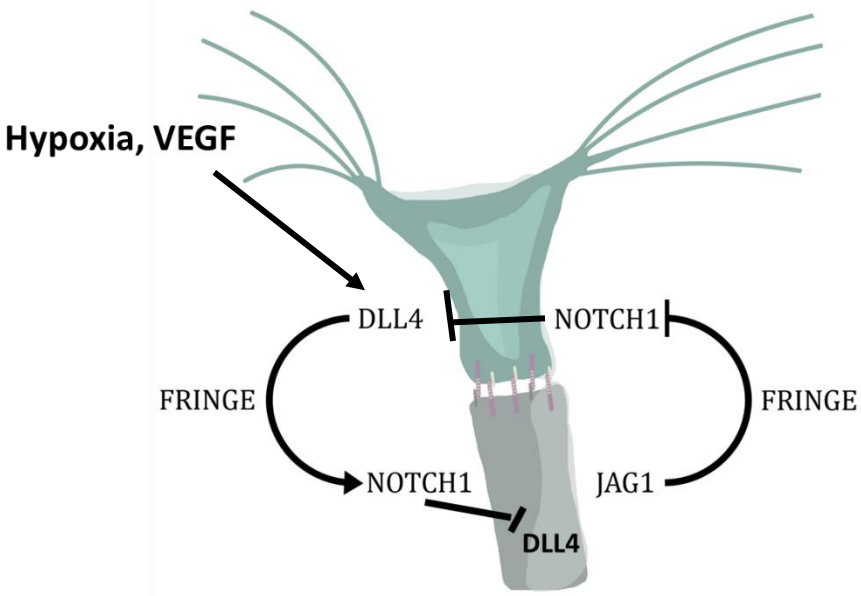

Cartoon depiction of sprouting angiogenesis beginning with binding of VEGF and increased expression of *Dll4*, both cells expressing Fringe. Enhanced activation of NOTCH1 in the adjacent cell by stimulation with DLL4 results in NOTCH1 regulation of *Dll4* expression in the signal-receiving cell, causing it to express more JAG1 at the cell surface than DLL4. Its abundant JAG1 signals to adjacent cells to inhibition activation of NOTCH1, including in the originating DLL4-dominant cell. Because NOTCH1 activation regulates expression of *Dll4*, more *Dll4* is able to express in the already DLL4-dominnt cell, reinforcing its status as *Dll4*-high and activation of NOTCH1-low. When it signals to adjacent cells, it will propagate the JAG1-dominancy, which will propagate more JAG1-dominancy in adjacent cells unless they contact VEGF and induce expression of *Dll4* independently. The DLL4-dominant cells develop filopodia, while stalk cells actively divide and extend the vessel forward [34].

Specific Aims

The goal of this dissertation is to demonstrate that the molecular mechanism behind mammalian Fringe enhancement of Notch1 activation by the Delta family ligands and inhibition of Notch1 activation by the Jagged family ligands identified *in vitro* also applies to developmental contexts *in vivo.*

This will be achieved by :

1) Generating a mouse line carrying a conservative T/V point mutation at Notch1 EGF8 to demonstrate that *O*-fucosylation and Fringe elongation at this site contributes to enhancement of Notch1 activation by the Delta family ligands. The phenotypes being addressed are embryonic lethality due to direct participation of EGF8 *O*-fucose in Receptor-Ligand interaction as well as T cell development in the thymus. Finally, angiogenic development of the retina will reveal if EGF8 *O*-fucose and Fringe modification have a phenotype response consistent with Notch Pathway loss-of-function.

2) Generating a mouse line carrying a conservative T/V point mutation at Notch1 EGF6 to show that Fringe modification at this site significantly contributes to inhibition of Notch1 activation by Lunatic and Manic Fringe when stimulated by Jagged1. Retinal angiogenesis is the perfect tissue to analyze due to expression of *Notch1*, *Lfng*, *Mfng*, *Rfng*, *Jag1*, and *Dll4*. If EGF6 is mediating inhibition of JAG1-N1 activation, the phenotype will resemble a *Jag1* loss-of-function or Notch Pathway Gain-of-Function.

CHAPTER 2

TWO NOTCH1 *O*-FUCOSE SITES HAVE OPPOSING FUNCTIONS IN MOUSE RETINAL ANGIOGENESIS

Rachel K. LoPilato[1], Heike Kroeger[2], Sneha Mohan[2], James D. Lauderdale[2], Neil Grimsey[3*], and Robert S. Haltiwanger[1*]

[1]Complex Carbohydrate Research Center, Department of Biochemistry and Molecular Biology, University of Georgia, Athens, GA 30602

[2]Department of Cellular Biology, University of Georgia, Franklin College of Arts and Sciences, Athens, GA 30602

[3]Pharmaceutical and Biomedical Sciences, University of Georgia, College of Pharmacy, Athens, GA 30602

***Authors for Correspondence**
Email: NeilGrimsey@uga.edu and rhalti@uga.edu

This article has been accepted for publication in *Glycobiology* Published by Oxford University Press. Reprinted here with permission of publisher, April 28, 2023.

Abstract

Previous *in vitro* studies demonstrated that Fringe glycosylation of the NOTCH1 extracellular domain at *O*-fucose residues in Epidermal Growth Factor-like Repeats (EGFs) 6 and 8 is a significant contributor to suppression of NOTCH1 activation by JAG1 or enhancement of NOTCH1 activation by DLL1, respectively. In this study we sought to evaluate the significance of these glycosylation sites in a mammalian model by generating two C57BL/6J mouse lines carrying NOTCH1 point mutations which eliminate *O*-fucosylation and Fringe activity at EGFs 6 (T232V) or 8 (T311V). We assessed changes to morphology during retinal angiogenesis, a process in which expression of *Notch1, Jag1*, *Dll4*, *Lfng, Mfng,* and *Rfng* genes coordinate cell-fate decisions to grow vessel networks. In the EGF6 *O*-fucose mutant (*6f/6f*) retinas we observed reduced vessel density and branching, suggesting that this mutant is a hypermorph. This finding agrees with prior cell-based studies showing that the *6f* mutation rescued JAG1-NOTCH1 signal in the presence of Fringes. Although we predicted that the EGF8 *O*-fucose mutant (*8f/8f*) would not complete embryonic development due to the direct involvement of the *O*-fucose on EGF8 in engaging ligand, the *8f/8f* mice were viable and fertile. In the *8f/8f* retina we measured increased vessel density consistent with established hypomorphs. Overall, our data supports the importance of NOTCH1 *O*-fucose residues for pathway function and confirms that single *O*-glycan sites are rich in signaling instructions for mammalian development.

Introduction

The Notch pathway is a cell-cell communication channel for the direction of cell fate decisions, proliferation, and spatial patterning required for tissue development and homeostasis in metazoans [23, 95]. The family of Notch pathway genes was first identified and foundationally studied in *Drosophila* which express a single Notch receptor, two ligands (Delta, Serrate) and one Fringe glycosyltransferase [8, 96]. The mammalian Notch family is more diverse with four Notch receptors (NOTCH1-4), three Delta ligands (DLL1, 3, 4), two Jagged ligands (JAG1, 2), and three Fringe glycosyltransferases named Lunatic (LFNG), Manic (MFNG), and Radical (RFNG) [20, 30, 97]. Owing to the complex expression patterns of receptors, ligands, and Fringes, contextual functions of the mammalian Notch pathway are presently under considerable investigation across tissue and disease states.

Glycosylation of the Notch extracellular domain is essential for its trafficking and function [39, 68, 98]. The enzyme Protein *O*-fucosyltransferase I (POFUT1) catalyzes the addition of *O*-linked fucose to a Ser or Thr between Cys 2 and 3 of Epidermal Growth Factor-like (EGF) repeats containing the consensus sequence Cys^2-X-X-X-X-Ser/Thr-Cys^3, which is modified with high fidelity and found in 20 of the 36 EGF repeats within the extracellular domain of NOTCH1 [15, 32] **(Fig. 1 A and B)**. Efficient cell surface expression of the Notch receptor is disrupted in some tissues due to loss of POFUT1 [65], and knockout of *Pofut1* in a mouse leads to embryonic lethality with Notch phenotypes [62]. In humans, defects in Notch-related glycosyltransferases cause diseases such as Spondylocostal Dysostosis, Dowling-Degos Disease, Adams Oliver Syndrome, and numerous cancers [16, 73, 99-103].

Biophysical and biological studies show that some of these glycans directly participate in Notch activation. C*O*-crystal structures of receptor ligand complexes revealed significant

interactions between the *O*-fucose at NOTCH1 EGF8 with JAG1 [58] and at EGF12 with DLL4 in addition to JAG1 [57, 58]. Both EGF8 and 12 occur in the ligand-binding domain, a region necessary for pathway function [80]. Mutation at either NOTCH1 EGF8 (T311V) or EGF12 (T466V) showed significant reduction in activation by DLL1 and JAG1 in mammalian cell-based assays [32]. *In vivo*, mutating the *O*-fucose site at EGF12 (T466A) caused embryonic lethality in homozygous mice [83, 104] and hemizygous flies (S502A) [27]. Although the EGF8 (T348V) mutation did not induce lethality in flies, it demonstrated a combinatorial effect with EGF12 to intensify wing vein thickening, a Fringe phenotype [27, 105]. These results emphasize the nuance to site-specific effects of Notch *O*-fucose glycans *in vivo.*

The Fringe family of glycosyltransferases is known to tune the Notch pathway by addition of *N*-acetylglucosamine to *O*-fucose [12, 13]. In flies, expression of Fringe enhances Delta induced signaling while reducing Serrate responses [11]. In mammals, LFNG, MFNG, and RFNG all enhance activation of NOTCH1 by DLL1, while LFNG and MFNG inhibit activation by JAG1 [32]. Fringe acts to coordinate binary cell fate decisions, such as during angiogenesis, the process by which endothelial cells organize into vessel networks during development or hypoxia [34, 106].

Endothelial cells that broadly express NOTCH1, JAG1, DLL4, and the three mammalian Fringes initiate sprouting angiogenesis by binding free Vascular Endothelial Growth Factor, which increases DLL4 expression. A greater concentration of cell-surface DLL4 heightens activation of Fringe-modified NOTCH1 in adjacent cells. Because NOTCH1 signal regulates expression of DLL4, neighboring cells become JAG1-dominant. Finally, JAG1 cells signal back to the originating endothelial cell to suppress activation of Fringe-modified NOTCH1 and reinforce expression of DLL4 [34]. DLL4-dominant cells develop filopodia and extend towards

pr*O*-angiogenic factors while JAG1-dominant cells follow closely behind, together giving the appearance of a sprout and stalk in growing vessels [107].

Knockdown and knockout phenotypes in the retinal angiogenesis system provide a straightforward readout for gross levels of NOTCH1 activity. A hypomorphic *Dll4 +/-* retina, for example, resulted in over-sprouting of tip cells and a highly dense vessel network [94]. A *Lfng -/-*knockout retina resembled the *Dll4 +/-* phenotype with a similar overabundance of tip cells at the leading edge [34]. In the opposing direction, a hypermorphic *Jag1* knockdown displayed reduced vessel density that was rescued by the Notch inhibitor DAPT [34].

The rationale for inspecting retinal angiogenesis to draw conclusions about single EGF *O*-glycans comes from cell-based data showing that the Fringe effect on signal by NOTCH1-DLL1 can be uncoupled from NOTCH1-JAG1 through mutating certain *O*-fucose residues [32, 108]. Among the three mammalian Fringe glycosyltransferases, LFNG modifies the greatest number of *O*-fucose sites and most strongly enhances NOTCH1 activation by DLL1 and greatly reduces activation by JAG1. MFNG modifies fewer sites than LFNG and enhances DLL1 signal less strongly but reduces JAG1 signal similarly to LFNG. RFNG modifies only a subset of NOTCH1 *O*-fucose sites with the smallest, but still significant, increase in activation by DLL1 and a curious increase in activation by JAG1 [32, 108].

In an *in vitro* mutagenesis screen, NOTCH1-JAG1 signal inhibited in the presence of either LFNG or MFNG was rescued by loss of the *O*-fucose site at EGF6 (T232V) with no change to elevated activation by DLL1. The EGF6 mutation showed no impact on activation by either DLL1 or JAG1 through NOTCH1 modified by RFNG, which was a significant finding because only LFNG and MFNG modify EGF6. Thus, Fringe modification at EGF6 appears to distinguish NOTCH1 signal inhibition by JAG1 with no effect on signal by DLL1 **(Figure 1A)**.

Further, mutation at EGF6 does not affect activation of NOTCH1 in the absence of Fringes, meaning that its function appears to be regulatory alone, and its location outside the ligand binding domain points to an indirect mechanism for its influence [32].

Although the *O*-fucose monosaccharide at EGF8 is important for ligand interaction [57, 58], Fringe modification at this site also significantly tunes signal by DLL1 and JAG1. In a cell-based assay, mutation at EGF8 reduces DLL1 activation of NOTCH1 by approximately 50% when modified by any of the three Fringes. While some inhibition by JAG1 is lost, it is rescued only to the level of unmodified NOTCH1. Mutation at EGF12 produces similar effects, and combination of both mutations completely suppresses signal by both DLL1 and JAG1 [32].

In this publication we sought to investigate the *in vivo* contributions of single mammalian NOTCH1 *O*-fucose glycans by generating two mouse lines carrying conservative T/V point mutations at the EGF6 (*6f*) and EGF8 (*8f*) *O*-fucose sites **(Figure 1)**. By evaluating phenotypes during sprouting angiogenesis, we confirmed pathway gain-of-function via rescue of JAG1-NOTCH1 signal in our *6f/6f* mice. Conversely, we observed pathway loss-of-function in the retinas of our *8f/8f* mice and induced embryonic lethality through genetic cross with mice carrying one copy of *Notch1* lacking the ligand binding region.

Generation of Mice lacking O-fucose at EGF6 or EGF8 on NOTCH1

To knock out the *O*-fucose site most responsible for inhibiting NOTCH1 signal by JAG1 in the presence of LFNG and MFNG **(Figure 1A)**, we generated a T232V mutation at EGF6 in mouse *Notch1* **(Figure 2A)**. CRISPR/Cas9 homology-directed repair was performed on a C57BL/6J mouse background, and repair template carrying the ACC->GTG mutation at *Notch1* nt19507-19510 (NCBI Gene: 18128) was targeted to mouse *Notch1* Exon 4 **(Figure 2A)**. Pups were screened using the *AarI* restriction enzyme which cuts at an endogenous restriction site interrupted by the missense mutation **(Figure 2B)**. The presence of a band at 350 bp indicated a mouse carrying the allele encoding *Notch1* EGF6 T232V, referred to as *6f* **(Figure 2C)**.

The *6f/+* founder mouse was sequenced at *Notch1* nt19388 – 19712, which confirmed the presence of the ACC->GTG nucleotide base pair change in one allele **(Figure 2D)**. The founder mouse was backcrossed into the C57BL/6J background for three generations before intercrossing **(Table I)**. Mice bred at Mendelian ratios, and homozygotes were viable and fertile. Digestion of the PCR product with the *AarI* enzyme differentiated heterozygotes from homozygotes by loss of a DNA band at 250 bp **(Figure 2E)**, and sequencing results confirmed that homozygotes showed signal for the GTG substitution only **(Figure 2F)**.

To assess the phenotypic importance of NOTCH1 EGF8 *O*-fucose in either embryonic or postnatal development, we generated *8f* mice in parallel to the *6f* mice. Considering that EGF8 occurs within the ligand binding domain of NOTCH1 **(Figure 1A)** and that a previously published *12f/12f* mouse carrying T466A at EGF12 was embryonic lethal [80, 104], we predicted that the *8f/8f* mice would also be embryonic lethal with classic Notch phenotypes such as loss of somites, heart defects, and impaired vascularization of the yolk sac [80, 104].

After performing homology-directed repair at *Notch1* Exon 6 to generate T311V in NOTCH1 **(Figure 3A)**, we identified *8f* mice by *NIAIV* restriction digest with the presence of a DNA band at 300bp **(Figures 3B** and **3C)**. Sequence results from the *8f*/*N1* founder mouse showed signal for one allele carrying the ACC-> GTG base pair substitution **(Figure 3D)**. After backcrossing into the C57BL/6J background for three generations, *8f*/*N1* mice were intercrossed to generate homozygotes. Considering we predicted that the homozygotes would not complete embryonic development, it was surprising that the *8f/8f* mice bred at normal Mendelian ratios **(Table II)** with no visible abnormalities or effect on fertility **(Figures 3E and 3F)**.

To test if the *8f* mice could be induced to embryonic lethality, we crossed the *8f/8f* mouse with the *12f*/*N1* mouse [83, 104], and although only one cross was performed, roughly half the progeny genotyped at weaning as *8f/12f* **(Supplementary Table SI).** Progeny did not display any visible congenital defects, which suggests that the *12f* mutation was not potent enough to disrupt embryonic development. Next, *8f*/*N1* mice were crossed with mice carrying one WT *Notch1* allele and one allele lacking the region encoding for the NOTCH1 ligand-binding domain *(lbd/N1)*. Among 8 litters, no pups carrying both the *8f* and *lbd* alleles were identified at weaning **(Table III)**, indicating that the *8f* mutation is a partial loss-of-function.

To ensure that the introduced mutations did not affect the trafficking of NOTCH1, we collected thymocytes from *6f/6f* and *8f/8f* mice at 1 month and stained for cell surface NOTCH1 **(Figures 4A - C)**. A slight downward trend in staining was observed in the *8f/8f* thymocytes, which is consistent with previously published *in vitro* data showing that the *8f* mutation caused 10% lower staining of NOTCH1 on the surface of HEK293T cells [69]. Because this reduction in NOTCH1 expression is far lower than the change in levels of activation in these cells (~50% reduction), it is unlikely that the decrease in cell-surface expression is the primary mechanism for lowered levels of NOTCH1 activation in the cell-based system [32].

NOTCH1 and DLL4 are essential for T-cell development, and the *12f* mutation was shown to impede thymocyte development in mice [83]. We therefore performed T-cell analyses on thymocytes from both *6f/6f* and *8f/8f* mice to assess for a change in number of total thymocytes or breakdown of subpopulations. We observed a downward trend in the total number of thymocytes from the *8f/8f* mice but no significant changes in the CD4+ Single Positive, CD8+ Single Positive, Double Positive, or Double Negative T-cell populations. We also observed no changes in the number of *6f/6f* thymocytes **(Supplementary Figure S1)**, which is consistent with our initial prediction because JAG1 is not the dominant ligand in thymic T-cell development [109].

Defects in Vascular Outgrowth of the Retina

Although the importance of *O*-fucosylation and Fringe modification at EGF8 has been demonstrated in the development of the *Drosophila* wing vein [Pandey, 27], it has yet to be studied in a mammalian model, and the influence of EGF6 *in vivo* remains unknown altogether. Postnatal sprouting angiogenesis in the retina is highly sensitive to varying levels of Notch pathway signaling during development of the primary vascular plexus from P0 to P7 [91], which made it an attractive tissue to target our studies.

Mouse retinas were dissected at stage P6, a timepoint when vessels in the retinas are actively sprouting outward from their origins surrounding the optic nerve head [91]. When stained with the vessel marker Isolectin-B4, retinas from WT mice showed normal vascular outgrowth extending from the optic nerve head into the edges of the retinal leaflet [90, 91] **(Figure 5A)**. Using ImageJ to manually outline the area of leaflet occupied by vessel, we found that *6f/6f* retinas showed loss of vascular outgrowth by an average of 30% compared to WT **(Figures 5B and 5D)**. A Sholl mask analysis of vascularity confirmed a decrease in total staining across the leaflet [Refer to methods and 110] **(Figure 5E)**. These results indicate that Notch signaling is dysregulated in the retinal vasculature but cannot distinguish hypermorphic and hypomorphic states [34, 111].

Consistent with the idea that the *8f* mutation disturbs Notch signaling, retinas from *8f/8f* mice at P6 showed a loss of vascular outgrowth at P6 **(Figure 5C and 5F)**. The Sholl Mask analysis showed total loss of IB4 staining across the leaflet **(Figure 5G)** and that staining reached a similar peak density as WT but occurred closer to the optic nerve head **(Supplementary Figures S2C and D)**. This signature differs from the *6f/6f* retinas which reach

peak density at a similar radial distance as WT **(Supplementary Figures S2A and B)**, and the staining across the leaflet is greater in the *8f/8f* retinas **(Figure 5G)** vs. the *6f/6f* retinas **(Figure 5E)**.

Defects in Vascular Layer Development in the Retina

During postnatal development, the superficial plexus is the first layer of the retina to vascularize beginning P0 – P3 [91]. At P7, vertical sprouts emerge downward from the superficial level into the deep layer area where vessels seed and extend radially during P8 – P10. The intermediate space between the superficial and deep layers is primarily occupied by vertical vessel connections until P10 when vessels initiate radial expansion, the final layer to do so. Although the retinal vasculature continues to mature and remodel into adulthood, the three vessel layers are established within the first 16 days [112].

Another feature of dysregulated Notch signaling, either gain-of-function or loss-of-function, is developmental delay in the formation of the intermediate and deep layers [34, 111]. To assess any variances in our mutants, Z-stack images were acquired from the stained retinas at depths standardized to wildtype and oriented to the radial midpoint between the individual sample's angiogenic front and optic nerve head. The presence of stained vessels was identified in each layer in the wildtype samples, including some vessel expansion in the deep layer and unorganized sprouts in the intermediate space **(Figures 6A – C)**. While the intermediate layer appeared to be fragmented with potential connection points and vertical sprouting forming to the deep layer, no staining of the deep layers were observed in either the *6f/6f* **(Figures 6D – 6F)** or *8f/8f* **(Figures 6G – 6I)** samples.

Orthogonal projections representing all Z-stack images reconstruct the 3-dimensional vasculature in the WT retina **(Figure 6J)** and the less mature intermediate and deep layers in the *6f/6f* **(Figure 6K)** and *8f/8f* retinas **(Figure 6L)**. It is worth noting that progression of layer

development is better observed at P9 or P13, however some differences in the mutants can be detected at P6 compared to wildtype.

Changes to Vessel Density in the Retina

Both loss of vessel expansion and delay in 3-dimensional deep layer development are evidence of defective Notch signaling, either Gain-of-Function or Loss-of-Function [34, 94, 111]. To differentiate the two states, we performed a vessel density quantitation over a 300 x 300 mm^2 area using AngioTool v. 0.6a [113]. In a blind study, boxes were drawn one vessel junction inward from the angiogenic front **(Figures 7A – C)**. Vessel density was compiled from five boxes per retina and three retinas per group. Representative results from AngioTool are shown below **(Figures 7D – F)** where the red lines identify vessels, blue dots detect vessel junctions, and yellow define avascular areas.

A significant decrease in vessel density was observed in the *6f/6f* retinas **(Figure 7G)**, followed by a significant decrease in the number of vessel junctions **(Figure 7H)**. Both changes have been observed in published hypermorphs [34], suggesting that the *6f* mutation is hypermorphic. In contrast, there was a significant increase in vessel density observed in *8f/8f* retinas **(Figure 7G)**, a change established in published hypomorphs [94, 111]. This data is further evidence that the *8f* mutation is a partial loss-of-function.

We also performed a double-blind experiment to observe filopodia expression in tip cells across genotypes **(Supplementary Figure S3A-C)**. We calculated the total number of filopodia per sprout point in each image and found the ratio significantly lower in the *6f/6f* samples compared to WT and *8f/8f* **(Supplementary Figure S3D)**. Although we recognize that filopodia are necessary but not sufficient for vascular outgrowth [114], and that vascular outgrowth is primarily determined by the proliferation of stalk cells rather than tip cells [107], we wondered if

manipulating the Notch pathway would result in tip cell morphological changes rather than the quantity, which is already a known Notch phenotype.

Indeed, we measured a loss in efficiency of filopodial sprouting in the tip cells from *6f/6f* retinas, consistent with imbalance of Notch signal. Because we did not observe a similar change in filopodial sprouting in the *8f/8f* retinas which exhibited a similar defect in vascular outgrowth, we hypothesize that this is due to the greater vessel density observed in Notch hypomorphs which may compensate.

Discussion

The retinal angiogenesis model is a well-established readout for NOTCH1 loss-of-function and gain-of-function phenotypes. The push-pull dynamic between JAG1 and DLL4 expressing cells is facilitated by expression of LFNG, MFNG and RFNG which modify *O*-fucose sites on NOTCH1 to reduce activation by JAG1 and enhance activation by DLL4 [34]. Although EGF6 is outside the ligand-binding region, *in vitro* studies identified it as a significant contributor to limiting NOTCH1 activation by JAG1 when the receptor is modified by LFNG or MFNG. The site's primary function appears to be regulatory and not important for trafficking or activation of the receptor [32].

Supporting this idea, our *6f/6f* mice did not show any outward Notch phenotypes or change to viability. Flow cytometry confirmed that staining of cell-surface NOTCH1 on thymocytes was unaffected by the *6f* mutation. When analyzing the retina at P6, we found that vascular outgrowth in the superficial layer was restricted and three-dimensional vascularization was delayed. Both phenotypes have been published in conjunction with either Notch gain-of-function or loss-of-function [34, 94, 111]. To differentiate these, we calculated vessel density at regions adjacent to the angiogenic front. We found that there were fewer vessels and branchpoints similar to the published phenotype from a conditional knockdown of *Jag1* in retinal endothelial cells by *Benedito et al.* [34].

What is most interesting about this finding is that it suggests we limited the ability for JAG1 to regulate signal through NOTCH1 while preserving heightened activation by DLL4. In *Benedito et al.*, the authors also analyzed retinas from *Lfng* -/- mice and observed the opposite phenotype, a gain of vessel density [34], similar to that observed in *Dll4* +/- retinas by *Suchting*

et al. [94]. Within the context of published phenotypes, our *6f/6f* retina is consistent with loss of *Jag1* as opposed to loss of *Lfng*.

We were surprised to find that our *8f/8f* mouse showed no outward Notch defects, considering that the EGF12 T466A (*12f*) homozygote is embryonic lethal [104]. Although the *8f* allele appeared to be a partial loss-of-function, it is not as potent as the *12f* allele, either because the *8f* T/V mutation is more conservative than the *12f* T/A mutation or because the *O*-fucose at EGF12 is more influential than EGF8. Prior studies showed that the EGF12 T466V mutation had a smaller effect on Notch-ligand binding than did the T466A mutation [25], which may explain why of *12f/12f* was lethal while *8f/8f* was not.

What was most striking about the *8f/8f* retina is that it recapitulated the *Lfng -/-* and *Dll4 +/-* phenotypes, as well as that observed *in Eogt -/-* and *Rbpj +/-* retinas by *Sawaguchi et. al* [34, 94, 115]. These authors demonstrated gain of vascular branching and vessel overgrowth consistent with hypomorphic signaling through NOTCH1. Although we measured an increase in vessel density in the *8f/8f* retinas, we did not measure an increase in vessel branching. Given that some vessels in **Figure 7F** appear almost fused together, the most likely reason is that AngioTool is not a sensitive enough software for detecting the extent of vessel clustering and branching. Nonetheless, our data showing a very significant increase in vessel density, in combination with loss of vascular outgrowth and deep layer development, is in agreement with findings from published hypomorphs [34, 111]. The lack of progeny from our *8f/lbd* cross also suggests that the *8f* mutation is a partial loss-of-function.

To summarize both the outcome of our findings and the mechanisms by which they were achieved, **Figure 8** illustrates the role of NOTCH1 *O*-glycans at EGF6 and EGF8 in relation to pathway stimulation and regulation by DLL4 and JAG1 ligands. In brief, loss of pathway

stimulation by Fringe-enhanced DLL4-NOTCH1 signal from tip cell to stalk cell causes incomplete activation of the pathway in stalk cells. We observed phenotypes in *8f/8f* mice identified in known hypomorphs such as impaired vascular outgrowth, delay in three-dimensional development, and gain of vessel density. Reciprically, loss of pathway regulation by Fringe-suppressed JAG1-NOTCH1 signal from stalk cell in return to the originating tip cell causes destabilization of the tip cell fate. Phenotypes characterized in known hypermorphs such as reduced vascular outgrowth, delay in deep layer development, and lower vessel density were observed in our *6f/6f* mice.

We recognize the need for future experiments to better address changes in cellular activity, such as staining for cell proliferation and cell cycle markers p-ERK and p21 [116] known to be regulated by Notch *in vivo*. In this study we demonstrate that the *6f/6f* line is hypermorphic, and further inquiry into the transcriptional consequences of uncoupling feedback inhibition of Notch during angiogenesis is a worthy pursuit.

Mouse Line Generation and Breeding

All animal work was conducted according to relevant national and international guidelines and under approved protocols at the University of Georgia. The animal studies were approved by the Institutional Animal Care and Use and Committee (IACUC), which followed all of the guidelines outlined in: Public Health Service Policy on Humane Care and Use of Laboratory Animals, distributed by the National Institutes of Health's Office of Laboratory Animal Welfare; Animal Welfare Act and Animal Welfare Regulations, distributed by the United States Department of Agriculture; and Public Health Service Policy on Humane Care and Use of Laboratory Animals, distributed by the Office of Laboratory Animal Welfare, NIH; Animal Welfare Act and Animal Welfare Regulations distributed by United States Department of Agriculture and Guide for the Care and Use of Laboratory Animals distributed by the National Research Council.

The *6f* and *8f* heterozygous mice were generated at the Emory University Mouse Transgenic and Gene Targeting Core (https://www.cores.emory.edu/tmf/index.html) using C57BL/6J mice. The founder mice were backcrossed three generations to wild type C57BL/6J mice at the University of Georgia before beginning phenotypic analysis.

The *12f/N1* [83, 104] and *lbd/N1* [80] mice were generously supplied by Dr. Pamela Stanley (Albert Einstein College of Medicine).

Genotyping

Tail clips were lysed in 100 µl MGB Lysis Buffer containing 65 mM $MgCl_2$, 166 mM $(NH_4)_2SO_2$, 670 mM Tris-HCl pH 8.8, 10mM DTT, and 0.5% Triton X-100 by denaturing at 90°C for 10 min. Samples were spun down and cooled to RT followed by incubation with 2 µg Proteinase-K O/N at 55°C. Lysates were heat inactivated at 95°C for 20 min, spun down and stored in -80°C. For PCR, lysates were thawed on ice and spun down at 15,000g for 10 min. DNA samples were collected from the supernatants. PCR reactions were performed in 25 µl reaction volumes containing 2.5 U OneTaq Polymerase (NEB cat. no. M0480L), 0.4 µM primer pairs, 0.2mM dNTP, 2mM Mg^{2+}, and 1µl DNA in OneTaq buffer. See **Supplementary Table SII** for a list of primers used to genotype each mouse line. Refer to Ge and Stanley 2008 and Ge, Liu et al. 2008 for details on the genetic composition of the *12f* and *lbd* alleles for genotyping the lines [80, 83]. The thermocycler protocol started with denaturing at 95°C for 5 min, followed by 34 cycles of denaturing at 95°C for 30 sec, annealing at 62°C for 30 sec, and extension at 72°C for 1 min. Final extension was performed at 72°C for 5 min, and the reaction was kept at 4°C until restriction digest and analysis by SDS-PAGE. For restriction digest of the *6f* allele, 10 µl PCR product was incubated in 19 µl AarI Buffer containing 1 µl AarI enzyme (Thermo cat. no. ER1581) O/N in 37°C water bath. For the *8f* allele, 5 µl PCR product was incubated in 14 µl CutSmart Buffer containing 1 µl NIaIV enzyme (NEB cat. no. R0126S) in a 37°C water bath for 1 h.

Antibodies

For immunophenotyping T-cell populations: 1:200 anti-CD4 PE (BioLegend cat. #100512), 1:200 anti-CD8a APC (BioLegend cat. #100712), 1:125 anti-CD25 PerCP (BioLegend cat.

#102028), and 1:200 anti-CD44 APC-Cy7 (BioLegend cat. #103028). For cell surface staining of NOTCH1: 1:100 anti-IgG PE (BioLegend MOPC-21) isotype control or 1:100 anti-mouse NOTCH1 PE (BioLegend HMN1-12). For retina staining: 1:500 Isolectin GS-IB4 Alexa-Fluor 488 (Invitrogen cat. #I21411)

Flow Cytometry

Thymocytes were collected from fresh thymus strained through a 70 mm cell strainer (CELLTREAT cat. no. 229483) into cold FACS Buffer (2% FBS/PBS, 0.05% NaN_3). Cells were spun at 400 g for 7 min and resuspended in ACK Lysis Buffer (Thermo Fisher Scientific cat. no. A1049201) for 2 min. Cells were spun again at 400 g for 7 min, resuspended in FACS buffer, and counted. Three million cells were collected and blocked in 100 ml blocking solution containing 3 ml CD16/32 Fc antibody (BioLegend cat. 101319) in FACS buffer at room temperature for 10 min. 100 ml primary antibody in FACS buffer was added for a final antibody dilution relative to 200 ml total solution and incubated at room temperature for 20 min. Finally, cells were collected by centrifugation and resuspended in 500 ml FACS buffer for detection by the Quanteon (Agilent) owned by the University of Georgia Center for Tropical and Emerging Diseases. 100,000 events were counted, and FlowJo analysis software v. 10.8.1 was used to compensate fluorescence, gate cell populations, and calculate positive events.

Retina Collection

Immediately post-euthanasia with secondary method, eyes were removed and fixed in for 20 minutes 4% PFA (Electron Microscopy Sciences 15710) at room temperature, then washed and stored in ice cold PBS for at least 10 minutes prior to dissection. Eyes were dissected following

the protocol from from *Tual-Chalot et al.* [117]. In short, mouse eyes were opened via small incision just below the limbal region, allowing the removal of the anterior part of the eye. The lens was removed, followed by carefully disloging the Haloid Vessels. The sclera and the retinal pigment epithelial cell layer were gently separated from the retinal cup, which was opened by 4 small incisions allowing the formation of the retinal flatmount containing four leaflets. Flatmounts were further fixed and stored in -20C until further processing for immunofluorescence analysis.

Immunostaining

Fixed retinas were washed in 1x in PBS for 5 min with gentle rocking and 2x in PBS-T (0.3% Triton X-100 in PBS) and blocked in 1x PBS-T/5% Goat Serum/0.2% BSA for at least 1 hr at room temperature with gentle rocking. Primary antibody Isolectin GS-IB4 Alexa-Fluor 488 (Invitrogen cat. #I21411) was diluted 1:500 in blocking buffer, the dish covered in tin foil and incubated at 4°C with gentle rocking overnight. Retinas were washed 4x with 1x PBS-T at room temperature with gentle rocking for 15 min, followed by a final wash of 1x PBS before retinas were mounted using ProLong^{TM} Gold antifade mountant (ThermoFisher cat. #P36930), cured at room temperature overnight and stored at 4°C.

Imaging and retinal analysis

Mounted retinas were imaged using a Zeiss LSM 800 2 channel GaAsP confocal microscope with Axiocam 506, and 20x/0.8 M27 objective. Tiled 100-120 x confocal sections of 169 µm stitched using Zen blue software with additional tile/position, Dynamic physiology modules. For z-stacked confocal sections using a 63x/1.4 Oil DIC M27 objective, 1024x1024 frames size with

continuous 0.5µm z-stack slices (30-50µm depth) were collected. For extraction of the superficial (s), intermediate (i), or deep (d) vascular layers, z-positions were set for the wt s, i, and d, and comparable sections were extracted from 6f/6f and 8f/8f retina from 3 independent repeats. Confocal Z-stack imaging for tip cells collected as stated above, Z-slices displayed as an X-Y orthogonal-projection. Retinal vascular complexity was calculated as previously described [118] . Briefly, optically sectioned images of retina flat mounts were analyzed using FIJI. Images were filtered using a multiscale adaptive enhancement filter. Semiautomated network tracing was carried out on filtered images using APP-2.0. The resulting network trace was used to mask the retinal vasculature into a binary image. The binary image was analyzed using 2-D Sholl analysis for each image plane in FIJI. The number of intersections as a function of radius was normalized by the area of the circle for each focal plane.

Vascular coverage of retinal leaflets was calculated by image tracing the inner edge of the vascular front and the outer edge of the leaflet in ImageJ [119] and measuring the areas.

Retinal vascular networks were processed for automated network tracing using AngioTool (NCI) [113]. Samples were scrambled and blinded for a third party to select five 300 x 300-pixel areas at the angiogenic front from each retina. Selection areas were exported as .png files and uploaded to AngioTool for blind processing. Analysis parameters were visually modified for accurate skeletonization. Controls were set to a low threshold of 15, high threshold of 255, and vessel diameter of 15 and to fill holes at 2000. Output metrics included vessel percentage area, total number of junctions, junction density, total vessel length, average vessel length, total number of endpoints, and mean lacunarity.

Acknowledgements

This work was supported by a NIH grant GM061126 to R.S.H and the Georgia Research Alliance. R.K.L. was partially supported by NIH grant T32 GM107004.

Tables

Table 2.I *6f/6f* mice were viable and fertile

6f/N1 founder mouse carrying the EGF6 Thr to Val (*6f*) mutant allele was backcrossed for three generations and intercrossed to produce homozygotes. Mice were genotyped at weaning, and a Chi-Squared analysis was performed to detect deviations in Mendelian inheritance. A P-value < 0.05 was considered significant.

Cross Type	**No. of litters**	**Avg. Litter Size**	**Progeny**	**Expected %**	**Observed %**	χ^2	**Significance**
6f/N1 x WT	8	7.8	*6f/N1*: 24 WT: 30	*6f/N1*: 50% WT: 50%	*6f/N1*: 44.5% WT: 55.6%	Df=1 $\chi2 = 0.3$ $p = 0.6$	n.s.
6f/N1 x *6f/N1*	3	7.0	*6f/N1*: 12 WT: 3 *6f/6f*: 6	*6f/N1*: 50% WT: 25% *6f/6f*: 25%	*6f/N1*: 57.1% WT: 14.3% *6f/6f*: 28.6%	Df=2 $\chi2 = 0.6$ $p = 0.7$	n.s.
6f/6f x *6f/6f*	9	7.6	*6f/6f*: 68	*6f/6f*: 100%	*6f/6f*: 100%	---	---

Table 2.II *8f/8f* mice were viable and fertile

8f/N1 founder mouse carrying the EGF8 Thr to Val (*8f*) mutant allele was backcrossed for three generations and intercrossed to produce homozygotes. Mice were genotyped at weaning, and a Chi-Squared analysis was performed to detect deviations in Mendelian inheritance. A P-value < 0.05 was considered significant.

Cross Type	No. of litters	Avg. Litter Size	Progeny	Expected %	Observed %	χ^2	Significance
8f/N1 x *WT*	5	7.6	*8f*/N1: 23 WT: 15	*8f*/N1: 50% WT: 50%	*8f*/N1: 60.5% WT: 39.5%	Df=1 $\chi 2 = 0.9$ $p = 0.4$	n.s.
8f/N1 x *8f/N1*	19	6.3	*8f*/N1: 65 WT: 26 *8f/8f*: 15	*8f*/N1: 50% WT: 25% *8f/8f*: 25%	*8f*/N1: 61.3% WT: 24.5% *8f/8f*: 14.2%	Df=2 $\chi 2 = 4.7$ $p = 0.1$	n.s.
8f/8f x *8f/8f*	5	8.6	*8f/8f*: 43	*8f/8f*: 100%	*8f/8f*: 100%	---	---

Table 2.III. *8f/lbd* mice did not survive to weaning

A het cross was performed to assess the number of progeny at weaning carrying both *8f* and *lbd* alleles. A Chi-Squared analysis was performed to detect deviations in Mendelian inheritance where level of significance was defined by: $p < 0.05$ *, $p < 0.03$ ** and $p < 0.01$ ***

Cross Type	No. of litters	Avg. Litter Size	Progeny	Expected %	Observed %	χ^2	Significance
8f/N1 x *lbd/N1*	8	5.9	*8f/N1*: 18 WT: 22 *lbd/N1*: 7 *8f/lbd*: 0	*8f/N1*: 25% WT: 25% *lbd/N1*: 25% *8f/lbd*: 25%	*8f/N1*: 38.2% WT: 46.8% *lbd/N1*: 14.9% *8f/lbd*: 0%	Df = 3 $\chi 2 = 16.5$ $p = 0.001$	***

Figure Legends

Figure 2.1. *O*-glycosylation of NOTCH1 EGF repeats is important for signaling by ligands JAG1 and DLL1

(A) *O*-fucose modifications (red triangle) on EGF6 and 8 play important roles in NOTCH1 activity. Fringe adds GlcNAc (blue square) to *O*-Fucose, which can be further modified with a Galactose (yellow circle). EGF repeats in NOTCH1, DLL4 and JAG1 are denoted by ovals. Note that many other EGF repeats are modified by *O*-fucose, but only modifications on EGF6 and 8 are shown for simplicity [32]. **(B)** Cartoon of an EGF repeat showing the conserved disulfide bonding pattern between the six conserved cysteines as well as the *O*-fucose consensus sequence between Cys 2 and 3 where X represents any amino acid, and a T/V substitution prevents *O*-fucosylation by POFUT1.

Figure 2.2. *6f* mice were generated by CRISPR/Cas9 homology-directed repair

(A) Donor template (in box), sgRNA (bold), and nucleotide base pair change ACC->GTG (red) for CRISPR/Cas9 HDR in the C57BL/6J background at Exon 4 of mouse *Notch1* nt19507-19510 for expression of NOTCH1 EGF6 T232V. **(B)** Restriction digest with *AarI* enzyme to identify *6f/N1* progeny containing band at 350 bp. **(C)** DNA gel showing digested PCR product from WT and *6f* het mice with band at 350 bp indicating presence of *6f* allele. **(D)** Sequencing of *6f/N1* Founder at mouse *Notch1* Exon 4 nt19388 – 19712 spanning EGF6 ACC->GTG knock-in mutation. **(E)** *AarI* restriction digest of intercrossed mice following three generations of backcrossing showing that homozygotes lack a band at 250 bp. **(F)** Sequencing of *6f/6f* showing two alleles containing the EGF6 ACC->GTG knock-in mutation.

Figure 2.3. *8f* mice were generated by CRISPR/Cas9 homology-directed repair

(A) Donor template (in box), sgRNA (bold), and nucleotide base pair change ACC->GTG (in red) for CRISPR/Cas9 HDR in the C57BL/6J background at Exon 6 of mouse *Notch1* gene for expression of NOTCH1 EGF8 T311V. **(B)** Map of the PCR product when digested with *NIAIV* restriction enzyme to identify *8f/N1* progeny. **(C)** DNA gel shows band at 300 bp in progeny carrying the *8f* allele. **(D)** Sequencing of *8f/N1* Founder at mouse *Notch1* Exon 6 nt22507 – 22826 spanning EGF8 ACC->GTG knock-in mutation. **(E)** *NIAIV* restriction digest of intercrossed mice following three generations of backcrossing showing that homozygotes lack a band at 200 bp compared to heterozygotes and wildtype. **(F)** Sequencing of *8f/8f* mouse showing two alleles containing the EGF8 ACC->GTG knock-in mutation.

Figure 2.4. NOTCH1 expression on the cell surface of *6f/6f* thymocytes was unchanged but slightly reduced on *8f/8f* thymocytes

(A) Cell surface staining of thymocytes with anti-NOTCH1 PE D1E11 (Cell Signaling Technology) or isotype control and **(B)** quantitation of Mean Fluorescence Intensity (MFI) showing significant differences between isotype control and antibody. Increased isotype MFI for *8f/8f* is due to performing this analysis on a different day than the WT and *6f/6f* samples. **(C)** Relative Mean Fluorescence Intensity (MFI) quantitation from *6f/6f* and *8f/8f* thymocytes compared to WT. Independent T-tests were performed on results from 4 mice. P-value <0.05 was considered significant.

Figure 2.5. Vascular outgrowth was reduced in *6f/6f* and *8f/8f* retinas

Retinas from P6 WT (N=5) **(A)**, *6f/6f* (N=7) **(B)**, and *8f/8f* (N=3) **(C)** mice stained with Isolectin-B4 (green). Scale bars represent 500 mm. **(D)** Vascular outgrowth from *6f/6f* and WT retinas represented by percent % coverage was calculated by manually tracing the edges of inner leaflets and outer leaflets (yellow dashed line) and measuring the areas in ImageJ. **(E)** Sholl Mask Analysis graphing average pixels of positive IB4 staining (y-axis) from *6f/6f* retinas compared to WT across the leaflets measured by radial steps (x-axis) from the origin. **(F)** Percent % coverage in *8f/8f* retinas compared to WT. **(G)** Sholl Mask Analysis graphing average of *8f/8f* retinas compared to WT. Peak IB4 staining and corresponding radial step are noted. The area under the curve analysis was performed in GraphPad Prism with the curve of average values from the Sholl analysis, and non-overlapping areas within a 95% CI were considered significantly different. Each genotype was compared to WT through an independent T-test of compiled sample percentages. Three asterisks *** represent a P-value <0.01, two asterisks ** represent a P-value <0.03, and one asterisk * represents a P-value <0.05.

Figure 2.6. Intermediate and deep layer development was reduced in *6f/6f* and *8f/8f* retinas

P6 Retinas stained with IB4 were imaged in Z-stacks from the superficial layer to the Intermediate and Deep layers. **(A - C)** Representative images from WT (N=3), **(D - F)** *6f/6f* (N=3), and **(G-I)** *8f/8f* (N=3). Scale bars represent 20 mm. **(J – L)** Orthogonal projections of Z-stack images collected from the Superficial “S” through the Intermediate “I” and Deep “D” layers of the retina. **(J)** Representative projection from P6 WT **(K),** *6f/6f* **(L)** and *8f/8f* retinas stained with IB4. Scale bars represent 20 mm.

Figure 2.7. Vascular density was reduced in *6f/6f* retinas but enhanced in *8f/8f* retinas

Retinas from P6 WT (N=3) **(A)**, *6f/6f* (N=3) **(B)**, and *8f/8f* (N=3) mice **(C)** were stained with Isolectin-B4 (green) and five 300 mm x 300 mm areas were drawn blind at the angiogenic fronts. **(D – F)** Selected areas were blindly processed with AngioTool for analysis of vessels (red traces), percent vascularity (area excluding yellow circles) and number of junction points (blue circles). **(F)** Calculation of percent vascularity as described in Materials and methods. **(G)** Calculation of the number of vessel junctions. A T-test was performed to compare density between samples. Four asterisks **** represents a P-value <0.005 Three asterisks *** represents a P-value <0.01, two asterisks ** represents a P-value <0.03, and one asterisk * represents a P-value <0.05.

Figure 2.8. Fringe modification of key *O*-fucose sites at EGF6 and EGF8 in NOTCH1 significantly influences angiogenesis in opposing directions

A model depicting NOTCH1 *O*-fucose sites where a red triangle represents Fucose, a blue square represents GlcNAc, a yellow circle represents Galactose, and X represents knockout of glycan function in either enhancing NOTCH1 activation by DLL4 or inhibiting activation by JAG1. Conservative amino acid point mutations at EGFs 6 and 8 eliminate the Fringe effect asymmetrically. Because angiogenic development is a balancing act between the tip cell fate and stalk cell fate that is patterned by a negative feedback loop of alternating *Dll4* and *Jag1* expression and maintained by broad expression of *Lfng*, *Mfng*, and *Rfng*, the Fringe effect is required in both directions for proper vessel networking. Loss of pathway regulation by Fringe-suppressed JAG1-NOTCH1 signal from stalk cell to tip cell caused by gain-of-function mutation at EGF6 leads to lower vascular outgrowth, vessel density, and branching. In the other direction,

loss of pathway strength by Fringe-enhanced DLL4-NOTCH1 signal from tip cell to stalk cell caused by loss-of-function mutation at EGF8 leads to lower vascular outgrowth and higher vessel density.

Figure 2.1

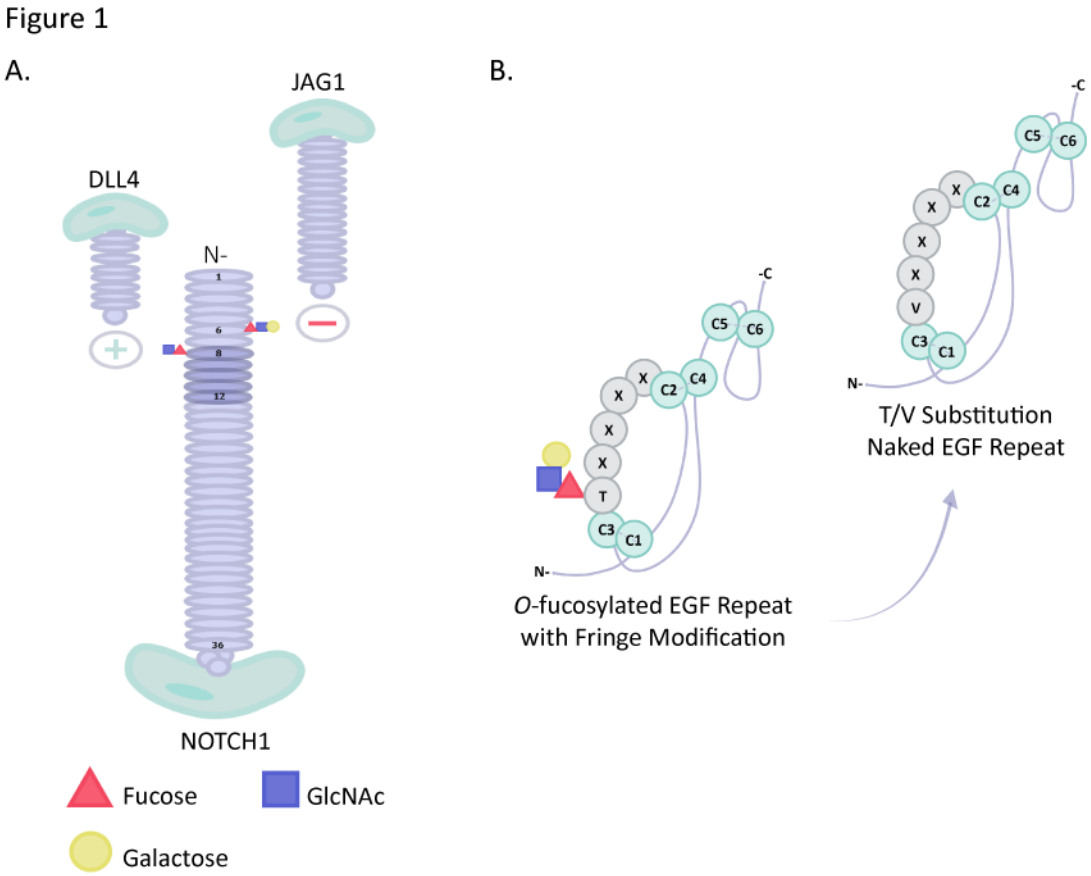
Figure 1
A.
JAG1
DLL4
N-
1
6
8
12
36
NOTCH1
Fucose
GlcNAc
Galactose
B.
-C
C5
C6
X
X
C2
C4
X
X
X
T
C3
C1
N-
O-fucosylated EGF Repeat
with Fringe Modification
-C
C5
C6
X
X
C2
C4
X
X
X
V
C3
C1
N-
T/V Substitution
Naked EGF Repeat

Figure 2.2

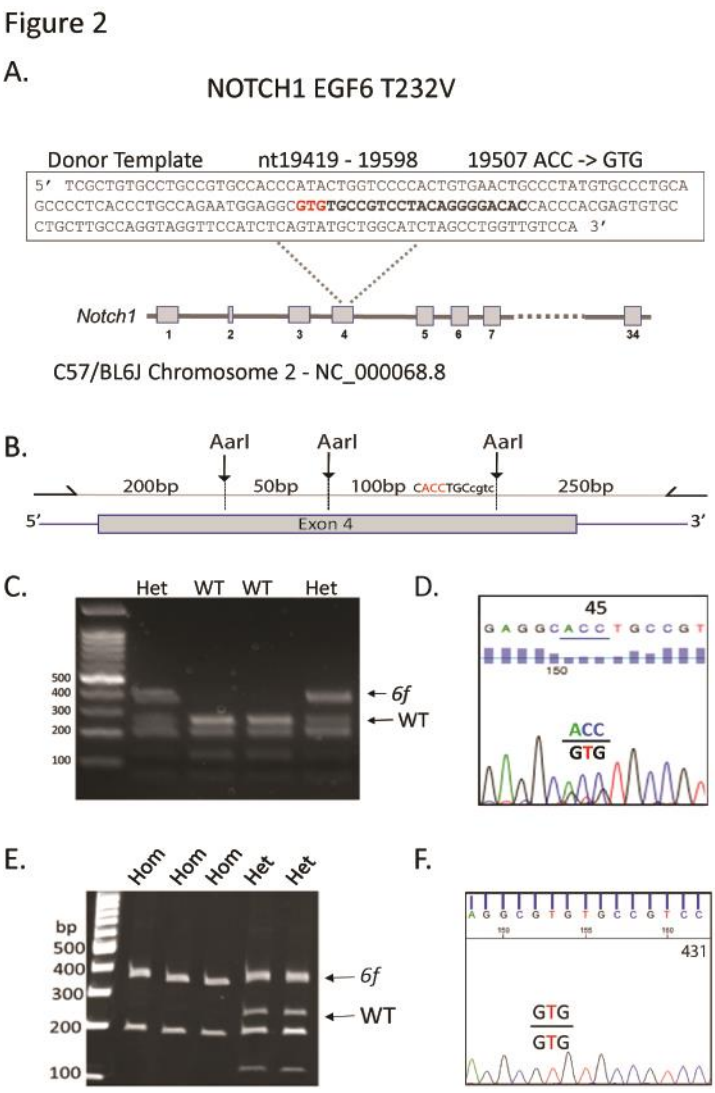
Figure 2
A.
NOTCH1 EGF6 T232V
Donor Template
nt19419 - 19598
19507 ACC -> GTG
5′ TCGCTGTGCCTGCCGTGCCACCCATACTGGTCCCCACTGTGAACTGCCCTATGTGCCCTGCA
GCCCCTCACCCTGCCAGAATGGAGGCGTGTGCCGTCCTACAGGGGACACCACCCACGAGTGTGC
CTGCTTGCCAGGTAGGTTCCATCTCAGTATGCTGGCATCTAGCCTGGTTGTCCA 3′
Notch1
1
2
3
4
5
6
7
34
C57/BL6J Chromosome 2 - NC_000068.8
B.
AarI
AarI
AarI
200bp
50bp
100bp CACCTGCCgtc
250bp
5′
Exon 4
3′
C.
Het
WT
WT
Het
500
400
300
200
100
6f
WT
D.
45
GAGGCACCTGCCGT
150
ACC
GTG
E.
Hom
Hom
Hom
Het
Het
bp
500
400
300
200
100
6f
WT
F.
AGGCGTGTGCCGTCC
150
155
160
431
GTG
GTG

Figure 2.3

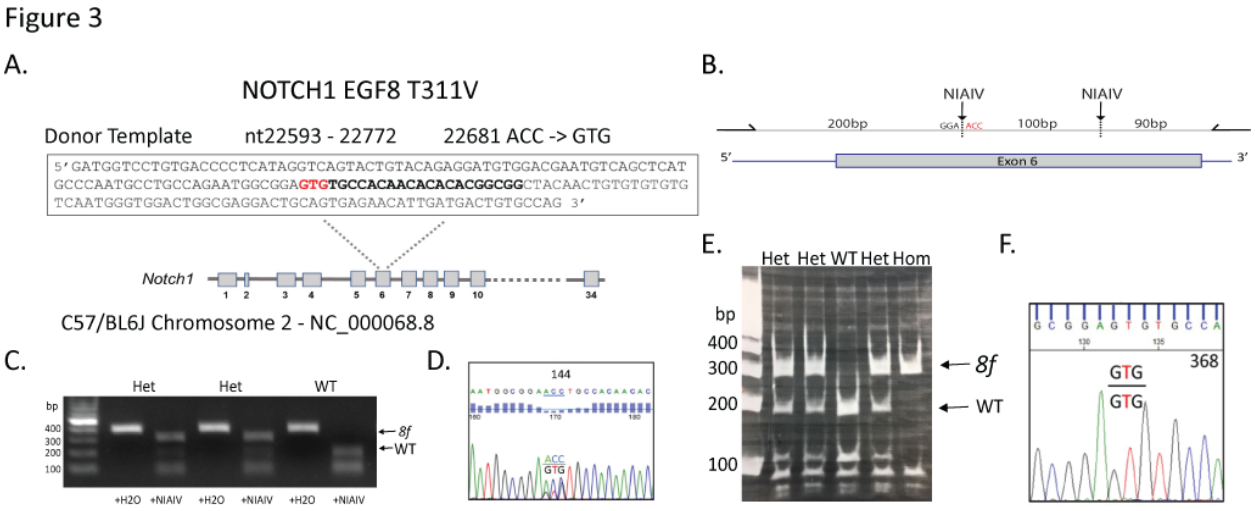
Figure 3
A.
NOTCH1 EGF8 T311V
Donor Template
nt22593 - 22772
22681 ACC -> GTG
5′ GATGGTCCTGTGACCCCTCATAGGTCAGTACTGTACAGAGGATGTGGACGAATGTCAGCTCAT
GCCCAATGCCTGCCAGAATGGCGGAGTGTGCCACAACACACACGGCGGCTACAACTGTGTGTGTG
TCAATGGGTGGACTGGCGAGGACTGCAGTGAGAACATTGATGACTGTGCCAG 3′
Notch1
1 2 3 4 5 6 7 8 9 10 34
C57/BL6J Chromosome 2 - NC_000068.8
B.
NIAIV
NIAIV
200bp
100bp
90bp
5′
Exon 6
3′
C.
Het
Het
WT
bp
400
300
200
100
8f
WT
+H2O +NIAIV +H2O +NIAIV +H2O +NIAIV
D.
144
ACC
GTG
E.
Het Het WT Het Hom
bp
400
300
200
100
8f
WT
F.
368
GTG
GTG

Figure 2.4

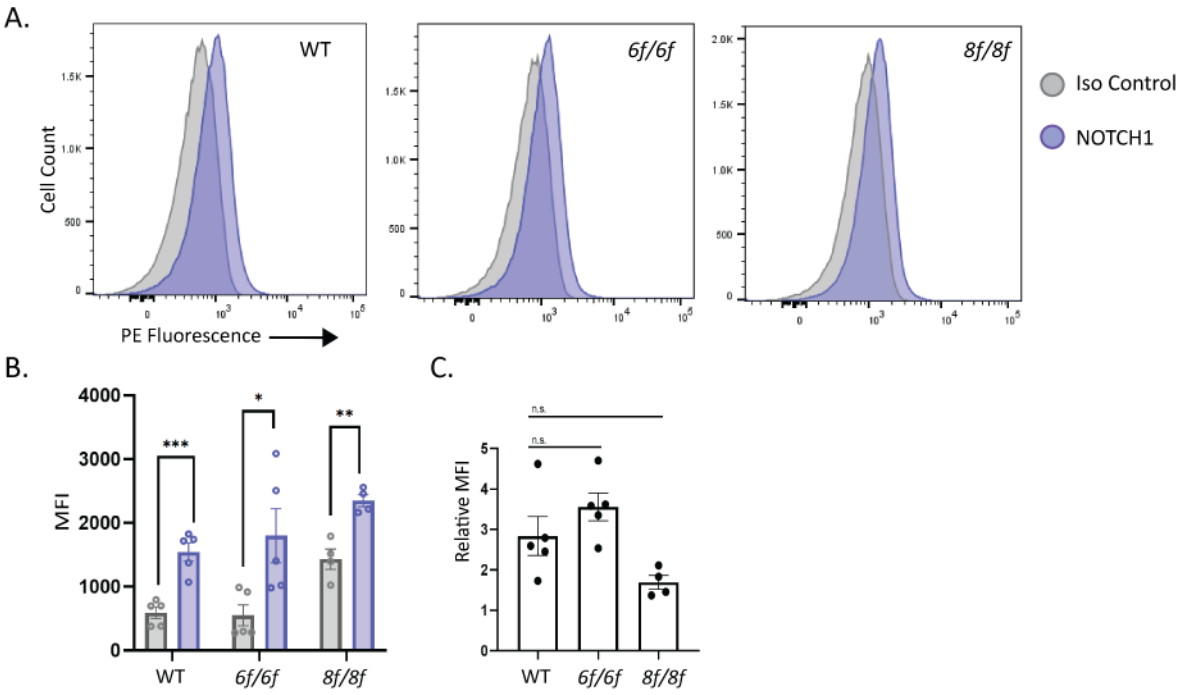
Figure 4
A.
WT
6f/6f
8f/8f
Cell Count
PE Fluorescence
Iso Control
NOTCH1
B.
MFI
***
*
**
WT
6f/6f
8f/8f
C.
Relative MFI
n.s.
n.s.
WT
6f/6f
8f/8f

Figure 2.5

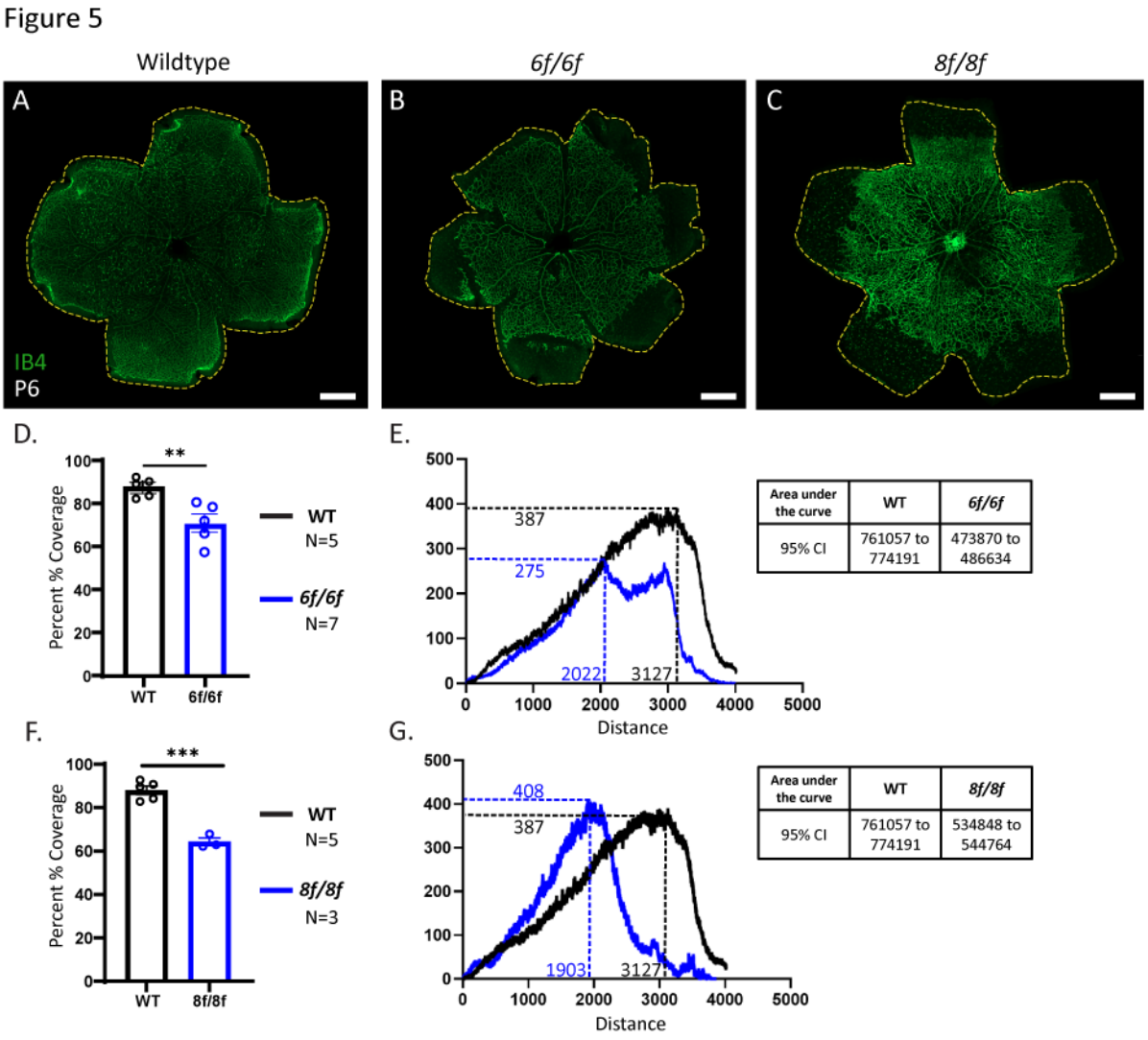
Figure 5
Wildtype
6f/6f
8f/8f
A
B
C
IB4
P6
D.
Percent % Coverage
**
WT
N=5
6f/6f
N=7
WT
6f/6f
E.
387
275
2022
3127
Distance
Area under the curve
WT
6f/6f
95% CI
761057 to 774191
473870 to 486634
F.
***
WT
N=5
8f/8f
N=3
WT
8f/8f
G.
408
387
1903
3127
Distance
Area under the curve
WT
8f/8f
95% CI
761057 to 774191
534848 to 544764

Figure 2.6

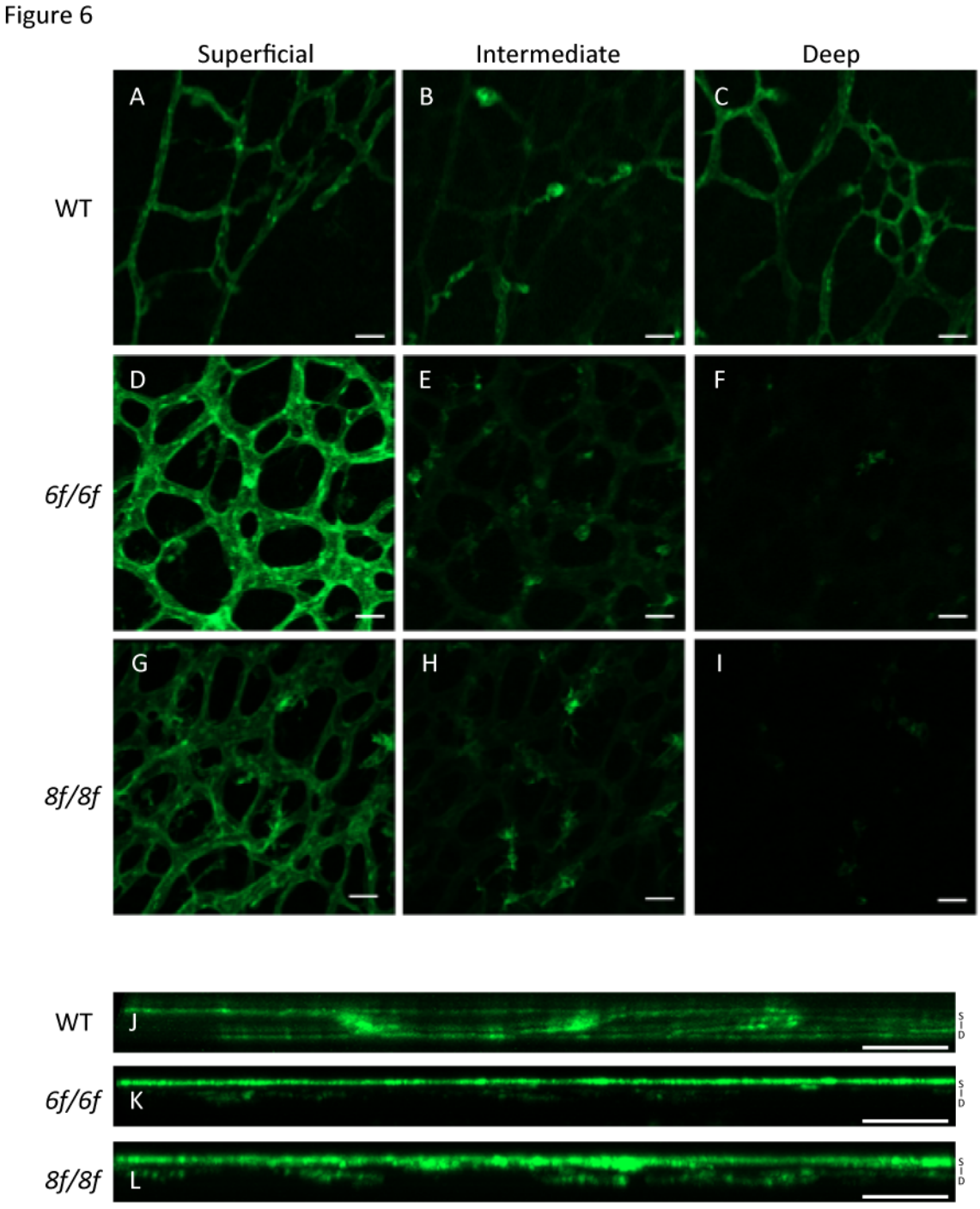
Figure 6
Superficial
Intermediate
Deep
A
B
C
WT
D
E
F
6f/6f
G
H
I
8f/8f
WT
J
6f/6f
K
8f/8f
L
S
I
D

Figure 2.7

Figure 7

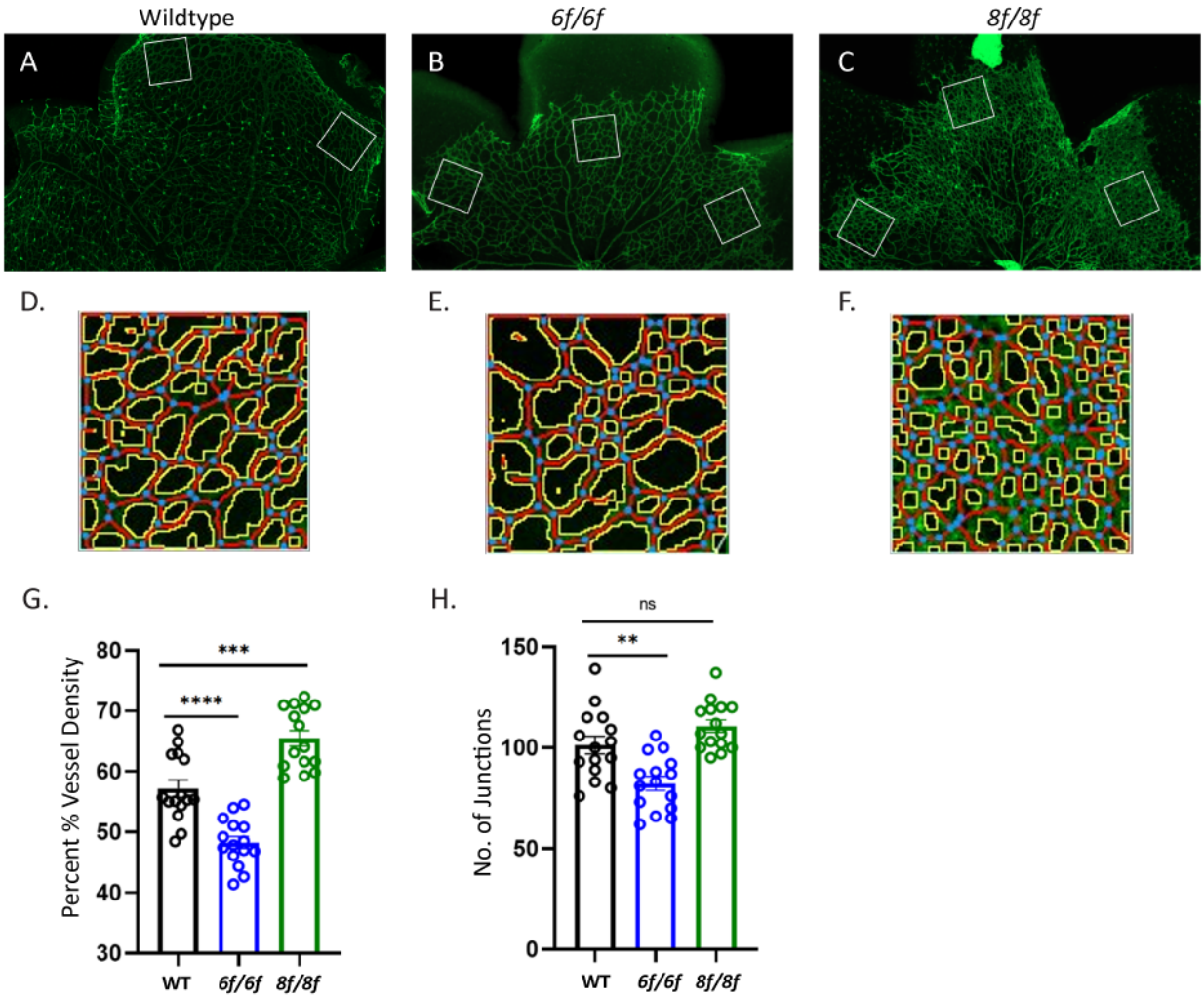

Figure 2.8

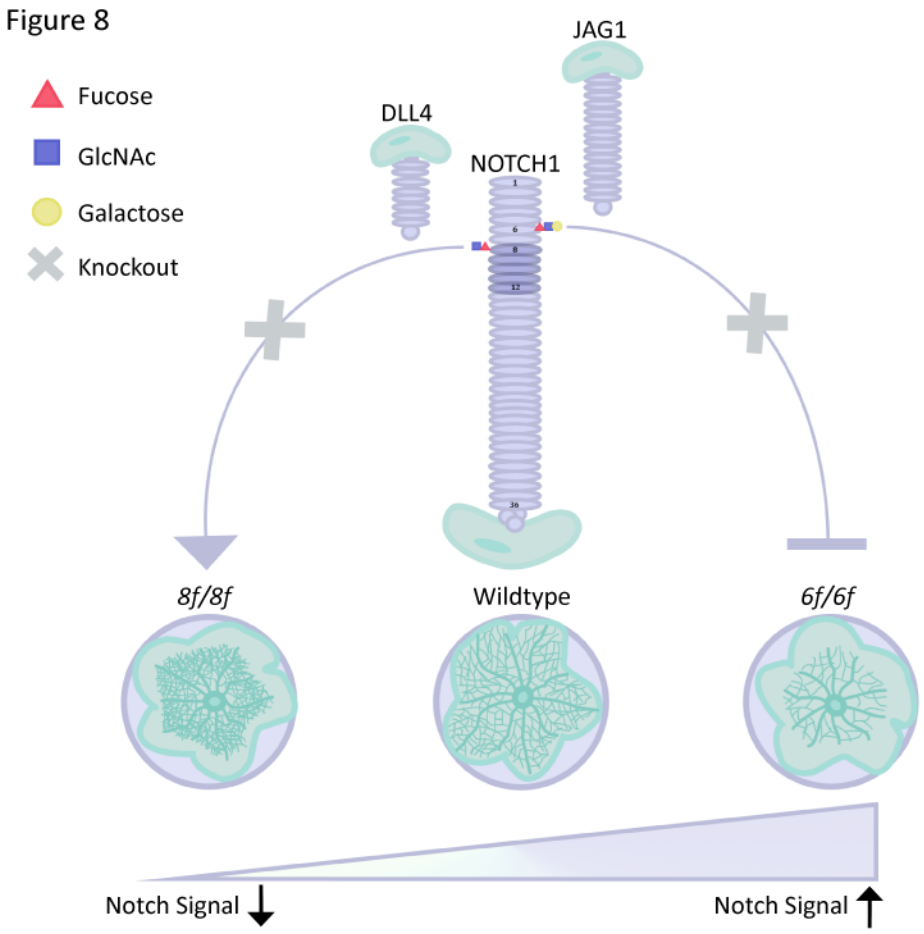
Figure 8
Fucose
GlcNAc
Galactose
Knockout
JAG1
DLL4
NOTCH1
8f/8f
Wildtype
6f/6f
Notch Signal
Notch Signal

Supplementary Table SI.

Cross Type	No. of litters	Avg. Litter Size	Progeny	Expected %	Observed %	χ^2	Significance
8f/8f x *12f/N1*	2	6	*8f/N1*: 8 *8f/12f*: 4	*8f/N1*: 50% *8f/12f*: 50%	*8f/N1*: 67% *8f/12f*: 33%	Df = 1 $\chi 2 = 0.7$ $p = 0.4$	n.s.

Supplementary Table SI. *8f/12f* mice survived until weaning
A cross was performed between *8f/8f* and *N1/12f* mice. Mice carrying both alleles were observed at weaning and showed no gross abnormalities.

Supplementary Table SII.

Allele	Forward Primer	Reverse Primer
6f	5' TCCAAATCTGCCCTGGGTTC 3'	5' AGTGTCCCCTCACTTCTGGT 3'
8f	5' CCAGCACTGAGCCATACAGGAGCTAGCATTCTGG 3'	5' CCTTCTCCCAGGACATTCCTGCACCGACTTACC 3'
lbd	5' GTATGTATATGGGACTTGTAGGCAG 3'	5' CTTCATAACCTGTGGACGGGAG 3'
12f	5' GTCAGTACTGTACAGAGGATGTGG 3'	5' GCATACATATGCATTGGAACTCCC 3'

Supplementary Table SII. Primer Sequences for Genotyping
Forward and reverse primers are listed for genotyping mice carrying the *6f*, *8f*, *lbd*, and *12f* alleles.

Supplementary Figures:

Supplementary Figure S1.

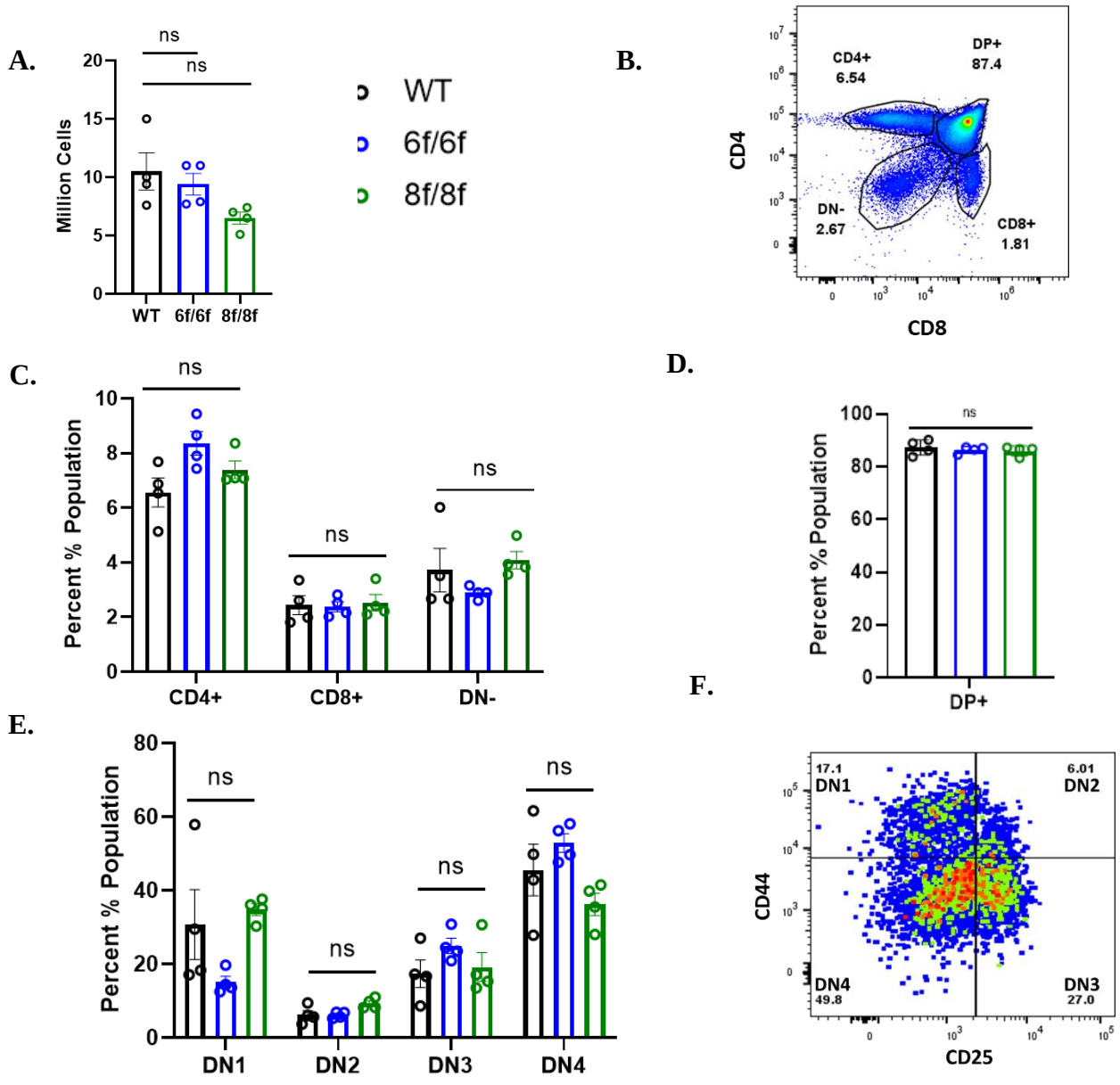

Supplementary Figure S1. T-cell development was not significantly affected in *6f/6f* or *8f/8f* mice, although there is a downward trend in total number of thymocytes from *8f/8f* mice. T-cell analysis was performed as described in Materials and methods. **(A)** The average number of thymocytes in one lobe of thymus from WT (n=4), *6f/6f* (n=4), and *8f/8f* (n=4) mice were calculated before staining with the T cell markers CD4, CD8, CD44, and CD25. **(B)** Representative plot showing gating of CD4+, CD8+, DN-, and DP+ cell populations **(C)** Distribution of single positive and double negative populations graphed by percent % population **(D)** Percent % Population of cells identified as double positive by CD4/CD8 markers (DP+) **(E)**

The DN- population of thymocytes were analyzed for changes in the DN1 to DN4 transition by markers CD44 and CD25 **(F)** Representative plot shows gating for DN1, DN2, DN3, and DN4 cell populations by CD44/CD25 staining. Independent T-tests were performed to compare values from mutants and WT. Three asterisks *** represents a P-value <0.01, two asterisks ** represents a P-value <0.03, and one asterisk * represents a P-value <0.05.; n.s., not significant.

Supplementary Figure S2.

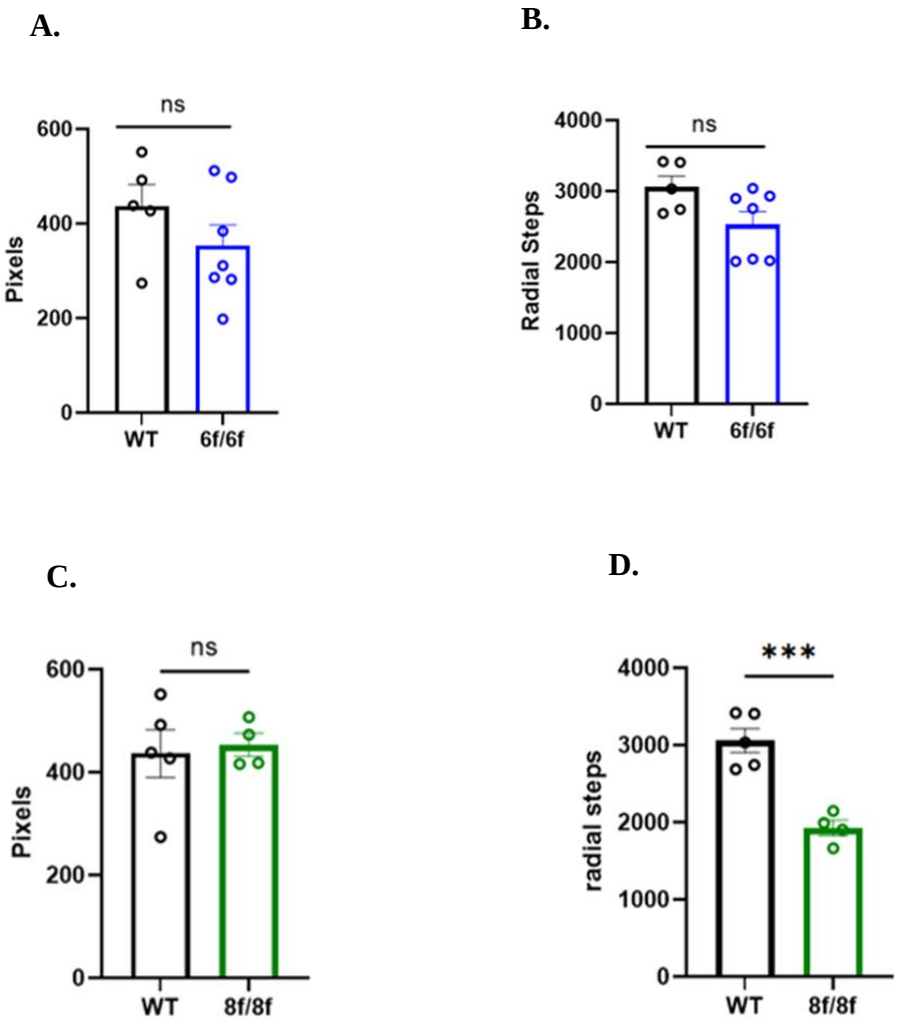

Supplementary Figure S2. Additional quantitation of Sholl mask analysis shows that *6f/6f* retinas reach similar peak staining at similar distance as WT and that *8f/8f* retinas reach comparable peak density closer to the optic nerve head than WT. Additional quantitation from the Sholl mask image analysis, parameters for peak staining and the radial steps from the optic nerve head at which peak staining is achieved as described in Materials and methods. **(A)** Change in *6f/6f* peak density compared to WT. **(B)** Distance from optic nerve head at which peak staining is achieved in *6f/6f* retinas compared to WT. **(C)** Difference in peak staining in *8f/8f* retinas compared to WT. **(D)** Distance from the optic nerve head at which peak staining is achieved in *8f/8f* retinas compared to WT. Independent T-tests were performed to compare values from mutants to WT. Three asterisks *** represents a P-value <0.01, two asterisks ** represents a P-value <0.03, and one asterisk * represents a P-value <0.05.; n.s., not significant.

Supplementary Figure S3:

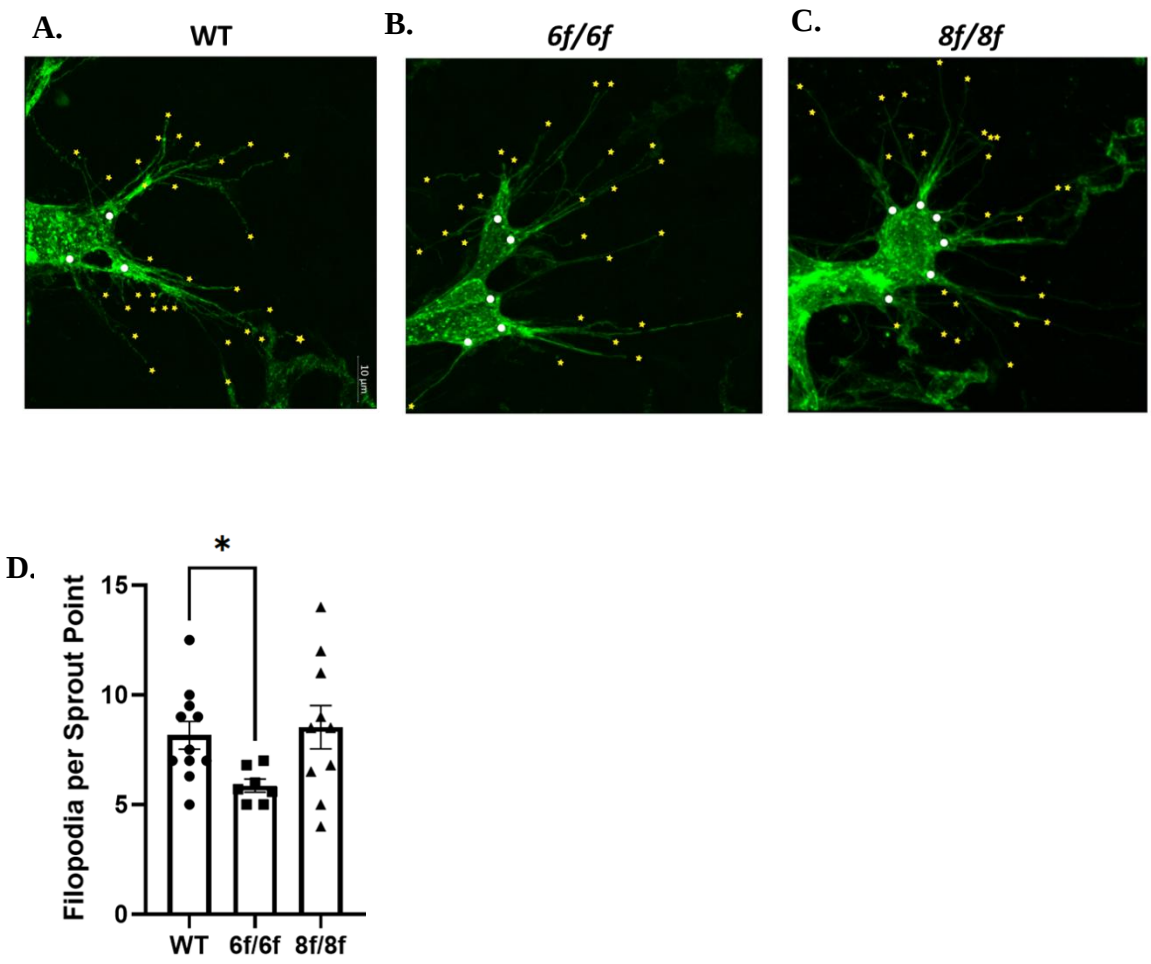

Supplementary Figure S3. Double blind analysis of tip cells shows fewer filopodia per sprout point from *6f/6f* retinas. Slides were mixed and blindly imaged by scanning from the upper-right-hand-corner of the retina downward to capture cells at the leading edge. Each genotype was represented by 3-4 retinas where WT (N=4), *6f/6f* (N=3), and *8f/8f* (N=3) with 3-5 images captured per retina. Representative images shown in **(A)-(C)**, where scale bar = 10 μm. **(D)** Quantitation of filopodia per sprout point, where each point represents the total number of filopodia per the total number of sprout points identified in each image. Calculations were

performed in GraphPad PRISM where outliers were removed by the ROUT method with FDR = 10%. Independent T-tests revealed significantly fewer filopodia per sprout point in the images from *6f/6f* retinas with a P-value <0.05 * considered significant.

CHAPTER 3

CONCLUSION

Summary of Experiments

In the roughly 100 years since the discovery of the first *notch* mutant described in *Drosophila* by John S. Dexter and Thomas Hunt Morgan, researchers have characterized components of the Notch signaling pathway across metazoans. Early phenotypes uncovered in *Drosophila* and mice defined the path to the next set of ligands, receptors, and proteases. While undefined at the time, parallel investigations into Notch *O*-glycans were pursued by chemists and geneticists piecing together predictive amino acid sequences and ordering events into the cascades that coordinate wing and bristle development. Finally, enough evidence would amass to draw attention across disciplines and open official study into *O*-glycosylation of Notch receptors and ligands.

After Notch began appearing relevant to human health, the pace of research increased. Connection to immune development was established by the accidental cloning of the human *NOTCH1* gene from T-ALL patient samples [5]. Notch was conditionally inactivated under promoters driving immune development, resulting in depletion of T cells [16, 79]. Although *Lfng-/-* mice exhibited a clear phenotype in concordance with human skeletal symptoms of Spondylocostal Dysostosis [75, 102], other phenotypes relating to the Fringe genes were not so easy to identify. By the process of working backwards from a Triple Knockout of all three mouse Fringe genes and re-introducing one Fringe gene at a time could clear contributions to specific immune phenotypes be distinguished [84].

Angiogenesis, the process through which vessels grow and organize into functional networks, has been extensively studied through the lens of NOTCH1 starting with the observation that yolk sacs from *Pofut1-/-* and *Jag1-/-* mice lack vascularization, both resulting in ~E10.5 lethality [62, 89]. Because vessel development is patterned by lateral inhibition coordinated by the regulated expression of *Notch1*, *Dll4*, *Jag1*, *Lfng*, *Mfng*, and *Rfng*, we wondered if we could confirm the molecular mechanisms for Fringe inhibition of NOTCH1 activation by JAG1 and Fringe enhancement of NOTCH1 activation by DLL4 *in vivo* by generating NOTCH1 mutant mice carrying T/V point mutations at either EGF6 or EGF8 *O*-fucose sites, respectively. Because pathway phenotypes had already been well documented, we predicted that EGF6 would cause loss of vessel density consistent with *Jag1* Loss-of-Function or NOTCH1 Gain-of-Function. Reciprocally, we predicted that the EGF8 mutation would induce a NOTCH1 Loss-of-Function phenotype observed in the *Dll4+/-* or *Lfng-/-* mice.

We also assessed changes to development of thymic T-cells, predicting that EGF6 would cause no change because EGF6 is only relevant in the context of *Jag1* and *Lfng or Mfng* expression, while the dominant ligand in the thymus is DLL4. This was an accurate prediction, however, we didn't measure a change to T-cell development in the EGF8 mutant. We predicted that eliminating EGF *O*-fucose would reduce necessary interactions between NOTCH1 and DLL4 in the thymus, as well as lost ability for LFNG-enhanced binding to DLL4 and a possible gain in the Double Positive population of T-cells [82]. We did notice a slight downward trend in the number of thymocytes harvested from EGF8 mouse thymi, but we decided to move towards assessment of angiogenesis and genetic crosses to induce embryonic lethality.

A homozygous NOTCH1 T/A mutation at the EGF12 *O*-fucose site caused embryonic lethality in a previous study [104], so we first crossed to this mouse. We identified viable mice

carrying the EGF8 mutation at one allele and EGF12 at the other, so we moved on to cross with a mouse lacking one copy of the NOTCH1 ligand binding domain. A cross this mouse yielded no live births of the EGF8/lbd transheterozygote. In a preliminary time-stage mating experiment, I was able to identify several embryos at E14.5 carrying both mutant alleles, so the embryos likely died after that timepoint and before birth.

Proposed in vivo Mechanisms

We confirmed that the EGF6 mutation did cause loss vessel density in the homozygotes consistent with pathway Gain-of-Function or *Jag1* Loss-of-Function. Because significant pivoting of JAG1 ligand was observed in the NOTCH1/JAG1 co-crystal structure indicative of a Catch Bond, a bond which lasts longer under greater tensile force, we wondered if the presence of GlcNAc in a region outside the ligand-binding domain would impart effects on a regulatory component other than soluble ligand binding at steady state conditions [32]. Preliminary data from a biophysical binding experiment under force suggests a conformational footprint when NOTCH1 is modified by LFNG and then mutated at EGF6. This could be a possible reasoning for the phenotype we observed in the retina.

Regarding the Loss-of-Activation observed in the EGF8 mice, the phenotype in the retina was highly consisten with *Lfng-/-* mice. Because mutation at EGF8 would lower activation by both JAG1 and DLL4 ligands in the absence of Fringe, and the evaluated angiogenic process is influenced by the global EGF8 allele, it likely wouldn't cause a change indicative of gene dosage. The more likely explanation is that the mutation knocked down the enhancement of *Mfng* and a little of *Lfng*, however *Rfng* does not modify that site so its expression is probably not relevant in this context.

Additional Considerations

Questions received during the defense process reflected a lack of consideration for the functional impact to the eye broadly or to vision in the context of loss of vessel density and gain of vessel desity. I'm of the mind that both states are equally bad because they likely cause disorganization to the vessels in the brain in addition to the eye. The vessels may also not be fully undergoing remodeling or stabilization, which was shown in a knockdown study into Eogt expression where leaky blood vessels were observed [115]. Thus, it is likely that aniogenic defects could cause the same issues in our mutants, not only in the retina, but in all vascular tissues.

Another consideration is the Alagille Syndrome defects observed in the eyes, especially anterior chamber defects to the iris and corneal tissue. These effects could be observed in a Jag1-/+ so it is possible that we could also observe these in our mice [89]. An easy phenotype to look for would be corneal clouding.

Further, no consideration was made for the nerve fiber layer which guides angiogenesis. This layer is made of ganglion cells which lead astrocytes and then endothelial cells. The neurogenic phenotype observed in the fly is the result of loss-of-function leading to overabundance of the differentiated neuronal cell type. Astrocyte progenitors derived from the optic nerve are likely held in a quiescent state until differentiation is needed around E18. This would require that Notch remain inactive until this point, then activate. I am uncertain if JAG1 and Fringe would be involved in this phenotype because proneural specification during lateral inhibition can be either JAG1 inhibition of NOTCH1 through Fringe or just expression of one ligand of the Delta family which would cause an alternating pattern in ligand expression and thus Notch activation. If you lose this through constitutive loss of the pathway, you may not generate

enough astrocytes (leading to loss of vessel development). It is a possible mechanism to explain this but further research into astrocytes is needed. It would be great to stain for astrocytes, as well as vessel stability factors such as pericytes, and cell cycle control genes or simply an Edu incorporation assay to look more closely at angiogenesis.

References

1. Bellen, H.J., C. Tong, and H. Tsuda, *100 years of Drosophila research and its impact on vertebrate neuroscience: a history lesson for the future.* Nat Rev Neurosci, 2010. **11**(7): p. 514-22.
2. Dexter, J.S., *The analysis of a case of continuous variation in Drosophila by a study of its linkage relations.* The American Naturalist, 1914. **48**(576).
3. Morgan, T.H., *The Theory of the Gene.* American Naturalist, 1917. **LI**(609).
4. Wharton, K.A., et al., *Nucleotide sequence from the neurogenic locus notch implies a gene product that shares homology with proteins containing EGF-like repeats.* Cell, 1985. **43**(3 Pt 2): p. 567-81.
5. Ellisen, L.W., et al., *TAN-1, the human homolog of the Drosophila notch gene, is broken by chromosomal translocations in T lymphoblastic neoplasms.* Cell, 1991. **66**(4): p. 649-61.
6. Swiatek, P.J., et al., *Notch1 is essential for postimplantation development in mice.* Genes Dev, 1994. **8**(6): p. 707-19.
7. Conlon, R.A., A.G. Reaume, and J. Rossant, *Notch1 is required for the coordinate segmentation of somites.* Development, 1995. **121**(5): p. 1533-45.
8. Irvine, K.D. and E. Wieschaus, *fringe, a Boundary-specific signaling molecule, mediates interactions between dorsal and ventral cells during Drosophila wing development.* Cell, 1994. **79**(4): p. 595-606.
9. Klueg, K.M., T.R. Parody, and M.A. Muskavitch, *Complex proteolytic processing acts on Delta, a transmembrane ligand for Notch, during Drosophila development.* Mol Biol Cell, 1998. **9**(7): p. 1709-23.
10. de Celis, J.F. and S. Bray, *Feed-back mechanisms affecting Notch activation at the dorsoventral boundary in the Drosophila wing.* Development, 1997. **124**(17): p. 3241-51.
11. Panin, V.M., et al., *Fringe modulates Notch-ligand interactions.* Nature, 1997. **387**(6636): p. 908-12.
12. Bruckner, K., et al., *Glycosyltransferase activity of Fringe modulates Notch-Delta interactions.* Nature, 2000. **406**(6794): p. 411-5.
13. Moloney, D.J., et al., *Fringe is a glycosyltransferase that modifies Notch.* Nature, 2000. **406**(6794): p. 369-75.
14. Rebay, I., M.E. Fortini, and S. Artavanis-Tsakonas, *Analysis of phenotypic abnormalities and cell fate changes caused by dominant activated and dominant negative forms of the Notch receptor in Drosophila development.* C R Acad Sci III, 1993. **316**(9): p. 1097-123.
15. Shao, L., D.J. Moloney, and R. Haltiwanger, *Fringe modifies O-fucose on mouse Notch1 at epidermal growth factor-like repeats within the ligand-binding site and the Abruptex region.* J Biol Chem, 2003. **278**(10): p. 7775-82.
16. Aster, J.C., W.S. Pear, and S.C. Blacklow, *The Varied Roles of Notch in Cancer.* Annu Rev Pathol, 2017. **12**: p. 245-275.
17. Yamamoto, S., et al., *A mutation in EGF repeat-8 of Notch discriminates between Serrate/Jagged and Delta family ligands.* Science, 2012. **338**(6111): p. 1229-32.
18. Rand, M.D., et al., *Calcium depletion dissociates and activates heterodimeric notch receptors.* Mol Cell Biol, 2000. **20**(5): p. 1825-35.
19. Gray, G.E., et al., *Human ligands of the Notch receptor.* Am J Pathol, 1999. **154**(3): p. 785-94.
20. D'Souza, B., A. Miyamoto, and G. Weinmaster, *The many facets of Notch ligands.* Oncogene, 2008. **27**(38): p. 5148-67.
21. Lindsell, C.E., et al., *Jagged: a mammalian ligand that activates Notch1.* Cell, 1995. **80**(6): p. 909-17.
22. Falo-Sanjuan, J. and S.J. Bray, *Decoding the Notch signal.* Dev Growth Differ, 2020. **62**(1): p. 4-14.

23. Kopan, R. and M.X. Ilagan, *The canonical Notch signaling pathway: unfolding the activation mechanism.* Cell, 2009. **137**(2): p. 216-33.
24. Panin, V.M., et al., *Notch ligands are substrates for protein O-fucosyltransferase-1 and Fringe.* J Biol Chem, 2002. **277**(33): p. 29945-52.
25. Taylor, P., et al., *Fringe-mediated extension of O-linked fucose in the ligand-binding region of Notch1 increases binding to mammalian Notch ligands.* Proc Natl Acad Sci U S A, 2014. **111**(20): p. 7290-5.
26. Kakuda, S. and R.S. Haltiwanger, *Analyzing the posttranslational modification status of Notch using mass spectrometry.* Methods Mol Biol, 2014. **1187**: p. 209-21.
27. Pandey, A., et al., *Glycosylation of Specific Notch EGF Repeats by O-Fut1 and Fringe Regulates Notch Signaling in Drosophila.* Cell Rep, 2019. **29**(7): p. 2054-2066 e6.
28. de Celis, J.F. and S.J. Bray, *The Abruptex domain of Notch regulates negative interactions between Notch, its ligands and Fringe.* Development, 2000. **127**(6): p. 1291-302.
29. Zheng, Y., et al., *A novel Notch1 missense mutation (C1133Y) in the Abruptex domain exhibits enhanced proliferation and invasion in oral squamous cell carcinoma.* Cancer Cell Int, 2018. **18**: p. 6.
30. Johnston, S.H., et al., *A family of mammalian Fringe genes implicated in boundary determination and the Notch pathway.* Development, 1997. **124**(11): p. 2245-54.
31. Rampal, R., et al., *Lunatic fringe, manic fringe, and radical fringe recognize similar specificity determinants in O-fucosylated epidermal growth factor-like repeats.* J Biol Chem, 2005. **280**(51): p. 42454-63.
32. Kakuda, S. and R.S. Haltiwanger, *Deciphering the Fringe-Mediated Notch Code: Identification of Activating and Inhibiting Sites Allowing Discrimination between Ligands.* Dev Cell, 2017. **40**(2): p. 193-201.
33. Kakuda, S., et al., *Canonical Notch ligands and Fringes have distinct effects on NOTCH1 and NOTCH2.* J Biol Chem, 2020. **295**(43): p. 14710-14722.
34. Benedito, R., et al., *The notch ligands Dll4 and Jagged1 have opposing effects on angiogenesis.* Cell, 2009. **137**(6): p. 1124-35.
35. Shifley, E.T. and S.E. Cole, *Lunatic fringe protein processing by proprotein convertases may contribute to the short protein half-life in the segmentation clock.* Biochim Biophys Acta, 2008. **1783**(12): p. 2384-90.
36. Artavanis-Tsakonas, S. and M.A. Muskavitch, *Notch: the past, the present, and the future.* Curr Top Dev Biol, 2010. **92**: p. 1-29.
37. Gerhardt, D.M., et al., *The Notch1 transcriptional activation domain is required for development and reveals a novel role for Notch1 signaling in fetal hematopoietic stem cells.* Genes Dev, 2014. **28**(6): p. 576-93.
38. Rana, N.A. and R.S. Haltiwanger, *Fringe benefits: functional and structural impacts of O-glycosylation on the extracellular domain of Notch receptors.* Curr Opin Struct Biol, 2011. **21**(5): p. 583-9.
39. Holdener, B.C. and R.S. Haltiwanger, *Protein O-fucosylation: structure and function.* Curr Opin Struct Biol, 2019. **56**: p. 78-86.
40. Varki, A. and S. Kornfeld, *Major Classes of Glycoconjugates and Glycans*, in *Essentials of Glycobiology*, A. Varki, et al., Editors. 2022: Cold Spring Harbor (NY).
41. Engel, J., *EGF-like domains in extracellular matrix proteins: localized signals for growth and differentiation?* FEBS Lett, 1989. **251**(1-2): p. 1-7.
42. Herbst, R.S., *Review of epidermal growth factor receptor biology.* Int J Radiat Oncol Biol Phys, 2004. **59**(2 Suppl): p. 21-6.

43. Semba, C.P., et al., *Alteplase and tenecteplase: applications in the peripheral circulation.* Tech Vasc Interv Radiol, 2001. **4**(2): p. 99-106.
44. Pohl, G., et al., *Tissue plasminogen activator: peptide analyses confirm an indirectly derived amino acid sequence, identify the active site serine residue, establish glycosylation sites, and localize variant differences.* Biochemistry, 1984. **23**(16): p. 3701-7.
45. Harris, R.J., et al., *Tissue plasminogen activator has an O-linked fucose attached to threonine-61 in the epidermal growth factor domain.* Biochemistry, 1991. **30**(9): p. 2311-4.
46. Kentzer, E.J., et al., *Carbohydrate composition and presence of a fucose-protein linkage in recombinant human pro-urokinase.* Biochem Biophys Res Commun, 1990. **171**(1): p. 401-6.
47. Rabbani, S.A., et al., *Structural requirements for the growth factor activity of the amino-terminal domain of urokinase.* J Biol Chem, 1992. **267**(20): p. 14151-6.
48. Harris, R.J., et al., *Identification and structural analysis of the tetrasaccharide NeuAc alpha(2-->6)Gal beta(1-->4)GlcNAc beta(1-->3)Fuc alpha 1-->O-linked to serine 61 of human factor IX.* Biochemistry, 1993. **32**(26): p. 6539-47.
49. Stults, N.L. and R.D. Cummings, *O-linked fucose in glycoproteins from Chinese hamster ovary cells.* Glycobiology, 1993. **3**(6): p. 589-96.
50. Hase, S., et al., *A new trisaccharide sugar chain linked to a serine residue in bovine blood coagulation factors VII and IX.* J Biochem, 1988. **104**(6): p. 867-8.
51. Nishimura, H., et al., *Identification of a disaccharide (Xyl-Glc) and a trisaccharide (Xyl2-Glc) O-glycosidically linked to a serine residue in the first epidermal growth factor-like domain of human factors VII and IX and protein Z and bovine protein Z.* J Biol Chem, 1989. **264**(34): p. 20320-5.
52. Acar, M., et al., *Rumi is a CAP10 domain glycosyltransferase that modifies Notch and is required for Notch signaling.* Cell, 2008. **132**(2): p. 247-58.
53. Wang, Y., et al., *Identification of a GDP-L-fucose:polypeptide fucosyltransferase and enzymatic addition of O-linked fucose to EGF domains.* Glycobiology, 1996. **6**(8): p. 837-42.
54. Wang, Y. and M.W. Spellman, *Purification and characterization of a GDP-fucose:polypeptide fucosyltransferase from Chinese hamster ovary cells.* J Biol Chem, 1998. **273**(14): p. 8112-8.
55. Wang, Y., et al., *Modification of epidermal growth factor-like repeats with O-fucose. Molecular cloning and expression of a novel GDP-fucose protein O-fucosyltransferase.* J Biol Chem, 2001. **276**(43): p. 40338-45.
56. Moloney, D.J., et al., *Mammalian Notch1 is modified with two unusual forms of O-linked glycosylation found on epidermal growth factor-like modules.* J Biol Chem, 2000. **275**(13): p. 9604-11.
57. Luca, V.C., et al., *Structural biology. Structural basis for Notch1 engagement of Delta-like 4.* Science, 2015. **347**(6224): p. 847-53.
58. Luca, V.C., et al., *Notch-Jagged complex structure implicates a catch bond in tuning ligand sensitivity.* Science, 2017. **355**(6331): p. 1320-1324.
59. Kao, Y.H., et al., *The effect of O-fucosylation on the first EGF-like domain from human blood coagulation factor VII.* Biochemistry, 1999. **38**(22): p. 7097-110.
60. Okajima, T. and K.D. Irvine, *Regulation of notch signaling by o-linked fucose.* Cell, 2002. **111**(6): p. 893-904.
61. Rebay, I., et al., *Specific EGF repeats of Notch mediate interactions with Delta and Serrate: implications for Notch as a multifunctional receptor.* Cell, 1991. **67**(4): p. 687-99.
62. Shi, S. and P. Stanley, *Protein O-fucosyltransferase 1 is an essential component of Notch signaling pathways.* Proc Natl Acad Sci U S A, 2003. **100**(9): p. 5234-9.
63. Okajima, T., et al., *Chaperone activity of protein O-fucosyltransferase 1 promotes notch receptor folding.* Science, 2005. **307**(5715): p. 1599-603.

64. Blaumueller, C.M., et al., *Intracellular cleavage of Notch leads to a heterodimeric receptor on the plasma membrane.* Cell, 1997. **90**(2): p. 281-91.
65. Takeuchi, H., et al., *O-Glycosylation modulates the stability of epidermal growth factor-like repeats and thereby regulates Notch trafficking.* J Biol Chem, 2017. **292**(38): p. 15964-15973.
66. Lee, T.V., et al., *Negative regulation of notch signaling by xylose.* PLoS Genet, 2013. **9**(6): p. e1003547.
67. Pandey, A., et al., *Sensitized genetic backgrounds reveal differential roles for EGF repeat xylosyltransferases in Drosophila Notch signaling.* Glycobiology, 2018. **28**(11): p. 849-859.
68. Varshney, S. and P. Stanley, *Multiple roles for O-glycans in Notch signalling.* FEBS Lett, 2018. **592**(23): p. 3819-3834.
69. Takeuchi, H., et al., *Two novel protein O-glucosyltransferases that modify sites distinct from POGLUT1 and affect Notch trafficking and signaling.* Proc Natl Acad Sci U S A, 2018. **115**(36): p. E8395-E8402.
70. Williamson, D.B., et al., *POGLUT2 and POGLUT3 O-glucosylate multiple EGF repeats in fibrillin-1, -2, and LTBP1 and promote secretion of fibrillin-1.* J Biol Chem, 2021. **297**(3): p. 101055.
71. Marshall, B.T., et al., *Direct observation of catch bonds involving cell-adhesion molecules.* Nature, 2003. **423**(6936): p. 190-3.
72. Gordon, W.R., et al., *Mechanical Allostery: Evidence for a Force Requirement in the Proteolytic Activation of Notch.* Dev Cell, 2015. **33**(6): p. 729-36.
73. Wang, W., T. Okajima, and H. Takeuchi, *Significant Roles of Notch O-Glycosylation in Cancer.* Molecules, 2022. **27**(6).
74. Hicks, C., et al., *Fringe differentially modulates Jagged1 and Delta1 signalling through Notch1 and Notch2.* Nat Cell Biol, 2000. **2**(8): p. 515-20.
75. Zhang, N. and T. Gridley, *Defects in somite formation in lunatic fringe-deficient mice.* Nature, 1998. **394**(6691): p. 374-7.
76. Williams, D.R., et al., *Disruption of somitogenesis by a novel dominant allele of Lfng suggests important roles for protein processing and secretion.* Development, 2016. **143**(5): p. 822-30.
77. Moran, J.L., et al., *Manic fringe is not required for embryonic development, and fringe family members do not exhibit redundant functions in the axial skeleton, limb, or hindbrain.* Dev Dyn, 2009. **238**(7): p. 1803-12.
78. Zhang, N., C.R. Norton, and T. Gridley, *Segmentation defects of Notch pathway mutants and absence of a synergistic phenotype in lunatic fringe/radical fringe double mutant mice.* Genesis, 2002. **33**(1): p. 21-8.
79. Radtke, F., et al., *Deficient T cell fate specification in mice with an induced inactivation of Notch1.* Immunity, 1999. **10**(5): p. 547-58.
80. Ge, C., et al., *In vivo consequences of deleting EGF repeats 8-12 including the ligand binding domain of mouse Notch1.* BMC Dev Biol, 2008. **8**: p. 48.
81. Lei, L., et al., *An O-fucose site in the ligand binding domain inhibits Notch activation.* Development, 2003. **130**(26): p. 6411-21.
82. Visan, I., et al., *Regulation of T lymphopoiesis by Notch1 and Lunatic fringe-mediated competition for intrathymic niches.* Nat Immunol, 2006. **7**(6): p. 634-43.
83. Ge, C. and P. Stanley, *The O-fucose glycan in the ligand-binding domain of Notch1 regulates embryogenesis and T cell development.* PNAS, 2008. **105**(5): p. 1539–1544.
84. Song, Y., et al., *Lunatic, Manic, and Radical Fringe Each Promote T and B Cell Development.* J Immunol, 2016. **196**(1): p. 232-43.
85. Basch, M.L., et al., *Fine-tuning of Notch signaling sets the boundary of the organ of Corti and establishes sensory cell fates.* Elife, 2016. **5**.
86. Alagille, D., *Alagille syndrome today.* Clin Invest Med, 1996. **19**(5): p. 325-30.

87. Spinner, N.B., et al., *Alagille Syndrome*, in *GeneReviews((R))*, M.P. Adam, et al., Editors. 1993: Seattle (WA).
88. Krantz, I.D., et al., *Spectrum and frequency of jagged1 (JAG1) mutations in Alagille syndrome patients and their families.* Am J Hum Genet, 1998. **62**(6): p. 1361-9.
89. Xue, Y., et al., *Embryonic lethality and vascular defects in mice lacking the Notch ligand Jagged1.* Hum Mol Genet, 1999. **8**(5): p. 723-30.
90. Hofmann, J.J. and M. Luisa Iruela-Arispe, *Notch expression patterns in the retina: An eye on receptor-ligand distribution during angiogenesis.* Gene Expr Patterns, 2007. **7**(4): p. 461-70.
91. Fruttiger, M., *Development of the retinal vasculature.* Angiogenesis, 2007. **10**(2): p. 77-88.
92. Nguyen-Ba-Charvet, K.T. and A. Rebsam, *Neurogenesis and Specification of Retinal Ganglion Cells.* Int J Mol Sci, 2020. **21**(2).
93. Punal, V.M., et al., *Large-scale death of retinal astrocytes during normal development is non-apoptotic and implemented by microglia.* PLoS Biol, 2019. **17**(10): p. e3000492.
94. Suchting, S., et al., *The Notch ligand Delta-like 4 negatively regulates endothelial tip cell formation and vessel branching.* Proc Natl Acad Sci U S A, 2007. **104**(9): p. 3225-30.
95. Bray, S.J., *Notch signalling in context.* Nat Rev Mol Cell Biol, 2016. **17**(11): p. 722-735.
96. Artavanis-Tsakonas, S., M.D. Rand, and R.J. Lake, *Notch signaling: cell fate control and signal integration in development.* Science, 1999. **284**(5415): p. 770-6.
97. Gridley, T., *Notch signaling in vertebrate development and disease.* Mol Cell Neurosci, 1997. **9**(2): p. 103-8.
98. Pandey, A., N. Niknejad, and H. Jafar-Nejad, *Multifaceted regulation of Notch signaling by glycosylation.* Glycobiology, 2021. **31**(1): p. 8-28.
99. Matsumoto, K., K.B. Luther, and R.S. Haltiwanger, *Diseases related to Notch glycosylation.* Mol Aspects Med, 2021. **79**: p. 100938.
100. Basmanav, F.B., et al., *Mutations in POGLUT1, encoding protein O-glucosyltransferase 1, cause autosomal-dominant Dowling-Degos disease.* Am J Hum Genet, 2014. **94**(1): p. 135-43.
101. Cohen, I., et al., *Autosomal recessive Adams-Oliver syndrome caused by homozygous mutation in EOGT, encoding an EGF domain-specific O-GlcNAc transferase.* Eur J Hum Genet, 2014. **22**(3): p. 374-8.
102. Sparrow, D.B., et al., *Mutation of the LUNATIC FRINGE gene in humans causes spondylocostal dysostosis with a severe vertebral phenotype.* Am J Hum Genet, 2006. **78**(1): p. 28-37.
103. Pennarubia, F., et al., *Cancer-associated Notch receptor variants lead to O-fucosylation defects that deregulate Notch signaling.* J Biol Chem, 2022. **298**(12): p. 102616.
104. Varshney, S. and P. Stanley, *A modifier in the 129S2/SvPasCrl genome is responsible for the viability of Notch1[12f/12f] mice.* BMC Dev Biol, 2019. **19**(19).
105. Correia, T., et al., *Molecular genetic analysis of the glycosyltransferase Fringe in Drosophila.* Proc Natl Acad Sci U S A, 2003. **100**(11): p. 6404-9.
106. Benedito, R. and M. Hellstrom, *Notch as a hub for signaling in angiogenesis.* Exp Cell Res, 2013. **319**(9): p. 1281-8.
107. Fernandez-Chacon, M., et al., *Role of Notch in endothelial biology.* Angiogenesis, 2021. **24**(2): p. 237-250.
108. Pennarubia, F., et al., *Modulation of the NOTCH1 Pathway by LUNATIC FRINGE Is Dominant over That of MANIC or RADICAL FRINGE.* Molecules, 2021. **26**(19).
109. Martin-Gayo, E., et al., *Spatially restricted JAG1-Notch signaling in human thymus provides suitable DC developmental niches.* J Exp Med, 2017. **214**(11): p. 3361-3379.
110. Schmuck, M.R., et al., *Automated high content image analysis of dendritic arborization in primary mouse hippocampal and rat cortical neurons in culture.* J Neurosci Methods, 2020. **341**: p. 108793.

111. Hultgren, N.W., et al., *Slug regulates the Dll4-Notch-VEGFR2 axis to control endothelial cell activation and angiogenesis.* Nat Commun, 2020. **11**(1): p. 5400.
112. Milde, F., et al., *The mouse retina in 3D: quantification of vascular growth and remodeling.* Integr Biol (Camb), 2013. **5**(12): p. 1426-38.
113. Zudaire, E., et al., *A computational tool for quantitative analysis of vascular networks.* PLoS One, 2011. **6**(11): p. e27385.
114. Figueiredo, A.M., et al., *Endothelial cell invasion is controlled by dactylopodia.* Proc Natl Acad Sci U S A, 2021. **118**(18).
115. Sawaguchi, S., et al., *O-GlcNAc on NOTCH1 EGF repeats regulates ligand-induced Notch signaling and vascular development in mammals.* Elife, 2017. **6**.
116. Pontes-Quero, S., et al., *High mitogenic stimulation arrests angiogenesis.* Nat Commun, 2019. **10**(1): p. 2016.
117. Tual-Chalot, S., et al., *Whole mount immunofluorescent staining of the neonatal mouse retina to investigate angiogenesis in vivo.* J Vis Exp, 2013(77): p. e50546.
118. Singh, J.N., et al., *Quantifying three-dimensional rodent retina vascular development using optical tissue clearing and light-sheet microscopy.* J Biomed Opt, 2017. **22**(7): p. 76011.
119. Schneider, C.A., W.S. Rasband, and K.W. Eliceiri, *NIH Image to ImageJ: 25 years of image analysis.* Nat Methods, 2012. **9**(7): p. 671-5.